AD-E950 021

②

TECHNICAL REPORT RL-CR-80-4

LEVEL III

FLOWS IN THE ANNULAR REGION WHEN AN UNDEREXPANDED NOZZLE IS EXHAUSTED INTO A STEPPED LAUNCH TUBE

by

Stanley A. Bouslog; John J. Bertin
Department of Aerospace Engineering and Engineering Mechanics
The University of Texas of Austin
Austin, Texas 78712

U.S. ARMY MISSILE COMMAND
Redstone Arsenal, Alabama 35809

DTIC
ELECTE
SEP 2 1980

B

1 March 1980

80 8 1 077

DISPOSITION INSTRUCTIONS

DISCLAIMER

TRADE NAMES

REPORT DOCUMENTATION PAGE		READ INSTRUCTIONS BEFORE COMPLETING FORM
1. REPORT NUMBER Technical Report RL-CR-80-4	2. GOVT ACCESSION NO.	3. RECIPIENT'S CATALOG NUMBER
4. TITLE (and Subtitle) FLOWS IN THE ANNULAR REGION WHEN AN UNDEREXPANDED NOZZLE IS EXHAUSTED INTO A STEPPED LAUNCH TUBE		5. TYPE OF REPORT & PERIOD COVERED Final on one phase 1 March 1979 - 30 Sept. 1979
		6. PERFORMING ORG. REPORT NUMBER
7. AUTHOR(s) Stanley A. Bouslog John J. Bertin		8. CONTRACT OR GRANT NUMBER(s) DAAK 40-79-C-0021
9. PERFORMING ORGANIZATION NAME AND ADDRESS Department of Aerospace Engineering & Engineering Mechanics, The University of Texas at Austin Austin, Texas 78712		10. PROGRAM ELEMENT, PROJECT, TASK AREA & WORK UNIT NUMBERS
11. CONTROLLING OFFICE NAME AND ADDRESS Commander, US Army Missile Command Attn: DRSMI-RPT Redstone Arsenal, AL 35809		12. REPORT DATE 1 March 1980
		13. NUMBER OF PAGES 101
14. MONITORING AGENCY NAME & ADDRESS(if different from Controlling Office) Commander, US Army Missile Command Attn: DRSMI-RLH Redstone Arsenal, AL 35809		15. SECURITY CLASS. (of this report) Unclassified
		15a. DECLASSIFICATION/DOWNGRADING SCHEDULE

16. DISTRIBUTION STATEMENT (of this Report)

Approved for public release; distribution unlimited

17. DISTRIBUTION STATEMENT (of the abstract entered in Block 20, if different from Report)

18. SUPPLEMENTARY NOTES

The findings of this report are not to be construed as an official
Department of the Army position unless so designated by other
authorized documents.

19. KEY WORDS (Continue on reverse side if necessary and identify by block number)

Free-Flight Rockets
Mallaunch of Free Rockets

Launch Tube Flow Fields

20. ABSTRACT (Continue on reverse side if necessary and identify by block number)

An experimental program has been conducted in which unheated air was ex-
hausted through a stationary rocket nozzle into a constant-area-tube launcher
modified with a constrictive ring. The constrictive ring simulates a constraint
which could be a permanent or temporary part of the launch tube. For the first
phase of the test program the static wall-pressure distribution, upstream and
downstream of the ring, and the mass flow-rates in the annular gap were measured.
Given an underexpanded nozzle, a correlation between the generation blow-by, or
reverse flow in the annular gap, and the position of the nozzle exit-plane rela-

DD FORM 1473 1 JAN 73   EDITION OF 1 NOV 65 IS OBSOLETE

20.   (Continued)

tive to the front face of the ring was developed.   The flow phenomena pre-
sent in the launcher for different nozzle positions has also been investi-
gated.   For the second phase of the test program the static pressure distri-
bution on the surface of the rocket and the mass flow-rates in the annular
gap were measured.   The differential pressure distributions on the rocket
were related to the mass flow-rate in the annular gap with increasing blow-
by flow, and with increasing ejector flow.

FLOWS IN THE ANNULAR REGION WHEN AN UNDEREXPANDED NOZZLE IS
EXHAUSTED INTO A STEPPED LAUNCH TUBE*

by

Stanley A. Bouslog and John J. Bertin
Aerospace Engineering Report 80001

Department of Aerospace Engineering
and Engineering Mechanics

The University of Texas at Austin

March 1980

ACKNOWLEDGEMENTS

DTIC
S ELECTE D
SEP 2 1980
B

ACCESSION for		
NTIS	White Section	☑
DDC	Buff Section	☐
UNANNOUNCED		☐
JUSTIFICATION		
BY		
DISTRIBUTION/AVAILABILITY CODES		
Dist.	AVAIL. and/or SPECIAL	
A		

ABSTRACT

An experimental program has been conducted in which unheated air
was exhausted through a stationary rocket nozzle into a constant-area-
tube launcher modified with a constrictive ring. The constrictive ring
simulates a constraint which could be a permanent or temporary part of
the launch tube. For the first phase of the test program the static wall-
pressure distribution, upstream and downstream of the ring, and the mass
flow-rates in the annular gap were measured. Given an underexpanded nozzle,
a correlation between the generation of blow-by, or reverse flow in the
annular gap, and the position of the nozzle exit-plane relative to the
front face of the ring was developed. The flow phenomena present in the
launcher for different nozzle positions has also been investigated. For
the second phase of the test program the static pressure distribution
on the surface of the rocket and the mass flow-rates in the annular gap
were measured. The differential pressure distributions on the rocket
were related to the mass flow-rate in the annular gap with increasing
blow-by flow, and with increasing ejector flow.

TABLE OF CONTENTS

Page

INTRODUCTION

The designer of a tube-launched rocket system must consider the flow field inside the launch tube as the rocket is launched. Unless the annular gap between the rocket and the launch tube is sealed by a ring (e.g., an obturator ring), viscous interactions associated with the expansion of the exhaust flow as it leaves the nozzle and the subsequent impingement of the exhaust on the launcher wall will produce a "secondary" flow in the annular gap. Barnette et. al. (ref. 1) have shown that the trajectory of a tube-launched rocket can be significantly affected by the unbalanced forces associated with this secondary flow. To predict the magnitude and the direction of the flow in the annular gap, one must be able to describe the exhaust plume of the rocket and the viscous/shock interaction structure that results when the plume encounters the launcher wall. The strength of the impingement shock-wave and the characteristics of the viscous interaction at the wall depend on the structure of the exhaust plume and on the geometry of the launch tube. When an under-expanded, supersonic nozzle exhausts into a constant-area tube, the strength of the impingement shock wave depends on the Mach number of the inviscid flow along the inner edge of the mixing zone at the plume boundary, on the velocity profile in the mixing zone, on the ratio of the specific heats (γ), and on the inclination of the impinging flow relative to the launcher wall.

When there is negligible secondary flow, the pressure in the annular gap varies only slightly and, therefore, is approximately equal to the

1

atmospheric pressure. Thus, the static pressure in the annular gap is less than that downstream of the impingement shock wave. Nevertheless, experimental measurements (ref. 2) obtained in the Rocket Exhaust Effects Facility (REEF) of the University of Texas at Austin indicate that, when the stagnation pressure is relatively low, air from outside of the launcher can be drawn into the annular gap toward the exhausting jet. As the under-expanded nozzle flow accelerates into the straight launch tube it entrains air from the region surrounding the nozzle at the exit plane. A fraction of the entrained air is given sufficient momentum so that it passes through the impingement shock wave. Using the atmosphere at the upstream end of the launcher as its source, a low-velocity, ejector-type flow, develops in the annular region to supply the mass flow-rate of air that is carried through the shock wave.

As the stagnation pressure is increased, the ratio p_{ne}/p_b increases and the exhaust flow must expand through a larger angle as it leaves the nozzle. As a result, the Mach number at the plume boundary and the angle at which the flow encounters the wall increase, causing the impinging shock wave to become stronger. Once the impingement shock-wave becomes sufficiently strong, the resultant adverse pressure gradient causes a fraction of the exhaust to be turned upstream. The exhaust flow that is turned upstream is known as blow-by blow.

An experimental program has been conducted to determine the secon-dary flow-rates that result when an underexpanded, supersonic nozzle was exhausted into a constant-area-tube (ref. 3). Flow-field data were ob-tained for nine nozzle/launch-tube configurations over a range of stagnation pressures from 6.89×10^5 N/m^2 (100 psi) to 9.65×10^6 N/m^2 (1400 psi). The configurations tested included three different nozzles

(a 20°-half-angle conical nozzle, a 10°-half-angle conical nozzle, and a contoured nozzle whose exit angle was 10°) and three launch tubes such that the internal radius of the launch tube was either 1.20 r_{ne}, 1.275 r_{ne}, or 1.50 r_{ne}. Significant blow-by flow occurred only for the 20°-half-angle conical nozzle and only at the higher reservoir pressures.

But not all launch tubes are straight. The presence of rails, frangible bore riders, and changes in cross section serve as constrictions to the exhaust flow. Constrictions located in the exhaust flow downstream of the nozzle can produce dramatic changes in the launch tube flow. Significant blow-by flow can result when the flow at the boundary of the exhaust plume impinges directly on the constriction (or step) and "splashes" forward into the annular gap. For a relatively small constriction this splash-back phenomenon diminishes as the nozzle moves away from the step. However, if the constriction is relatively large, the reduction in the cross-section area of the launch tube may be large enough so that it serves as a second throat, choking the exhaust flow. Choking of the exhaust flow by a constrictive change in cross-section has been observed both in cold-gas tests at the University of Texas at Austin (ref. 1) and in flight tests at the White Sands Missile Range (ref. 4). For these flows, the strong shock wave which is generated when the plume impinges on the wall produces a large pressure gradient that turns a significant fraction of the flow upstream into the annular gap. Flow downstream of the shock wave is subsonic.

For the present program, two of the constant-area tubes used in the tests described in ref. 3 were modified by placing a ring in them. Thus, the ring formed a constrictive step in the tube similar to those

which might appear on a shoulder fired system. For the first phase of the test program, the relation between the nozzle-exit position relative to the ring and the flow field in the launch tube was investigated. A 10°-half-angle conical nozzle was exhausted into one of the modified launch tubes, and static wall-pressure distributions and mass flow-rates in the annular gap were measured over a range of stagnation pressures from 6.89×10^5 N/m^2 (100 psi) to 8.96×10^6 N/m^2 (1300 psi). Data were taken with the ring located from one to ten h downstream of the nozzle exit-plane, where h is the vertical (radial) height of the ring.

In the second phase of the test program the relation between the mass flow-rates in the annular gap and the generation of differential pressures across the rocket, when a constrictive ring is placed downstream of the nozzle exit was investigated. As shown by Barnette (ref. 1), small differential pressures across the rocket can significantly affect the initial trajectory of the rocket. An instrumented 10°-half-angle nozzle, as used by Barnette (ref. 1), was exhausted into a constant-area tube modified with a ring. Static-pressure distributions on the surface of the rocket and mass flow-rates in the annular gap were measured over a stagnation pressure range from 6.89×10^5 N/m^2 (100 psi) to 7.58×10^6 N/m^2 (1100 psi). Again, data were taken with the ring located from zero to ten h downstream of the nozzle exit-plane.

NOMENCLATURE

A	Cross-sectional area
d	Diameter
h	Radial height of ring
M	Mach number
$\dot{m}$	Mass flow-rate
p	Pressure
r	Radius
T	Temperature
x,y,z	Axes of a right-handed Cartesian coordinate frame
x	Distance relative to nozzle exit-plane
$\tilde{x}$	Distance relative to front face of ring
γ	Ratio of specific heats
θ,ϕ	Variables used to denote angular displacements

Subscripts

ag	Denotes static properties evaluated at the upstream end of the annular gap
aft	Refers to geometry of ring
atm	Atmospheric value
b	Denotes static properties evaluated in the base region
cyl	The cylindrical outer surface of the simulated rocket
ex	Referenced to exhaust flow
for	Refers to forward portion of launch tube
ne	Denotes properties in the nozzle exit-plane

5

pit   Denotes value measured by the pitot-probe

t   The inner surface of the launch tube

tl   Denotes properties evaluated in the stagnation chamber of the simulated rocket

Superscripts

*   Denotes properties evaluated at the throat (sonic region) of the nozzle

EXPERIMENTAL PROGRAM

Test Facility

The tests were conducted at the Rocket Exhaust Effects Facility (REEF) located at the Experimental Aerodynamics Laboratory (EAL) of the University of Texas at Austin. A schematic diagram of this blow-down type facility is presented in Fig. 1. Simulated rocket exhaust plumes were obtained by accelerating unheated, compressed air (the test gas) through a convergent-divergent nozzle (the simulated rocket). The simulated launch tube was mounted on a movable table. By moving the table in the x or (streamwise) direction, the location of the launch tube relative to the exit plane of the simulated rocket nozzle could be varied. The simulated rockets (C4 and C1) and the simulated launch tubes (L1 and L3), as modified for use in this test program, are illustrated by the sketches presented in Figs. 2 through 4. Data for the C4 nozzle and for the L1 and the L3 launch tubes have been presented in ref. 3. The C1 nozzle fitted with an instrumented sleeve to measure differential pressures acting on the rocket was used in the tests described in ref. 1. Although both the C4 and the C1 nozzles have 10° half-angles, the area ratio A_{ne}/A^* differs, being 2.315 and 2.242, respectively. If one assumed isentropic flow in the nozzle, these ratios can be used to define their respective Mach numbers at the nozzle exit-plane: M_{ne} = 2.360 for C4 and M_{ne} = 2.325 for C1. The two launch-tubes were modified with a constrictive ring with a radial height equal to the annular gap. For the C4/L1 configuration, h = 0.1499 cm (0.059 in.), and for C1/L3, h = 0.2286 cm (0.090 in.).

Data were obtained for two nozzle/launch-tube configurations. The
first configuration, C4/L1, that was tested, had only the launch-tube
instrumented. As shown in Fig. 4, the static wall pressures could be
measured 4.64 cm (1.83 in.) upstream and 4.64 cm downstream of the ring.
Upstream of the ring the pressure orifices were spaced 0.309 cm (0.122 in)
apart while downstream of the ring the orifices were spaced 0.618 cm
(0.243 in) apart. The launch-tube also had pitot-probes that could face
either upstream or downstream in order to determine the mass flow-rate
of the secondary flow. It should be noted that the pitot-probes were made
from 0.091 cm (0.036 in.) outside-diameter, stainless-steel tubing. Since
the annular gap was only 0.1499 cm (0.059 in.) wide, the probes were
relatively large for this configuration. Based on an analysis of the
data, it appears that secondary-flow rates were not accurately measured.
Therefore, only the trends of these measurements should be considered.

The principal objective of the tests conducted with the second
configuration, C1/L3, was to determine a correlation between the secon-
dary flow rates and the pressure distribution on the rocket. Therefore,
the tests involving the C1/L3 configuration did not make use of the static-
pressure orifices on the launcher. Instead, the C1 nozzle was fitted
with an instrumented sleeve containing 32 static-pressure orifices. The
cross-section views of the particular axial location at which the pressure
taps were installed are illustrated in the sketch of Fig. 3. All of the
corss-sections (called "stations") which contain pressure taps were
located at distances equal to integer multiples of the nozzle exit radius
(r_{ne}) from the nozzle exit-plane. The station number of a group of
circumferentially-located pressure taps refers to the distance (in nozzle

exit radii) the taps are located upstream of the nozzle exit-plane. For
example, station 1 refers to those orifices which are located at a dis-
tance of 1.0 r_{ne} from the nozzle exit. As shown in the figure, pressure
taps were located at stations 1, 2, 3, 5, and 10. Of the launch-tube
instrumentation, only the pitot-probes were used, as discussed earlier.
Since the annular gap was 0.2286 cm (0.090 in) for the C1/L3 configuration
the relative size of the pitot-probes did not appear to affect seriously
the measurement of the secondary flow-rates.

Coordinate Systems

For this test program two coordinate systems were used. The non-
dimensionalized coordinate x/r_{ne} was used in measuring the position of
the static-pressure taps, either on the wall of the launcher or on the
surface of the rocket, relative to the nozzle exit-plane, downstream
being positive. The non-dimensionalized coordinate $\tilde{x}/h$, where h is
the height of the ring, was introduced to define the distance from the
front face of the ring. These two coordinate systems are illustrated in
Fig. 5.

Data Acquisition and Reduction

To determine the effects of the rocket/launch-tube geometry on
the secondary flow characteristics and on the pressure differentials
acting on the rocket, three types of data were obtained: (1) static-
pressure distributions on the launcher wall (for the C4/L1 configuration
only, (2) static-pressure distributions on the surface of the rocket

(for the C1/L3 configuration only), and (3) the mass flow-rates in the annular gap (for both the C4/L1 and the C1/L3 configurations).

Nylon pressure tubing connected all of the instrumentation to the scannivalve system and HP-9825A minicomputer, as described by Idar (ref. 3). The static wall-pressures and the pitot pressures were recorded using either a 100 psid or a 500 psid transducer (rated at $\pm$ 0.06% of full scale). During the runs in which the pressure differentials across the rocket were to be computed, the accuracy was found to be $\pm$ 0.0012 psid. The minicomputer was used to control the scannivalve system and to convert the transducer output directly into the non-dimensionalized static-pressures, p/p_{t1}, and the mass flow-rates in the annular gap. Assuming a one-dimensional, adiabatic flow in the annular gap and perfect-gas properties, then the dimensionless mass flow-rate is given by:

$$\frac{\dot{m}_{ag}}{\dot{m}_{ex}} = M_{ag} \sqrt{\frac{T_{t1}}{T_{ag}}} \; \frac{p_{ag}}{p_{t1}} \; \frac{(r_t^2 - r_{cyl}^2)}{\sqrt{\frac{2}{\gamma+1}} \left(\frac{2}{\gamma-1}\right)^{\frac{1}{\gamma-1}} (r^*)^2}$$

Note that $\gamma = 1.4$ for all tests. Since $r_t = 1.4844$ cm (0.5844 in), $r_{cyl} = 1.3335$ cm (0.525 in), and $r^* = 0.8130$ cm (0.320 in), for the C4/L1 configuration, the mass flow-rate equation becomes:

$$\frac{\dot{m}_{ag}}{\dot{m}_{ex}} = 1.1120 \; M_{ag} \sqrt{\frac{T_{t1}}{T_{ag}}} \; \frac{p_{ag}}{p_{t1}}$$

Since r_t = 1.8555 cm (0.7305 in), r_{cyl} = 1.626 cm (0.640 in), and r^* = 0.9703 cm (0.382 in), for the C1/C3 configuration, the mass flow-rate equation becomes:

$$\frac{\dot{m}_{ag}}{\dot{m}_{ex}} = 1.4687 \ M_{ag} \sqrt{\frac{T_{t1}}{T_{ag}}} \ \frac{P_{ag}}{P_{t1}}$$

For those runs where blow-by occurred, p_{ag} was the average value of the static pressures measured nearest the pitot-probes. The measured pitot-pressures were divided by p_{ag} and were used to calculate M_{ag}. For the ejector flow calculations, the pitot-pressures were assumed to be the atmospheric value while the value of p_{ag} was measured. The resultant ratio of p_{pit}/p_{ag} was used to calculate M_{ag}.

Test Program

Before the test program was begun, the C4 simulated rocket nozzle was threaded into the air supply line, and the modified L1 launch tube was mounted on the movable table. Then, efforts were made to align the rocket with the tube to insure that they were colinear within ± 0.05 degrees.

After alignment, the table was moved so that the nozzle exit-plane was one h, or 0.1499 cm (0.059 in), from the face of the ring, i.e., $\tilde{x}_{ne}$ = 1.0h. The pitot-probe assembly was oriented to sense blow-by, i.e., pointing downstream, and tufts were placed on the rocket just outside the forward end of the launch tube. These tufts provided visualization of the secondary flow and its direction. Tests were run, and

wall pressure and pitot pressure measurements were taken at three different stagnation pressures: 8.96×10^6 N/m^2 (1300 psi), 6.21×10^6 N/m^2 (900 psi), and 2.76×10^6 N/m^2 (400 psi). Data were obtained with $\tilde{x}_{ne}$ in multiples of h from one through ten. Then, the pitot-probes were reversed and measurements for ejector flow were taken at $\tilde{x}_{ne}/h$ equal to two, four, six and eight. For the ejector flow tests measurements were taken for p_{t1} equal to 2.07×10^6 N/m^2 (300 psi), 1.38×10^6 N/m^2 (200 psi), and 6.89×10^5 N/m^2 (100 psi).

Once the C4/L1 tests had been completed, the C1 nozzle and the modified L3 launch tube were positioned, as described above. Each pressure lead was checked for leaks, and the pitot-probes were oriented in the blow-by position. At this time, tests were run at each $\tilde{x}_{ne}$ for $\tilde{x}_{ne}/h$ equal to 2,4,6,8 and 10. At each nozzle position, the static-pressures on the surface of the rocket and the pitot pressures were measured for three values of the reservoir stagnation pressure, i.e., 7.58×10^6 N/m^2 (1100 psi), 5.52×10^6 N/m^2 (800 psi), and 2.76×10^6 N/m^2 (400 psi). Then, the pitot-probes were reversed and the constrictive ring was removed. With the ring removed ejector flow in the annular gap was more easily achieved. Again, the static-pressures and pitot-pressures were measured. However, since ejector-type flows were of interest, the data were obtained at stagnation pressures of 3.45×10^6 N/m^2 (500 psi), 2.07×10^6 N/m^2 (300 psi), 1.38×10^6 N/m^2 (200 psi), and 6.89×10^5 N/m^2 (100 psi). Since the ring was removed, the tests were run at only one position. A location of $\tilde{x} = 10.0h$ will be assigned to this test. A small piece of tape was then placed on the outer surface of the rocket

between station 2 and 3. This tape simulated a small protuberance on the surface of the rocket, such as a folded fin. The tape was 0.013 cm (0.005 in) thick and 0.377 cm (0.150 in) wide. Once again, pitot and static pressures were taken during runs at the same stagnation pressures, except for the 3.45×10^6 N/m^2 (500 psi) case.

DISCUSSION OF RESULTS

An experimental program has been conducted in which unheated air
was accelerated through two different rocket nozzle/launch-tube con-
figurations. The C4 nozzle (r_{ne} = 1.237 cm), which is a 10° conical
nozzle without instrumentation, was exhausted into a launch-tube (L1)
whose internal radius was 1.20 r_{ne} and that had been modified with a ring
as shown in Fig. 4. The C1 nozzle (r_{ne} = 1.453 cm), which is a 10° coni-
cal nozzle with an instrumented sleeve, was exhausted into a modified
launch-tube (L3) whose internal radius was 1.28 r_{ne}. For the C4/L1 con-
figuration, the mass flow-rates measured in the annular gap and the static
pressure distribution measured on the internal wall of the launch-tube
when a constrictive ring was placed downstream of the nozzle exit are
discussed in the present report. For the C1/L3 configuration, the mass
flow-rates in the annular gap will be discussed, along with the differential
pressure distribution on the rocket itself.

The Generation of Blow-by Due to a Constrictive Ring

When an underexpanded rocket exhausts into a launch-tube, a
significant fraction of the exhaust gas may be turned upstream by the
adverse pressure gradient associated with the impingement process,
creating a secondary flow in the annular gap. This flow reversal, or
blow-by, can be caused by many factors such as a strong shock created as
the exhaust impinges upon the launcher wall at a relatively high angle.
Bertin et al. (ref. 5) have investigated the generation of blow-by for

14

exhaust flows from various nozzles into constant-area launch-tube con-
figurations. They observed that, whenever 10° conical nozzles are exhausted
into constant-area tubes, little or no blow-by would be expected for
$P_{t1} \leq 8.87 \times 10^6$ N/m^2 (1386 psia).

The launch-tubes used by Bertin et al. were modified with a ring
(or step) for the present tests. A constriction (the ring) located down-
stream of the nozzle exit-plane may serve as a second throat, choking the
flow in the launch-tube. This possibility will be considered first.
Barnette et al. (ref. 1) have shown that a constriction downstream that
chokes the exhaust flow will cause massive blow-by. Also, Bertin and
Batson (ref. 6) found "that the constrictive area ratio, A_{aft}/A_{for}, was
a dominant parameter in the generation of blow-by flow." If the area
ratio is below a critical value the exhaust flow will become choked
creating a strong (normal) impingement shock and the flow is subsonic as
it passes through the constriction. Because the impingement shock-wave
is strong, some of the exhaust flow does not have sufficient momentum to
overcome the adverse pressure gradient and will turn upstream.

The critical area ratio was calculated as follows. Assuming that
the flow upstream of the normal shock wave is one-dimensional and expands
isentropically to the area of the launch-tube, an equation was developed
to calculate the minimum constrictive area ratio through which the rocket
exhaust flow can pass without choking. The correlation is presented in
Fig. 6. Referring to this figure, one sees that the C4/L1 configuration
with the ring is well above the "critical value". Hence, the ring would
not be expected to act as a second throat choking the flow. However,
the C1/L3 configuration has an area ratio slightly greater than the

"critical value." Based on data from previous tests (ref. 1), choked flow due to viscous effects could be expected for some conditions. Nevertheless, choked flow in the launch tube was not observed for either configuration during this experimental program. Therefore, any generation of blow-by cannot be attributed to the choking of the exhaust flow and the shock system that a second throat would establish. Instead, another cause of blow-by must be investigated, such as splash-back.

Even though the constrictive ring does not choke the exhaust flow, i.e., act as a second throat, relatively large blow-by flow-rates were obtained for some nozzle positions. To understand why blow-by occurs for some nozzle positions and not for others, an investigation of the flow phenomena in the launch tube is in order. An investigation of these phenomena must begin with an understanding of the interaction between the rocket exhaust plume and the launcher wall including the ring. The theoretical plume for the C4 nozzle (for which θ_{ne} was 10°) exhausting into the ambient atmosphere (ref. 7), superimposed on the geometry of the launch tube with a ring, is shown in Fig. 7. The reader should note that this sketch is only a general guide, since the exhaust flow could be significantly altered by viscous/shock interactions. Such interactions depend on the position of the nozzle with respect to the ring. With the nozzle exit-plane very close to the ring, i.e., within 1.0h or 2.0h of the step (ring), the basic plume is such that the boundary intersects the front face of the ring. This creates a splash-back of the exhaust into the annular gap. Moving the nozzle further upstream, i.e., x_{ne} greater than 3.0h, the plume boundary intersects the wall before encountering the ring. The relative distance between the plume impinge-

ment and the front face of the ring will influence the flow field and, hence, the mass flow-rates of the secondary flow and the static-pressure distribution on the launcher wall. Using these data, flow models, which depend on the nozzle-exit plane position, can be developed. Sketches of these "assumed" flow models appear in Figs. 8 and 9.

In the first sketch on Fig. 8, the nozzle is shown very close to the ring, i.e., $\tilde{x}_{ne}$ less than 1.0h. At this nozzle location the exhaust plume does not impinge on the front face of the ring. Instead, it expands into the aft section of the launcher, and no secondary flow in the annular gap occurs. As the nozzle exit-plane is moved forward, the exhaust plume boundary will impinge directly on the front face of the ring. Although most of the exhaust flow will continue downstream, past the constrictive ring, a significant fraction of the flow splashes off the ring back into the annular gap. Thus, there is a secondary flow in the annular gap in the negative x direction, i.e., blow-by. Given the basic plume of Fig. 7 blow-by due to splash-back occurs at $\tilde{x}_{ne}$ approximately equal to 2.0h (see Fig. 8(b)) for stagnation pressures in excess of 1.38×10^6 N/m^2 (200 psi). When the nozzle is moved further upstream, the exhaust flow impinges on the launcher wall ahead of the ring. But the impingement location is not yet far enough from the ring (step) to establish a flow field similar to that which results when a uniform flow encounters a forward-facing step. Charwat et al. (ref. 8) have investigated notches in supersonic flows. It was found that if the notch is long enough (larger than a critical closure length), then the flow will separate and expand from the corner of the downstream-facing step, reattach on the floor of the notch, and then separate from the flow creating a recompression

wake in front of the forward-facing step. The recompression wake
reattaches at the corner of the step. The nozzle exhaust flow can be
modeled as the flow past a notch. The exhaust flow expands out of the
nozzle and impinges upon the launcher wall. However, what happens next
depends on the distance between the impingement location and the front
face of the step (ring). Charwat et al. (ref. 8) have designated this
distance L_f. According to their data, a distance of approximately five
step heights is needed to create a recompression wake in front of a step
for a supersonic turbulent flow (M = 2 to 4) over a Reynold's number
range of 1 x 10^6 to 1 x 10^7 (ref. 8, Fig. 4). Clearly, for $\tilde{x}_{ne}$ = 3.0
to 7.0h (Fig. 8(c)), L_f is below the critical value, and therefore, a
recompression wake will not form. Instead, a curved shock that is essen-
tially normal near the launcher wall stands in front of the step. A
significant fraction of the exhaust flow encounters the shock and, due to
the large adverse pressure gradient, is turned back into the annular gap.
Again, significant blow-by occurs.

Once the rocket passes the $\tilde{x}_{ne}$ = 7.0h point (Fig. 9), the exhaust
plume impinges 5 or more step heights upstream of the step. Therefore,
the critical "closure" length has been attained and a "pressure-rise-
induced separation of the oncoming boundary layer", as described by
Charwat et al. (ref. 8), can occur. The separation from the wall and
the recompression of the flow deflects the external flow maintaining
a constant angle until the flow reattaches at the corner of the step.
Below the separated flow, a separation "bubble" forms in front of the
step. For these conditions, the step becomes isolated from the exhaust
flow and no longer influences the generation of secondary flow. A

sketch of this flow phenoemna is presented in Fig. 9. Also presented in

9 is the pressure distribution ahead of a step in a supersonic flow,

as reported by Chapman, Kuehn, and Larson (ref. 9). A pressure rise,

induced by the presence of the step and the thickening boundary layer,

causes the flow to separate at a constant angle of deflection. Beneath

the separated shear layer, a region exists with constant pressure through-

out, defining the pressure plateau. Very near the front fact of the

step another sharp pressure rise occurs due to the recompression of the

shear layer against the face of the step. Both the data of Chapman et al.

for a step in a uniform flow, which is reporduced in Fig. 9 for comparison,

and the present-test data for a step in an impingement plume exhaust show

the existence of the pressure plateau and the peak pressure very near the

face of the step.

Mass flow-rate data and the wall pressure distributions for the

C4/L1 configuration are presented in Fig. 10(a) and 11, respectively. In

order to measure the mass flow-rate in the annular gap, two pitot-probes

were positioned diameterically apart, midway between the launcher wall and

the rocket. Again, the reader is reminded about the questionable accuracy

of the pitot pressure measurements for this particular nozzle/launch-tube

configuration due to the relative size of the pitot-probe. Nevertheless,

the trends of the data can give meaningful conclusions. Referring to

Fig. 10(a), one can see that if the rocket nozzle is within 6.0h of the

ring, significant blow-by occurs for all stagnation pressures above

approximately 1.38×10^6 N/m^2 (200 psi), which is the stagnation pressure

at which the nozzle is properly expanded. This observation was also con-

firmed by the use of tufts placed on the rocket. Below 1.38×10^6 N/m^2

(200 psi), an adverse pressure gradient large enough to turn a fraction
of the exhaust flow upstream does not exist. Instead, air from the nozzle
base-region is entrained by the exhaust flow and is given sufficient
momentum to pass through the weak impingement shock wave, creating an
ejector flow. The mass flow-rate data show that an ejector flow exists
for all nozzle positions when the stagnation pressure is below 1.38×10^6
N/m^2 (200 psi). Above 1.38×10^6 N/m^2 (200 psi) there seems to be little
correlation between the stagnation pressure and $\dot{m}_{ag}/\dot{m}_{ex}$. A large con-
tributer to the scatter in the data is attributed to the experimental
uncertainty caused by having the probe in the relatively small annular gap
(as noted earlier).

The location of the nozzle-exit plane relative to the ring ($\tilde{x}_{ne}/h$
coordinate) is an extremely important parameter for the generation of
blow-by. As the nozzle exit-plane of the rocket moves from $\tilde{x}_{ne}$ = 0.0h
to $\tilde{x}_{ne}$ = 2.0h, the mass flow-rate increases. Because a larger fraction
of the exhaust flow impinges on the front face of the ring (see the
approximate plume boundaries of Fig. 7), more of the exhaust flow is
turned (i.e., splashes back) into the annular gap, creating blow-by.
Between $\tilde{x}_{ne}$ = 2.0h and $\tilde{x}_{ne}$ = 6.0h the mass flow-rate in the annular gap
is relatively constant. In this range of $\tilde{x}_{ne}$, the exhaust impinges upon
the wall of the launcher upstream of the ring. A signifiant fraction of
the exhaust flow is turned upstream due to the impingement shock and the
viscous interaction created by the close proximity of the ring. From
$\tilde{x}_{ne}$ = 6.0h to x_{ne} = 10.0h the mass flow-rate in the annular gap decreases
to almost zero. When the exhaust flow impinges far enough upstream of
the step (greater than 5.0 $\tilde{x}_{ne}/h$), a flow field similar to that for a

forward-facing step in a supersonic flow exists. After impinging upon the wall, the flow separates from the launcher wall, forms a separation "bubble" ahead of the step (ring), and reattaches at the corner of the step (see Fig. 9). Since the constrictive ring is not large enough to choke the flow, the ring serves as a forward-facing step which becomes essentially isolated from the exhaust flow. Little or no blow-by occurs, which is consistent with the data obtained for the C4/L1 configuration without the ring (ref. 3).

From the mass flow-rate data, three flow regions have been defined as a function of the nozzle-exit position. For each nozzle position in each of these flow regions, the pressure distribution on the wall of the launcher was measured. The static wall-pressure distributions for the three nozzle positions for a stagnation pressure of 8.96×10^6 N/m^2 (1300 psi) are presented in Fig. 11. The wall pressure data introduced in Fig. 11 are typical of all the wall pressure data obtained. For completeness, the remainder of the static wall pressure data are included in the Appendix. When $\tilde{x}_{ne} = 2.0h$ (Fig. 11(a)) the wall pressures upstream of the nozzle exit, i.e., for negative values of x/r_{ne}, are essentially constant along the length of the gap and approximately equal to two atmospheres. This high pressure in the annular gap indicates the presence of a large mass flow-rate, i.e., massive blow-by, as confirmed by Fig. 10. It should be noted that the flow in the annular gap is almost choked. Downstream of the ring, the pressure distribution can be quite complex due to the expansion of the exhaust flow over the downstream corner and to the possible existence of reflected shock waves.

Moving the nozzle to $\tilde{x}_{ne}$ = 6.0h (Fig. 11(b)), the wall pressure distribution ahead of the ring becomes more complicated. Just downstream of the nozzle exit, a local peak pressure exists where the flow impinges on the wall. At the base of the nozzle a dip in the pressure data ia observed which is an indication of the initial acceleration of a portion of the exhaust as it is turned upstream into the annular gap. Upstream of the nozzle exit the flow decelerates and maintains a relatively large pressure, i.e., greater than two atmospheres. Again, the high pressure in the annular gap reconfirm the presence of massive blow-by. The reader should note that ahead of the step (ring) no pressure plateau is observed for the limited data that are available. Since a pressure plateau is typical of a forward-facing step in a supersonic flow, the flow field at $\tilde{x}_{ne}$ = 6.0h is not similar to one for a forward-facing step. The close proximity of the step to the exhaust plume impingement modifies the impingement process, possibly strengthening the impingement shock. From the data available one cannot obtain a clear picture of the flow field at this nozzle position. However, it is apparent that a large fraction of the exhaust flow is turned upstream, creating mass flow-rates equal to, if not larger than, those for the splash-back case.

Shown in Fig. 11(c) are the wall pressure data for $\tilde{x}_{ne}$ = 10.0h. Upstream of the nozzle exit-plane, the wall pressures are essentially atmospheric, as would be expected since there was little or no secondary flow. Therefore, both the wall pressure data and the mass flow-rate data indicate very little or no blow-by. Downstream of the nozzle exit the exhaust flow impinges upon the wall sufficiently far from the ring as to not modify the impingement process. The impingement process resembles

that for a 10°-half-angle nozzle exhausted into a constant-area-tube, as described by Idar et al. (ref. 3). The pressure distribution ahead of the step (ring) is typical of that for a forward-facing step in a supersonic flow (see Fig. 9). The data indicate the presence of a pressure plateau in the region where the separation "bubble" exists and the pressure peak just in front of the step. Both the mass flow-rate data and the wall pressure data indicate that the step is isolated in the flow.

As an illustration of the effect of nozzle-exit position relative to the ring on the generation of blow-by, photographs of oil flows on the surface of the rocket just ahead of the launcher were taken, and are presented in Figs. 12, 13, and 14. Fig. 12 captures transient blow-by and steady-state blow-by when $\tilde{x}_{ne} = 2.0h$. The second photograph was taken at a stagnation pressure of 2.76×10^6 N/m^2 (400 psi). The reader should note the high shear as the blow-by flow exits the front of the launch tube and its decrease further from the launcher. These observations are also evident in the series of photographs taken at $\tilde{x}_{ne} = 4.0h$. As the rocket moves away from the ring, the ring becomes essentially isolated in the flow and no blow-by occurs. Fig. 14(a) shows the presence of little blow-by when $\tilde{x}_{ne} = 10.0h$. Also, shown in Fig. 14 is an oil flow during an ejector run. Obviously, little effect is felt by the rocket forward of the launcher during an ejector run.

For the C4/L1 configuration, the following observations were made.
1) A constrictive ring downstream of the rocket nozzle-exit can cause significant blow-by even though it does not choke the exhaust flow.
2) As long as the rocket nozzle is underexpanded, the generation of blow-by is a function of the distance of the rocket nozzle-exit plane from the front face of the ring.

3) The mass flow-rate data and the wall pressure data seem to define four different flow fields.

    a) When the nozzle location is less than 1.0h from the ring, the exhaust flow by-passes the ring, and little or no blow-by occurs.

    b) As the nozzle moves forward ($\tilde{x}_{ne}$ = 2.0h), the exhaust flow impinges directly on the front face of the ring and splashes back into the annular gap, creating blow-by.

    c) In the range of 3.0 $\tilde{x}_{ne}$/h to 7.0 $\tilde{x}_{ne}$/h, the exhaust flow impinges on the wall upstream of the ring. The relative closeness of the exhaust impingement location to the ring establishes a shock strong enough to turn a significant portion of the exhaust flow upstream.

    d) Beyond 7.0 $\tilde{x}_{ne}$/h the impingement shock is similar to that of a 10°-half-angle nozzle exhausting into a constant-area-tube in which no blow-by occurs. The flow phenomena near the ring, such as the pressure plateau and the peak pressure near the face, are characteristic of a forward-facing step in a supersonic flow. Essentially, the step (ring) is isolated from the impingement flow field.

Pressure Differentials Acting on a Rocket Due to
Flows in the Annular Gap

It has been established that considerable blow-by can occur when
an underexpanded rocket nozzle is exhausted into a simulated launch-tube
with a constrictive ring placed downstream of the nozzle exit-plane.
However, the question immediately arises as to what the effect these large
blow-by flow-rates can have on the initial trajectory of the rocket.
Barnette et al (ref. 1) have investigated this problem for a rocket ex-
hausting into a variable-area launch-tube. For those tests, the area
ratio of the constriction was such that the aft tube choked the flow in
the launch tube. It was concluded that if massive blow-by occurs,
asymmetric pressure differentials can exist on the rocket, even though
the axes of the nozzle and of the launch-tube were colinear.
The magnitude of the pressure-induced forces and moments are not sufficient
to cause a lateral displacement of the rocket in the tube. However,
these forces and moments can significantly affect the pitch angle and the
pitch rate of the rocket. Since these pressure-induced forces and moments
could affect the initial trajectory of a free-flight rocket, the relation
between the mass flow-rate in the annular gap of a launch tube with a
constrictive ring and the pressure differentials acting on the rocket
was studied.

In order to detect the presence of pressure differentials on the
rocket, the 10°-half-angle nozzle that was used by Barnette et al (ref. 1)
was used with one of the present launch-tubes. The pressure differentials
were determined at several nozzle-exit positions relative to the ring

25

over a range of stagnation pressures. Before discussing the pressure
distributions on the surface of the rocket, the flow phenomena in the
tube will be discussed.

The mass flow-rate data for the C1/L3 configuration with con-
strictive ring is presented in Fig. 10(b). Even though the exhaust
plume geometry for the C1 nozzle differs from the plume geometry
for the C4 nozzle, the flow fields are roughly similar for these two
configurations. Again, it is observed that the mass flow-rate in the
annular gap is relatively large when the nozzle-exit plane is close to
the ring, i.e., less than $\tilde{x}_{ne} = 7.0h$. Note that the non-dimensionalized
mass flow-rate increases rapidly as P_{t1} is increased for $\tilde{x}_{ne} = 2.0h$.
These data suggest that the blow-by for this nozzle location is caused
by splash-back since the flow rate increases rapidly as the plume expands
to larger dimensions. For $4.0h \leq \tilde{x}_{ne} \leq 6.0h$, the dimensionless blow-by
flow-rates are relatively insensitive to P_{t1}. Although the nozzle is
far enough away so that the exhaust impinges on the launcher wall up-
stream of the ring, the close proximity of the ring modifies the impinge-
ment process and significant blow-by still occurs. Eventually, the
exhaust impingement location moves sufficiently far from the ring, so
that a flow field similar to the one for a forward-facing step is
established ahead of the ring. The ring (step) becomes essentially
isolated in the flow and little or no blow-by occurs. This fact is
illustrated by the data for $\tilde{x}_{ne} = 10.0h$.

Also, shown in Fig. 10(b) are the mass flow-rate data obtained
when the constrictive ring was removed and ejector tests were run.

One set of runs was made with a piece of tape placed around the rocket to simulate a small disturbance on the rocket, such as folded fins. The other set of runs was conducted without the tape. All ejector runs indicated a strong dependence of the mass flow-rate on the stagnation pressure. Bertin et al. (ref. 5) describe this phenomenon. As the stagnation pressure decreases, the ejector mass flow-rate increases.

Since the flow field in the launcher may consist of massive blow-by flow due to splash-back or of entrained air (while the system is acting as an ejector), it is instructive to examine the pressure distribution on the rocket during either flow field situation. Presented in Figs. 15-17 and in Figs. 19-22, therefore, are the experimentally determined differential pressures across the rocket nozzle. The differential pressures, normalized by the appropriate stagnation pressure, are presented as a function of ϕ. Here, ϕ represents the angle between the x_n-y_n plane and a plane containing the diametrically-opposed pressure orifices at which the differential pressures for that particular value of ϕ were measured (see Fig. 3). For example, a value of $\phi = 0$ corresponds to pressure taps 1 and 5, whereas $\phi = 90$ corresponds to pressure taps 3 and 7. The dimensionless pressure ratio, $\Delta P/P_{t1}$, is plotted such that positive values correspond to the higher pressures being measured at taps 1,2,3, or 4. Negative values correspond to higher pressures being measured at taps 5,6,7, or 8. By presenting the data in this manner, the circumferential variation in the differential pressures can be seen for the various axial locations at which data were obtained. To determine the variation in the pressure distribution in the axial direction, the reader should note the pressure differentials at a particular ϕ and record them

as a function of x/r_{ne}, the axial distance from the nozzle exit-plane to the pressure orifice.

The pressure distributions on the surface of the Cl nozzle during blow-by tests for stagnation pressures of 7.58 x 10^6 N/m^2 (1100 psi), 5.52 x 10^6 N/m^2 (800 psi) and 2.76 x 10^6 N/m^2 (400 psi) are presented in Figs. 15, 16, and 17. The data for $\tilde{x}_{ne}$ = 2.0h, for $\tilde{x}_{ne}$ = 6.0h and for $\tilde{x}_{ne}$ = 10.0h, are presented in Figs. 15, 16, and 17, respectively. As a result of the occurrence of blow-by, it is observed that the pressures on the rocket have become asymmetric with a seemingly random variation. However, the variations in the pressure differential have been shown to be repeatable, i.e., Barnette et al (ref. 1). Therefore, an asymmetric pressure distribution is created on the rocket due to massive blow-by, despite the fact that the axes of the rocket and of the launch tube are "colinear", within experimental tolerance. Note that the larger asymmetric pressures occur near the nozzle exit. The large pressure differentials acting on the rocket near the nozzle exit are a result of the large pressure gradients which occur when the supersonic flow is turned 180° from the initial exhaust direction in such a short distance. Given the occurrence of the large pressure differentials near the nozzle exit-plane and the long moment-arm from the center of gravity of the rocket, the asymmetric pressures would significantly affect the pitch and the pitch rate of the rocket. The maximum differential pressures at an axial location for several test runs are presented in Fig. 18. The pressure differentials further away from the nozzle exit generally decrease since the static pressure in the annular gap must eventually equal the ambient pressure. Otherwise, no clear pressure distribution pattern has been

found.

Comparing the differential pressure data with the mass flow-rate data for the Cl/L3 configuration, a relation between blow-by flow-rates and differential pressure balues is observed. At $\tilde{x}_{ne}$ = 2.0h, significant blow-by occurs for the higher stagnation pressures (see Fig. 10(b)), while the corresponding differential pressures are also significant, see Fig. 15. When the stagnation pressure is decreased to 2.76 x 10^6 N/m^2 (400 psi), the blow-by flow-rate is nearly zero while the corresponding differential pressures are negligible. At $\tilde{x}_{ne}$ = 6.0h massive blow-by occurs for all stagnation pressures and again large asymmetric pressures were present, see Fig. 16. Once the ring becomes isolated in the flow, x_{ne} = 10.0h, little blow-by occurs and Fig. 17 indicates relatively symmetric static pressures act on the rocket. Plots have been made of the correlation between the mass flow-rate in the annular gap and the maximum differential pressure across the rocket at each station (see Fig. 23). For most stations during blow-by tests, an increase in the blow-by flow-rate meant an increase in the asymmetric pressures. It is not clear why station 3, x/r_{ne} = -3.0, did not follow this trend. However, the reader should remember that, since the asymmetric differentials are significant and vary rapidly with position, that it is possible to miss local maxima with the limited instrumentation. There were only four orifices for the stations at $-3r_{ne}$ and at $-10r_{ne}$.

When a portion of the air near the base of the nozzle is entrained by the exhaust plume, a secondary, "ejector", flow is created in the

annular gap. In order to investigate the relation between ejector flow-rates and the differential pressures across the C1 nozzle, the constrictive ring was removed. With the ring removed ejector flow would exist in the annular gap for a larger range of stagnation pressures. The first set of ejector runs were made for stagnation pressures of 3.45×10^6 N/m^2 (500 psi), 2.07×10^6 N/m^2 (300 psi), 1.38×10^6 N/m^2 (200 psi), and 6.89×10^5 N/m^2 (100 psi). For the second set of ejector runs, a piece of tape was placed between stations 2 and 3 to simulate a small disturbance on the rocket, such as a folded fin. These tests were conducted for stagnation pressures of 2.07×10^6 N/m^2 (300 psi), 1.38×10^6 N/m^2 (200 psi) and 6.89×10^5 N/m^2 (100 psi). The pressure differentials determined during each of these tests are presented in Figs. 19-22.

The differential pressure data for ejector tests indicate that significant asymmetric pressures exist on the rocket only in the presence of substantial ejector flow. At the higher stagnation pressures, 3.38×10^6 N/m^2 (490.5 psia) and 2.04×10^6 N/m^2 (295.9 psia), relatively small ejector flow-rates occurs, and the corresponding differential pressures, as shown in Figs. 19 and 20, are also small. Decreasing the stagnation pressure to 1.37×10^6 N/m^2 (198.5 psia), increases the ejector flow-rate, but it does not substantially change the differential pressures (see Fig. 21). Only when the ejector flow-rate increases considerably, i.e., at a stagnation pressure of 6.98×10^5 N/m^2 (101.2 psia), do the asymmetric pressures acting on the rocket become significant (see Fig. 22). Plots depicting the maximum differential pressures at a particular station as a function of the ejector flow-rate are presented in Fig. 23.

It is observed that for all stations, as the ejector flow-rates increased the maximum differential pressures increased. When the tape was placed between stations 2 and 3, the maximum differential pressures did not substantially change for low ejector flow-rates. However, when a large ejector flow-rate was present in the annular gap, the maximum differential pressures measured near the tape increased. Even though relatively large asymmetric pressures exist for large ejector flow-rates, the magnitudes of the differential pressures are not as large as those for blow-by, and the highest asymmetric pressures are not concentrated at a particular axial position. Therefore, a substantial ejector flow with its accompanying asymmetric pressures would not be expected to affect the initial trajectory of the rocket as much as blow-by would.

The following observations are made for the tests conducted with the C1/L3 configuration.

(1) For all the tests conducted for this experimental program, the flow fields for the C1/L3 configuration were similar to those discussed for the C4/L1 configuration.

(2) When significant blow-by exists in the rocket/launch-tube configuration, the highest asymmetric pressures acting on the rocket are concentrated near the nozzle exit. Since this area has a long momentum-arm, relatively small differential pressures could affect the pitch and the pitch-rate of the rocket.

(3) As the blow-by flow-rate increases, the differential pressures measured on the rocket also increase.

(4) Even though increasing the ejector flow-rate of a rocket/launch-tube configuration increases the differential pressures acting

on the rocket, these differential pressures are not as large as those induced by blow-by, and they are not concentrated at a particular axial location.

CONCLUDING REMARKS

An experimental program has been conducted in which underexpanded nozzles were exhausted into launch-tubes fitted with a constrictive ring (or step). In order to invesigate the flow fields present in a launch-tube with a step and in order to investigate a relation between the secondary flow-rates and the asymmetric pressures acting on the rocket, static wall-pressures, static pressures on the surface of the rocket, and pitot-pressures were measured. For the range of flow conditions and geometric configurations considered in the present program, the following conclusions are made:

1. When an underexpanded nozzle exhausts into a launch-tube with a constrictive ring that does not choke the exhaust flow, the blow-by flow-rate is a function of the nozzle exit-plane location relative to the front of the ring.

2. The mass flow-rate data and the static wall-pressure data seem to define four different flow fields.

    a. When the nozzle exit-plane is very close to the ring, the exhaust plume does not encounter the front face of the ring and no blow-by occurs.

    b. As the rocket moves upstream, the exhaust plume impinges directly on the face of the ring. A significant fraction of the exhaust flow splashes back into the annular gap creating blow-by.

c. With the rocket placed further upstream, the exhaust flow impinges on the launcher wall ahead of the ring. Due to the close proximity of the ring the impingement process is modified and a large adverse pressure gradient turns the flow upstream, generating blow-by.

d. When the exhaust plume impinges on the wall sufficiently far from the ring (step), a flow field similar to that for a forward-facing step in a supersonic flow is established. The wall pressure data just up-stream of the ring (step) confirm the existence of a pressure plateau and a local peak pressure typical of a forward-facing step pressure distribution. The ring becomes isolated in the exhaust flow and little or no blow-by occurs.

3. As the mass flow-rate (either blow-by or ejector) in the annular gap increases, the differential pressures acting on the rocket also in-crease. Thus, the possible effect on the initial trajectory of the rocket also increases with increasing mass flow-rates.

4. Since the asymmetric pressures induced by ejector-type flow are smaller than those associated with blow-by, and since the higher differential pressures associated with ejector flow are not concentrated near the nozzle exit, as they are for blow-by, it would be expected that blow-by flow would have more of an effect on the initial trajectory of the rocket than would ejector flow.

REFERENCES

1. D.W. Barnette, J.J. Bertin, and J.L. Batson, "Free-Flight Rocket's Initial Trajectory as Affected by Massive Blow-By", Journal of Spacecraft and Rockets, Vol. 15, No. 6, Nov.-Dec. 1978, pp. 334-340.

2. R.R. Morris, J.J. Bertin and J.L. Batson, "Flow Field for the Under-expanded, Supersonic Nozzle Exhausting into an Expansive Launch Tube", Presented at the 13th Annual Meeting of the Society of Engineering Science, Nov. 1976, Hampton, Virginia.

3. E.S. Idar, III, J.J. Bertin, and S. Bouslog, "The Effect of Geometry on Static Wall-Pressure Distributions and Secondary Flows for Tube-Launched Rocket Configurations", Aerospace Engineering Report 79005, November 1979, The University of Texas at Austin.

4. J.L. Batson and J.J. Bertin, "Experimental Study of Flow Field Produced when an Underexpanded Rocket Exhausts into Cylindrical Tube", AIAA Paper 73-1227, presented at AIAA/SAE 9th Propulsion Conference, Las Vegas, November 1973.

5. J.J. Bertin, E.S. Idar, and D.L. Booker, "Secondary Flows for a Tube-Launched Rocket Configuration", AIAA Paper 80-0372, Presented at the 18th Aerospace Sciences Meeting, Pasadena, California, Jan. 1980.

6. J.J. Bertin and J.L. Batson, "Comparison of Cold-gas Simulations and Rocket-Launch Data for Constrictive Launchers", Journal of Spacecraft and Rockets, Vol. 13, No. 11, Nov. 1976, pp. 684-691.

7. S.J. Sutter, J.J. Bertin, D.P. Dannemiller, and E.J. Zihlman, "Study of the Exhaust Plume for Highly Underexpanded Supersonic Nozzles Exhausting into Quiescent Air", Aerospace Engineering Report 79001, January 1979, The University of Texas at Austin.

8. A.F. Charwat, J.N. Roos, F.C. Dewey, Jr., and J.A. Hitz, "An Investigation of Separated Flows - Part I: The Pressure Field", Journal of the Aerospace Sciences, Vol. 28, No. 6, June 1961, pp. 457-470.

9. D.R. Chapman, D.M. Kuehn, and H.K. Larson, "Investigation of Separated Flows in Supersonic and Subsonic Streams with Emphasis on the Effect of Transition", Report 1356, 1956, NACA.
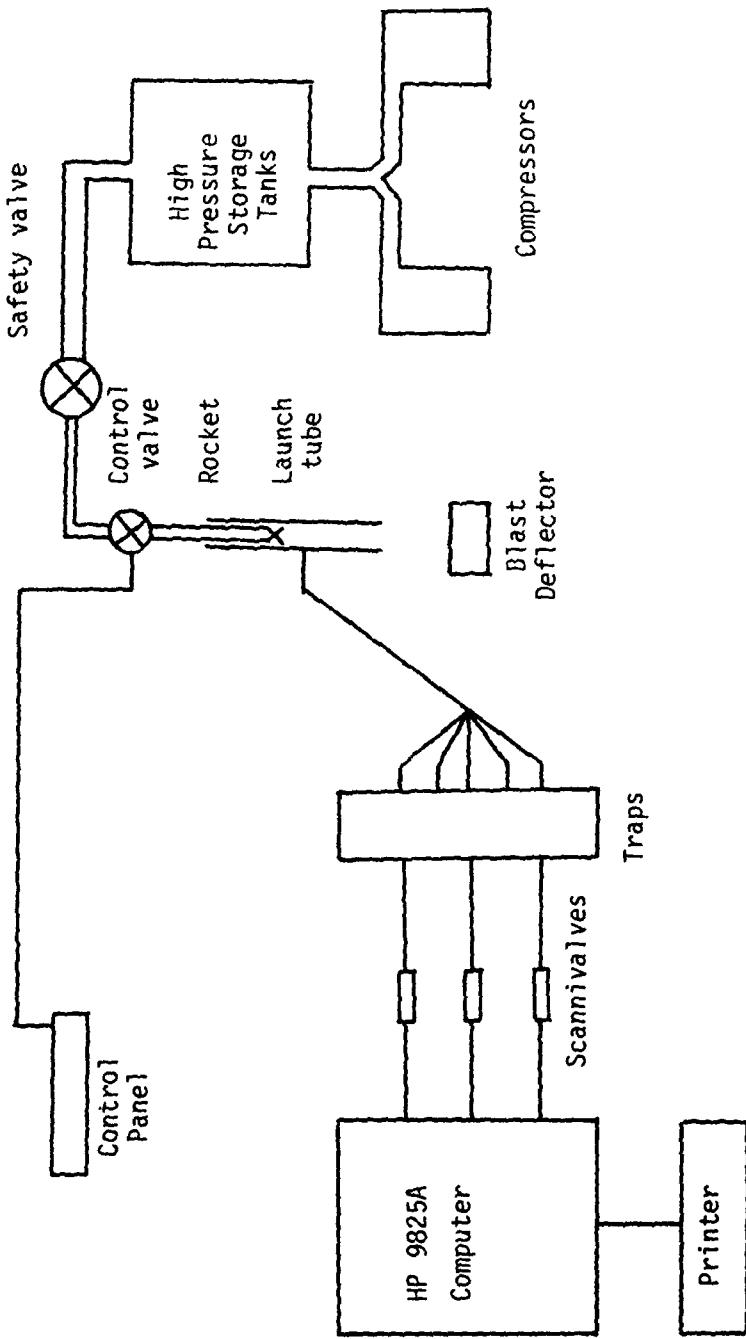
Figure 1. – Schematic of the University of Texas Rocket Exhaust Effects Facility.

Equations for Divergent Section (cm):

For $-2.479 \leq x \leq -2.338$

$$(x + 2.479)^2 + (r - 1.626)^2 = (0.813)^2$$

For $-2.338 < x \leq 0.0$

$$r = 0.176\, x + 1.237$$

$\theta = \theta_{ne} = 10°$

$r_{ne} = 1.237$
(0.487)

$r_r = 1.334$
(0.525)

r_{ne}

$x = 0.0$

$r^* = 0.813$
(0.320)

$x = -2.479$
(0.976)

1.080
(0.425)
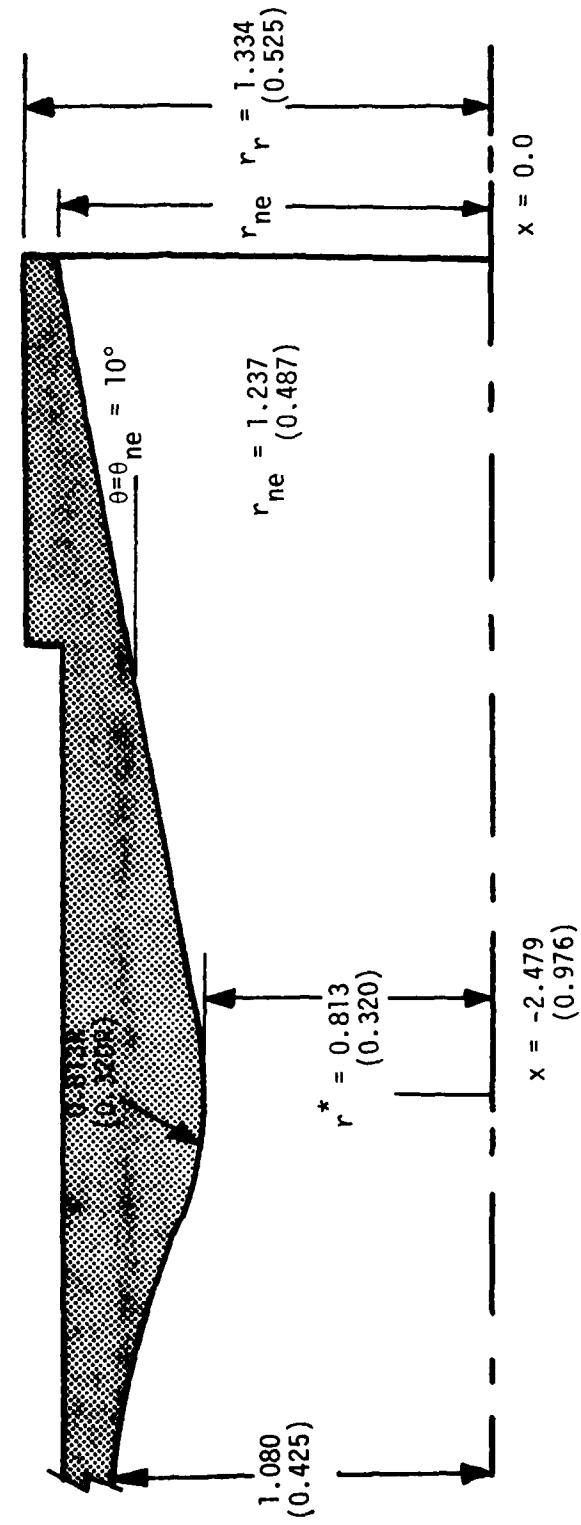
(a) 10° Conical Nozzle, the C4 Nozzle

Figure 2. - Sketches of rocket nozzles used in the present test program.

Note: dimensions in centimeters (inches)
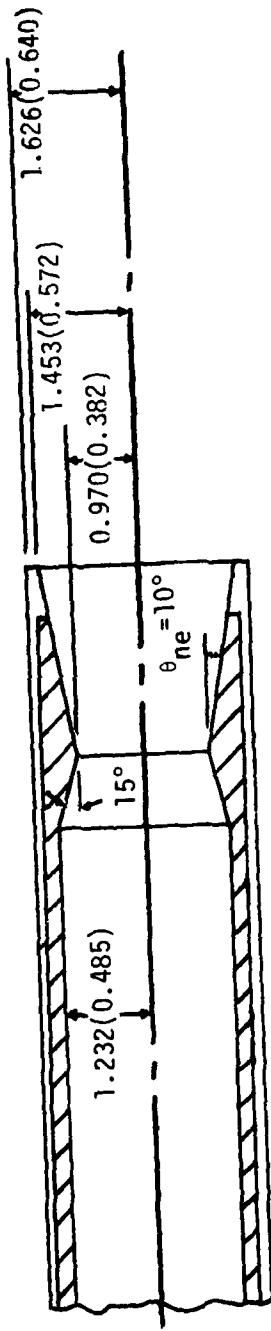
(b) 10° Conical Nozzle, the C1 Nozzle.

Figure 2. - Continued.
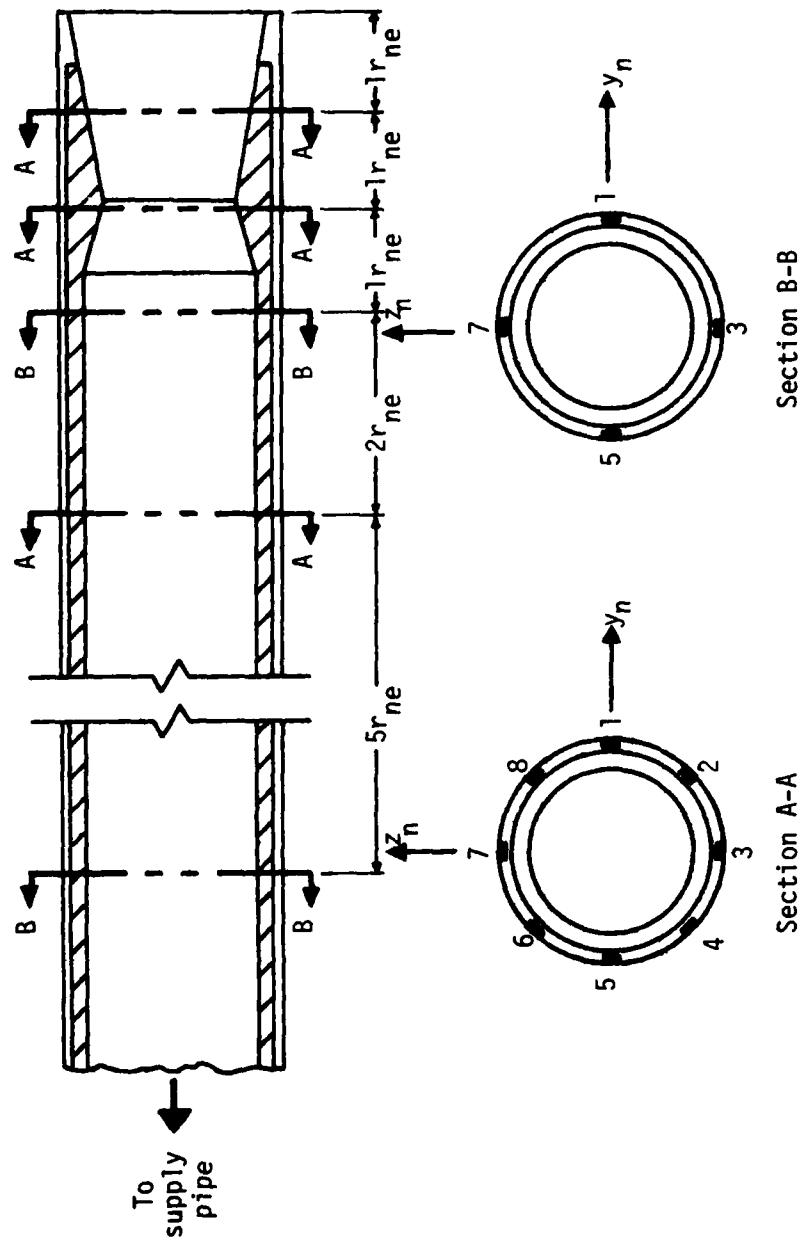
Figure 3. - Sketch of the C1 rocket nozzle illustrating pressure orifice locations. Scale: actual size. r_{ne} = 1.453 cm (0.572 in.).

Note: All dimensions in centimeters (inches)

Tube	$\frac{d_t}{}$
L1	2.969 (1.169)
L3	3.711 (1.461)

$\phi = 180°$

Exhaust flow

$\phi = 0°$

d_t

Ring

10°

Typical rocket nozzle

Static pressure orifices
(not used in C1/L3)

Pitot-static probe

4.128
(1.625)

1.270
(0.500)

15.621 (6.150)

38.10 (15.00)
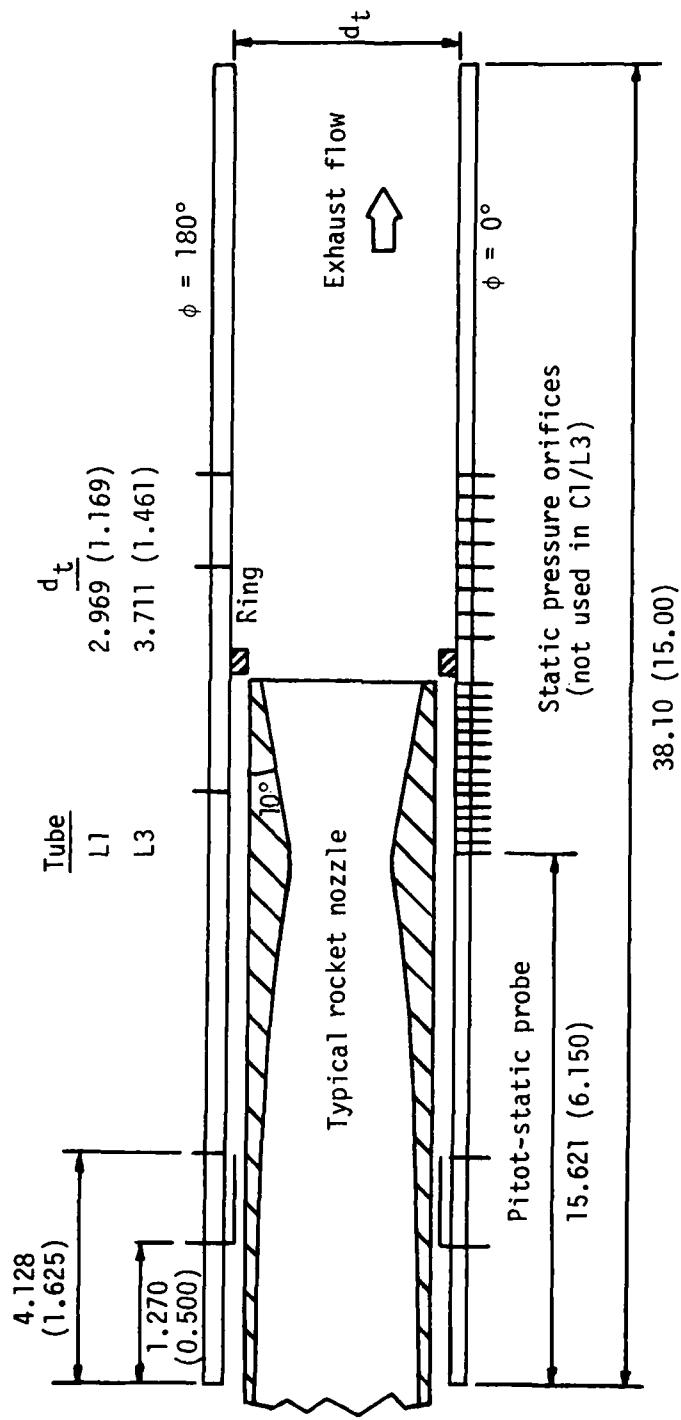
Figure 4. – Rocket-nozzle/launch-tube configuration.

Exhaust flow

Face of ring

h = 0.1499 cm (0.059 in) for L1
h = 0.2286 cm (0.090 in) for L3

$\tilde{x}/h$
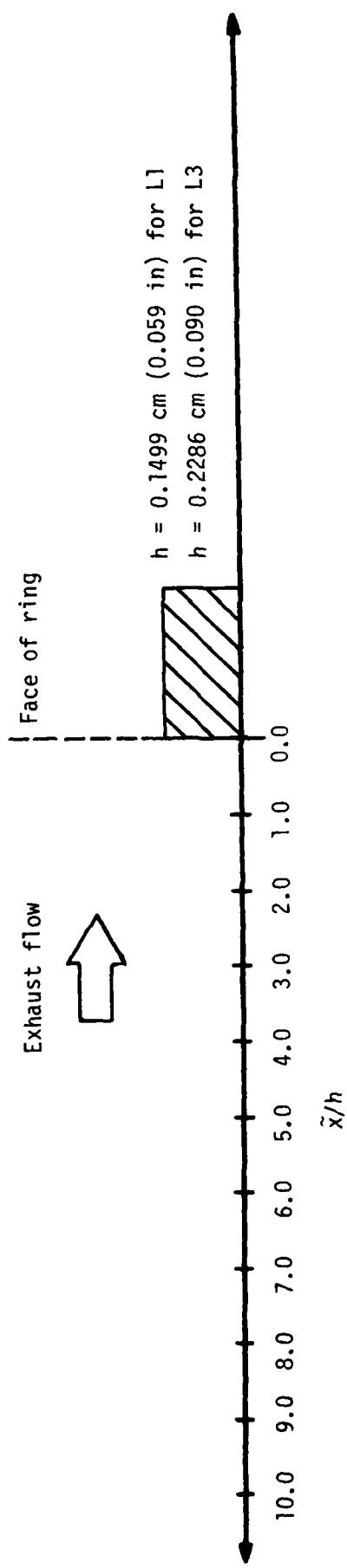
(a) $\tilde{x}/h$ - coordinate system, distances relative to the ring.

Exhaust
flow

Nozzle
exit-plane

r_{ne} = 1.237 cm (0.487 in) for C4
r_{ne} = 1.453 cm (0.572 in) for C1
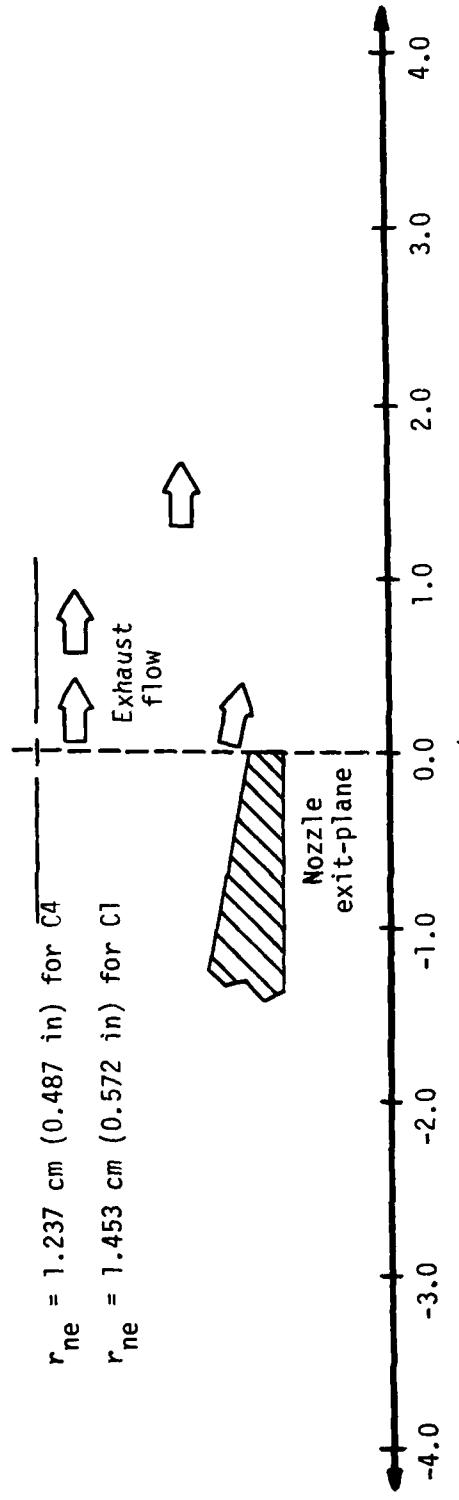
x/r_{ne}

(b) x/r_{ne} - coordinate system, distances relative to the nozzle exit-plane.

Figure 5. - Coordinate systems for present test program.

Unfilled symbols: unchoked flow

Filled symbols: choked flow

Half-filled symbol: flow is choked at some conditions, but not at others.
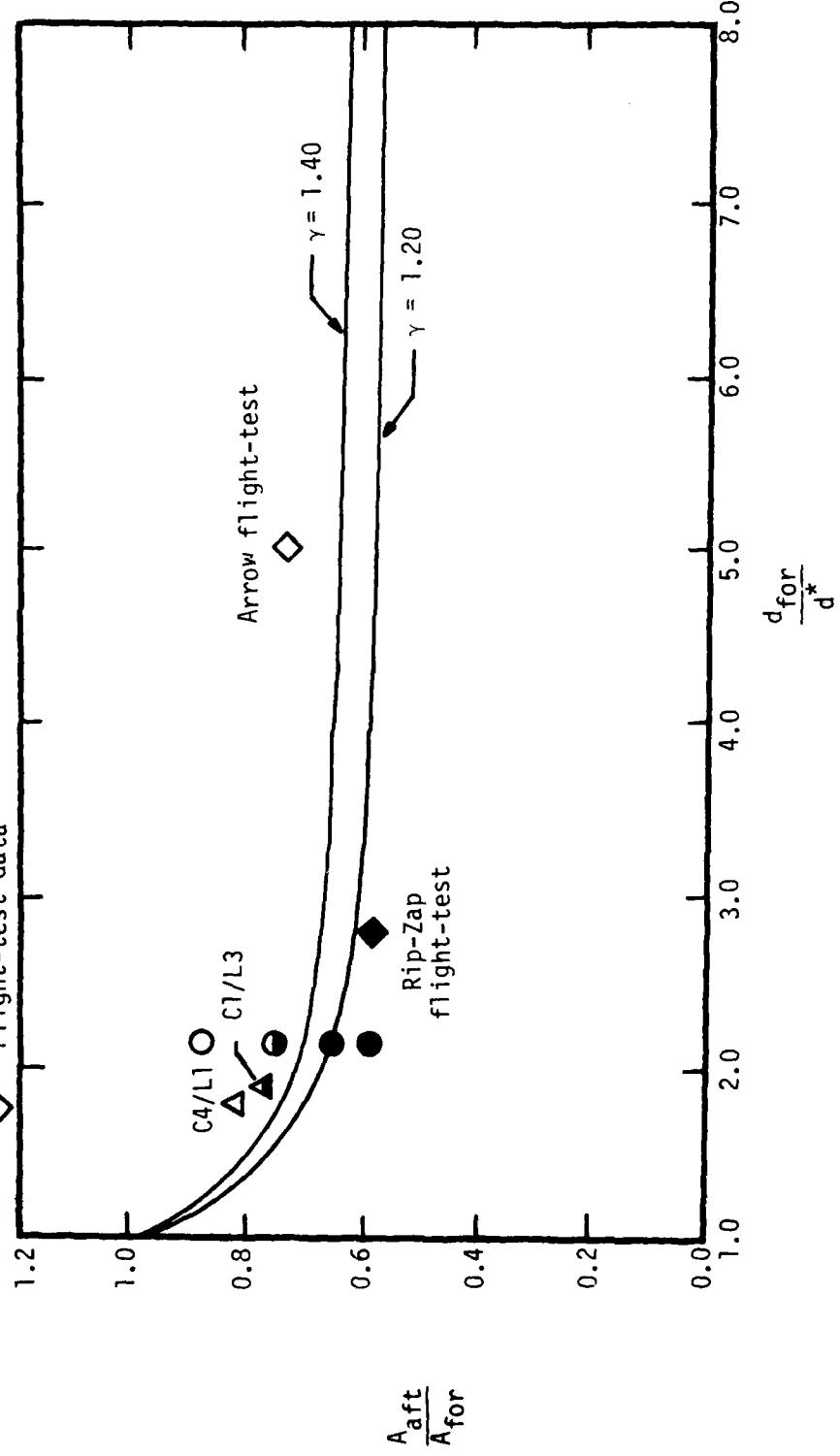
Figure 6. — The minimum constrictive area ratio through which the rocket exhaust flow can pass without choking the flow.

C4/L1 Configuration
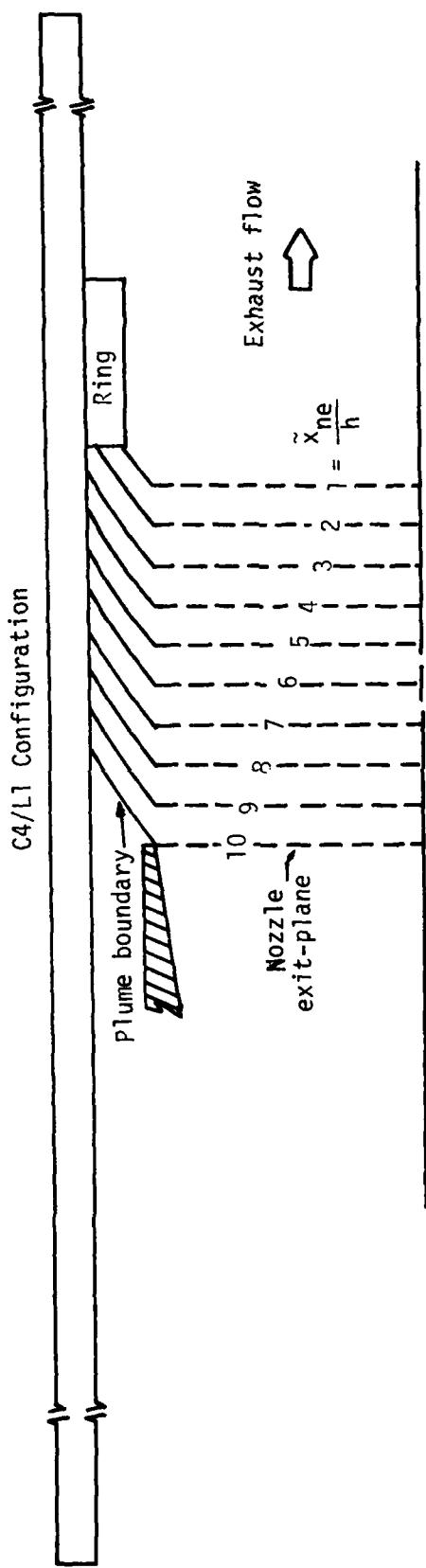
Figure 7. - The theoretical rocket-exhaust plume boundary for p_{t_1} = 8.71 x 10^6 N/m^2 (1264 psi) superimposed on a sketch of the L1 launch-tube with the ring.
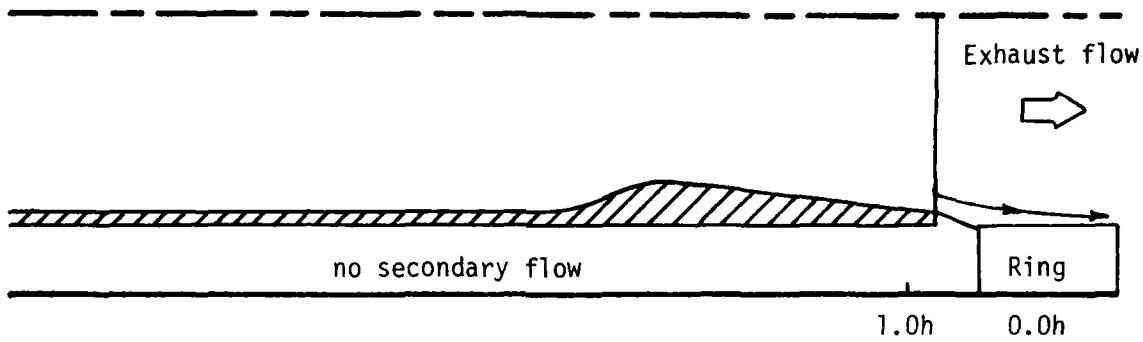
(a) Exhaust flow does not encounter front face of ring,
$\tilde{x}_{ne} < 1.0h$.
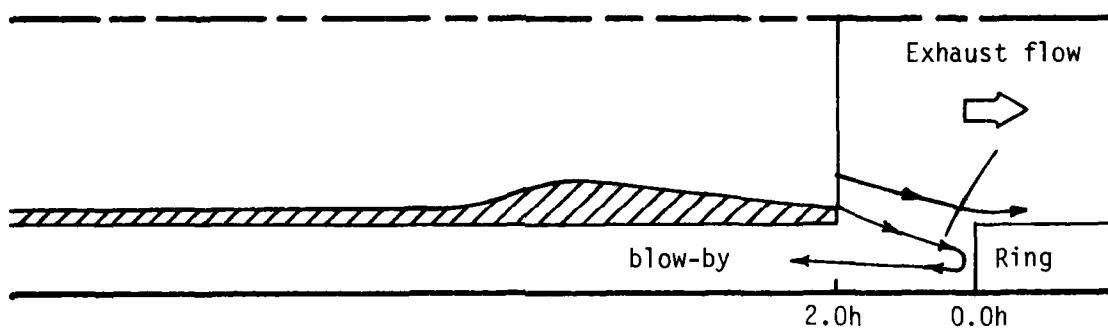
(b) Splash-back of exhaust flow into annular gap, $\tilde{x}_{ne} = 2.0h$.
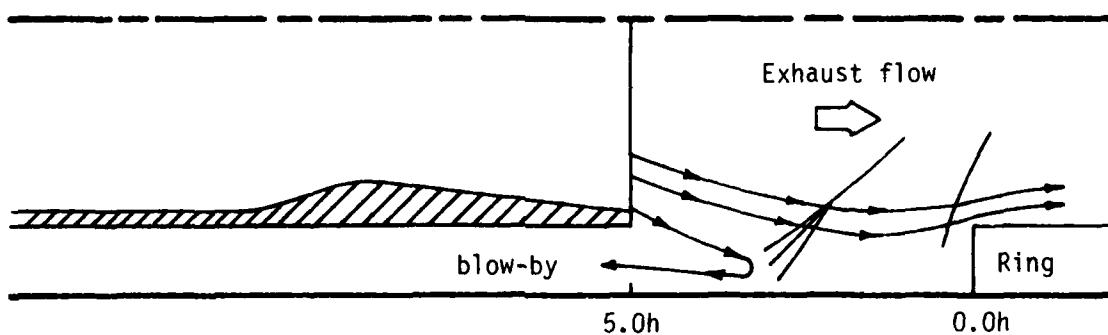
(c) Exhaust flow impinges on launcher wall ahead of ring,
$3.0h \leq \tilde{x}_{ne} < 7.0h$.

Figure 8. - Sketches of flow fields for a nozzle exhausting upstream of a constrictive ring.
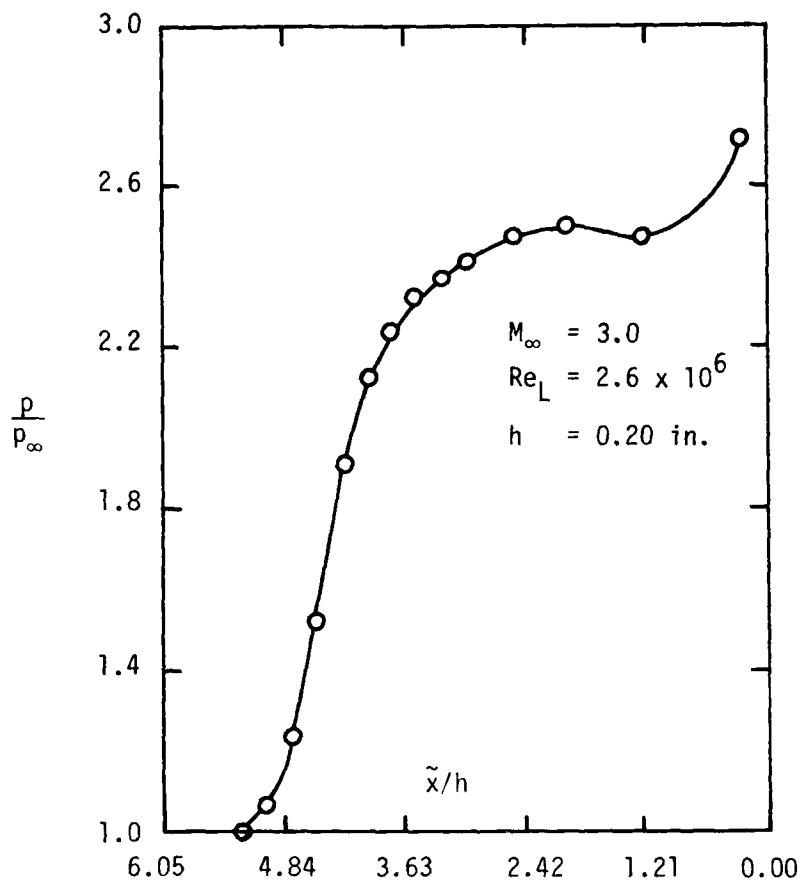
(a)   Pressure distribution in front of forward-facing step (data from ref. 9).
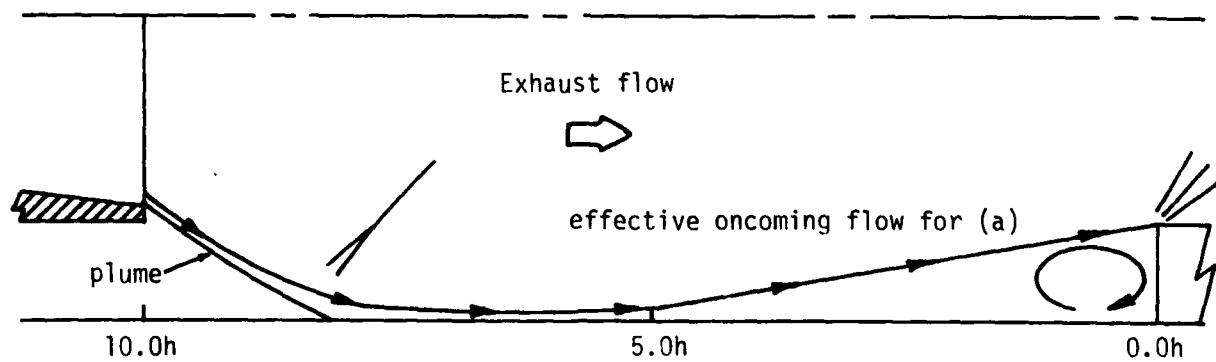
(b)   Sketch of plume encountering an "isolated" forward-facing step

Figure 9. - The flow field in front of a forward-facing step in a supersonic flow.

$\bigtriangledown$ $P_{t1} = 6.89 \times 10^5$ N/m^2 (100 psi)

$\diamondsuit$ $P_{t1} = 1.38 \times 10^6$ N/m^2 (200 psi)

$\triangle$ $P_{t1} = 2.76 \times 10^6$ N/m^2 (400 psi)

$\square$ $P_{t1} = 6.21 \times 10^6$ N/m^2 (900 psi)

$\bigcirc$ $P_{t1} = 8.96 \times 10^6$ N/m^2 (1300 psi)

ejector

$\tilde{x}_{ne}/h$

$\dfrac{\dot{m}_{ag}}{\dot{m}_{ex}}$

blow-by
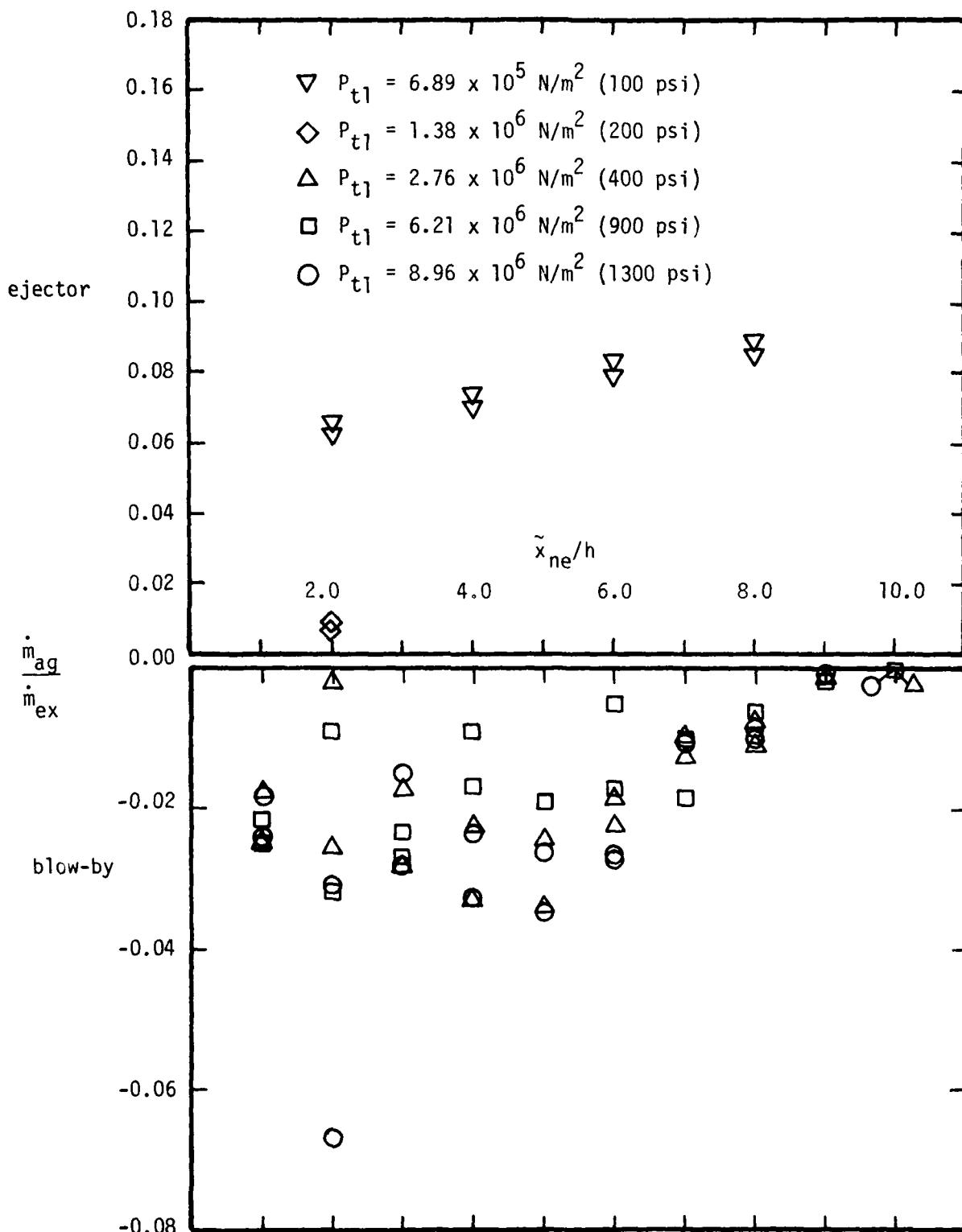
(a) The data for the C4/L1 configuration.

Figure 10. - Non-dimensional mass flow-rate in the annular gap as a function of the nozzle exit-plane position.

Filled symbols: Tape placed between -2.0 x/r_{ne} and -3.0 x/r_{ne}
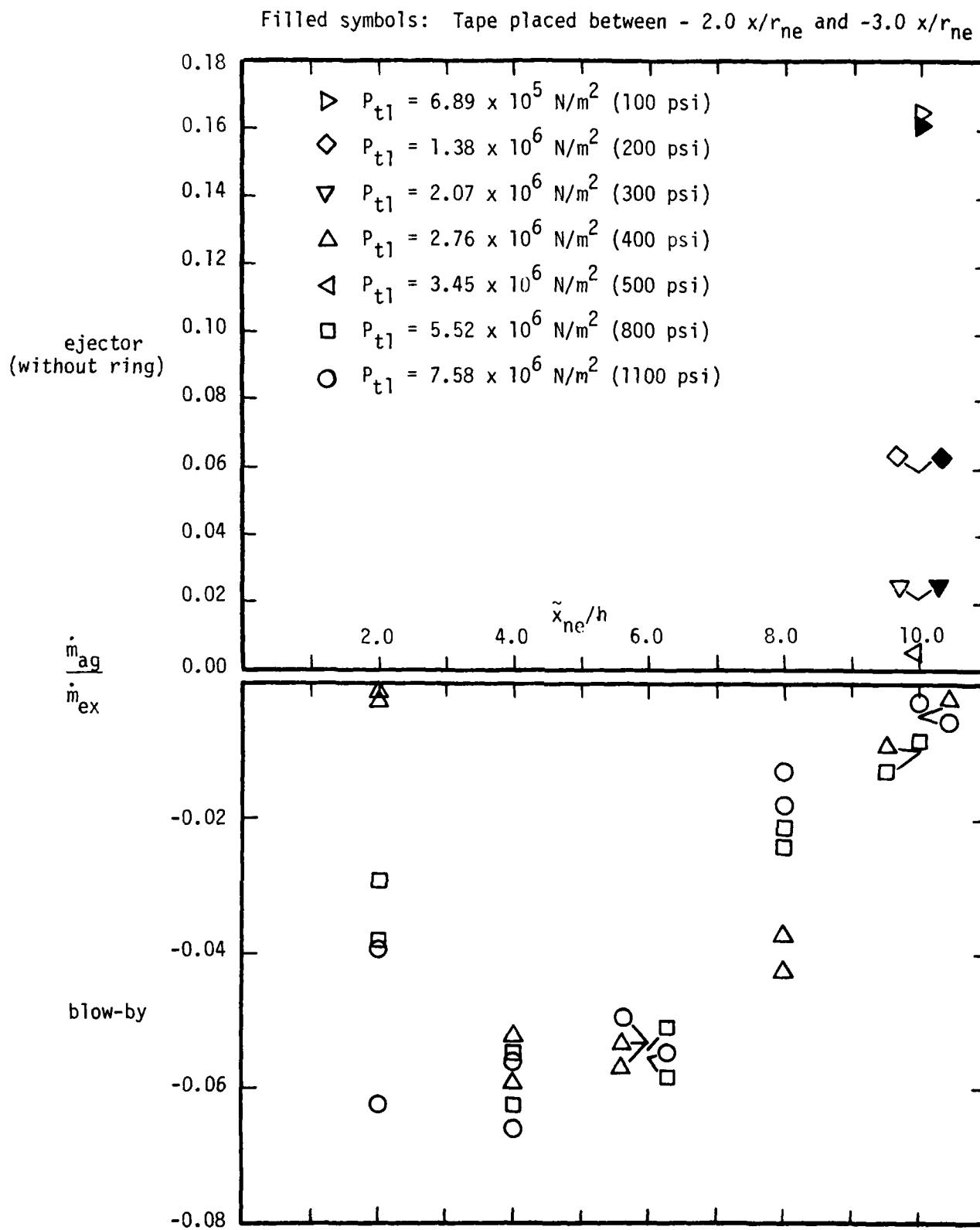
(b) The data for the C1/L3 configuration

Figure 10. - Concluded.
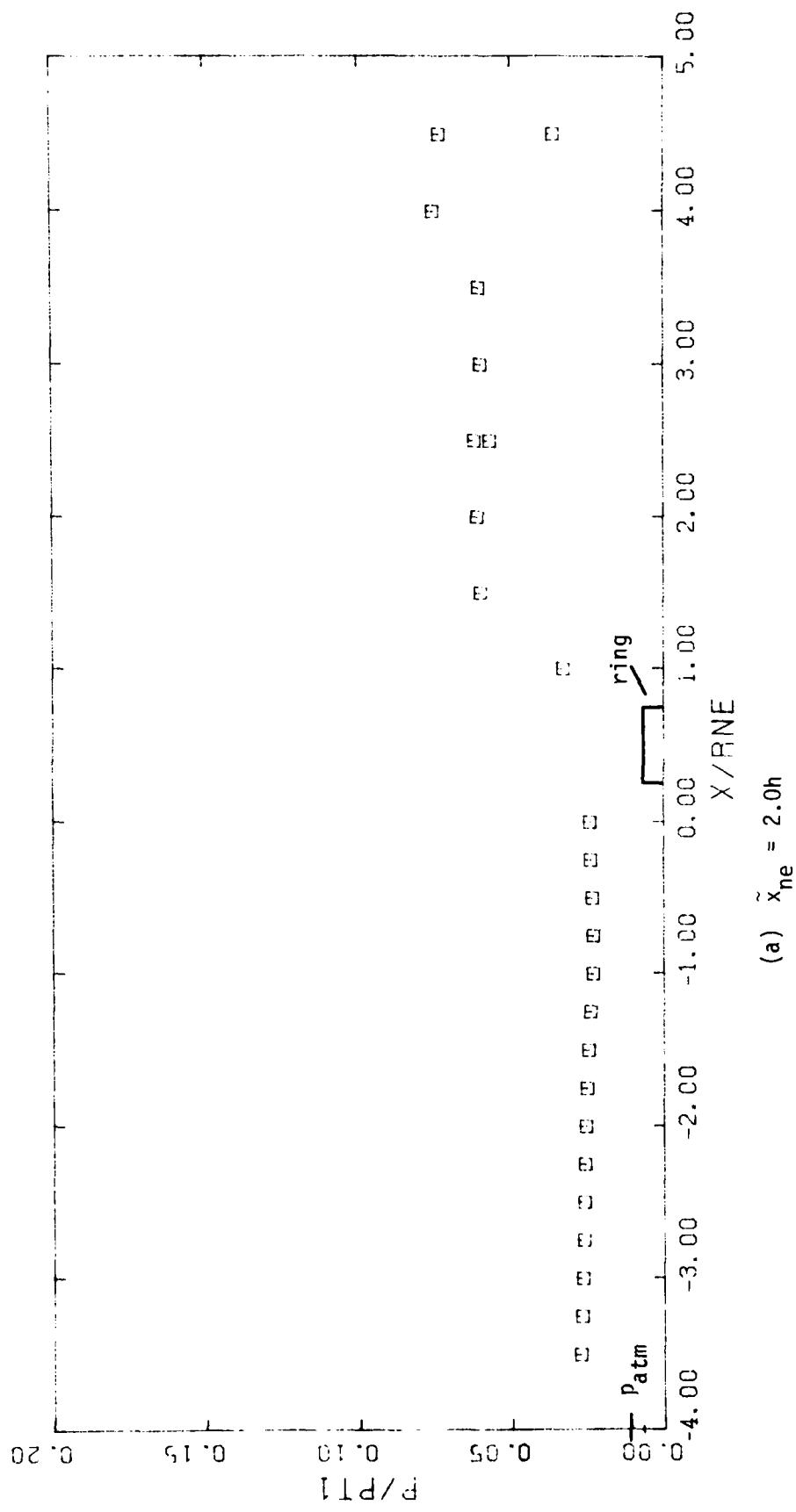
Figure 11. - The static wall pressure distribution for the C4/L1 configuration with the constrictive ring, $\tilde{P}_{t1} = 8.96 \times 10^6$ N/m^2 (1300 psi).

(a) $\tilde{x}_{ne} = 2.0h$

(b) $\tilde{x}_{ne} = 6.0h$
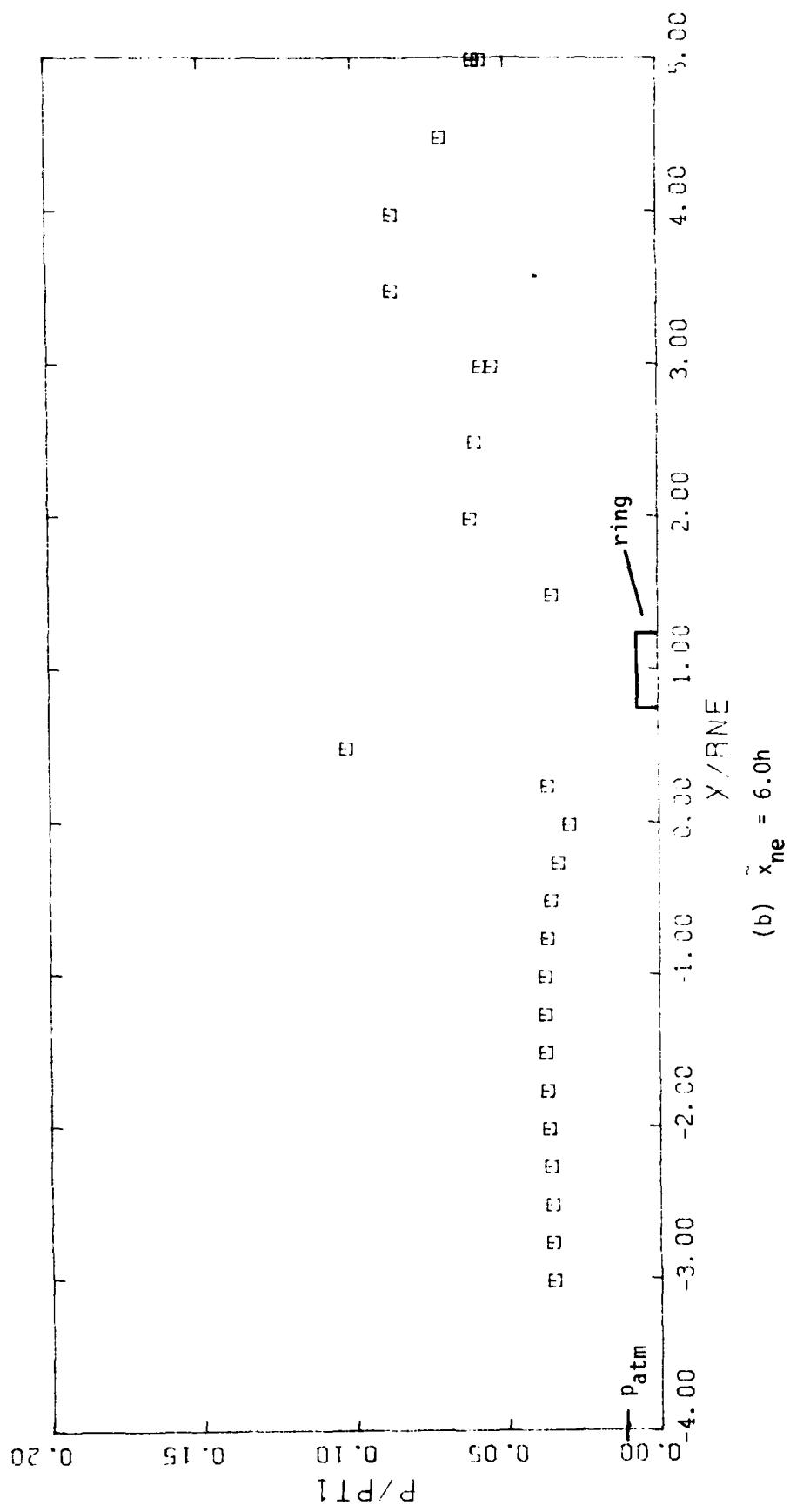
Figure 11. - Continued.

(c) $\tilde{x}_{ne} = 10.0h$
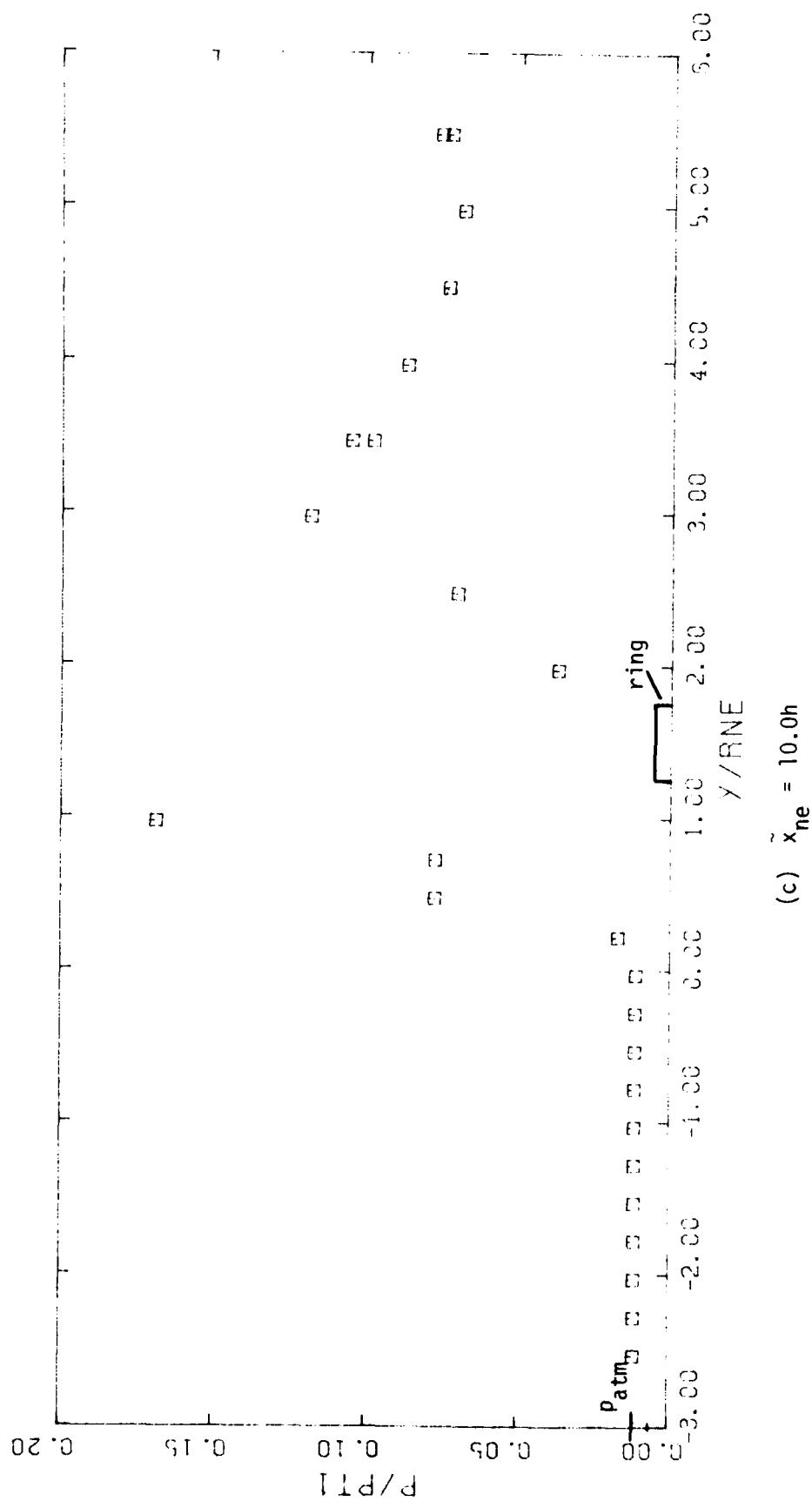
Figure 11. - Concluded.
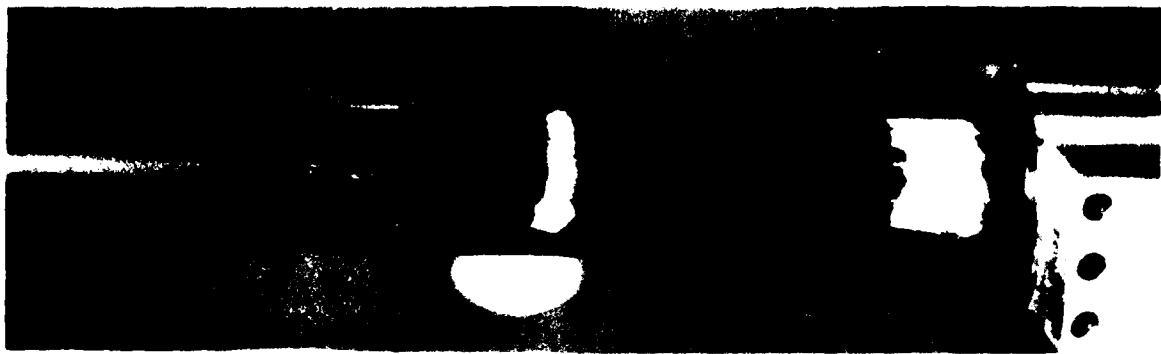
(a) Very early in the run.
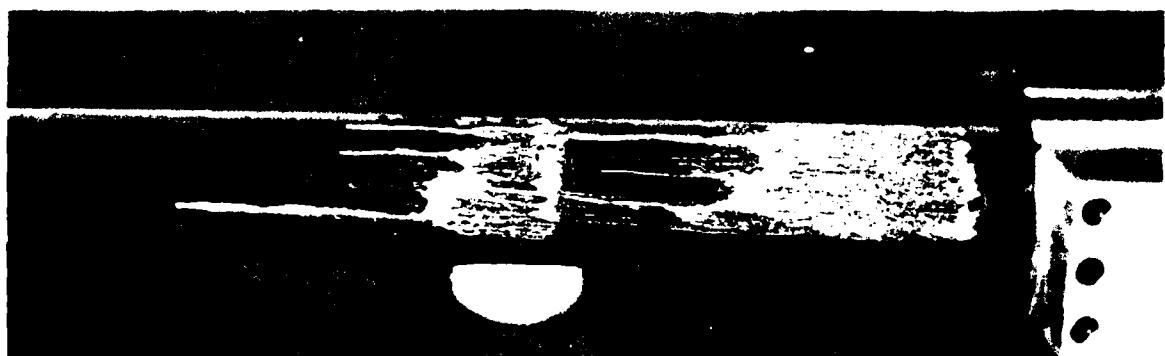
(b) Late in the run, i.e., steady-state flow
with $Pt_1 = 2.76 \times 10^6$ N/m^2 (400 psi).

Figure 12.- Photographs of an oil flow for the C4/L1 configuration,
$\tilde{x}_{ne} = 2.0h$.
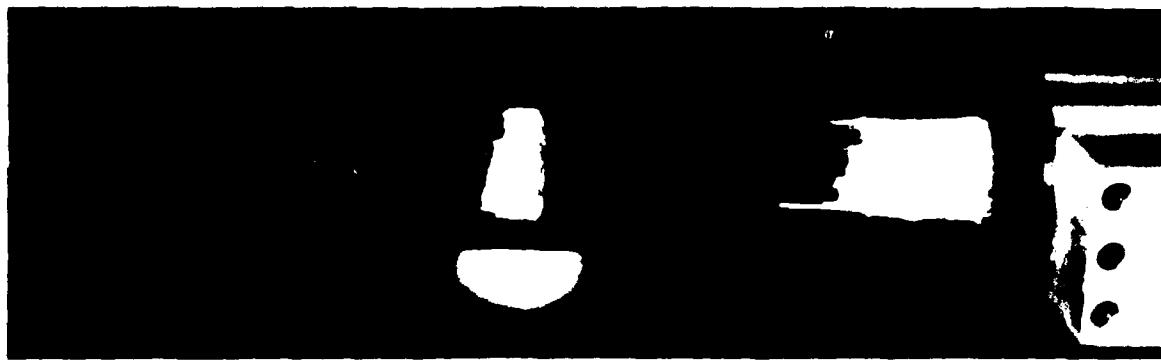
(a) Very early in the run.
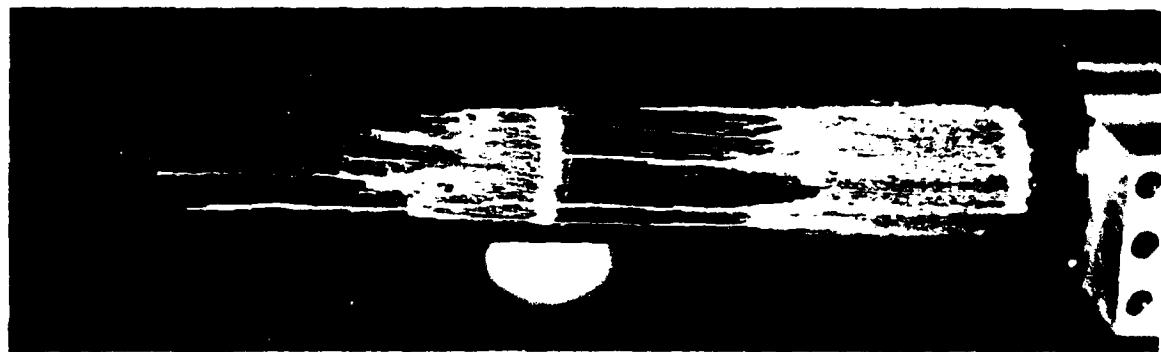
(b) Late in the run, i.e., steady-state flow with
$Pt_1 = 2.76 \times 10^6$ N/m^2 (400 psi).
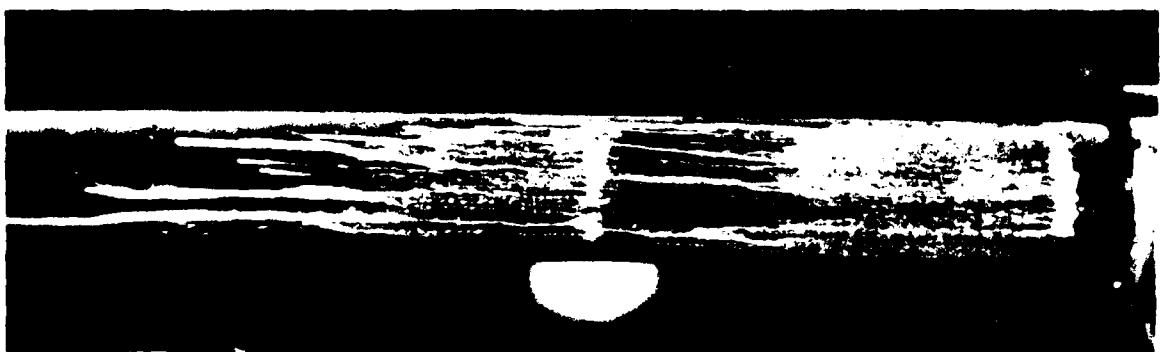
(c) After the run.

Figure 13.- Photographs of an oil flow for the C4/L1 configuration,
$\tilde{x}_{ne} = 4.0h$.
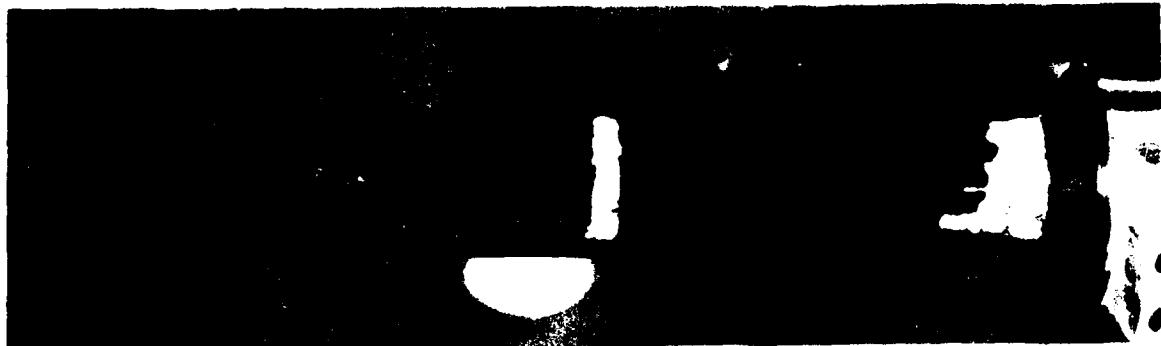
(a) Late in the run, i.e., steady-state flow with
$Pt_1 = 2.76 \times 10^6$ N/m^2 (400 psi).

(note: blow-by of relatively low magnitude resulted for this test
condition.)
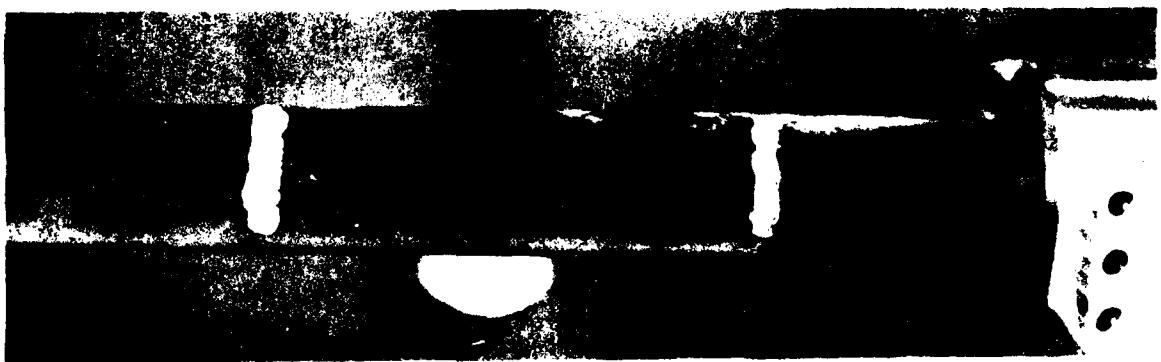
(b) Late in the run, i.e., steady-state flow with
$Pt_1 = 6.89 \times 10^5$ N/m^2 (100 psi).

(note: ejector flow of fairly large magnitude resulted for this
test condition.)

Figure 14.- Photographs of an oil flow for the C4/L1 configuration,
$\tilde{x}_{ne} = 10.0h$.

$\bigcirc$ p_{t1} = 7.375 x 10^6 N/m^2 (1069.7 psia)

$\square$ p_{t1} = 5.362 x 10^6 N/m^2 (777.7 psia)

$\triangle$ p_{t1} = 2.745 x 10^6 N/m^2 (398.1 psia)

Filled symbols are the corresponding values of Δp = 6.89 x 10^3 N/m^2 (1 psi)

(a) $\dfrac{x}{r_{ne}}$ = -1.0   (b) $\dfrac{x}{r_{ne}}$ = -2.0   (c) $\dfrac{x}{r_{ne}}$ = -3.0

Figure 15. - The pressure distribution on the surface of the Cl
nozzle during a blow-by test, $\tilde{x}_{ne}$ = 2.0h.

$\bigcirc \; p_{t1} = 7.375 \times 10^f \; N/m^2 \; (1069.7 \; psia)$

$\square \; p_{t1} = 5.362 \times 10^6 \; N/m^2 \; (777.7 \; psia)$

$\triangle \; p_{t1} = 2.745 \times 10^6 \; N/m^2 \; (398.1 \; psia)$

Filled symbols are the corresponding values of $\Delta p = 6.89 \times 10^3 \; N/m^2 (1psi)$

(d) $\dfrac{x}{r_{ne}} = -5.0$ \qquad (e) $\dfrac{x}{r_{ne}} = -10.0$

Figure 15. - Concluded.

O p_{t1} = 7.375 x 10^6 N/m^2 (1069.7 psia)

$\square$ p_{t1} = 5.362 x 10^6 N/m^2 (777.7 psia)

$\triangle$ p_{t1} = 2.711 x 10^6 N/m^2 (393.2 psia)

Filled symbols are the corresponding values of Δp = 6.89 x 10^3 N/m^2 (1psi)

(a) $\dfrac{x}{r_{ne}}$ = -1.0   (b) $\dfrac{x}{r_{ne}}$ = -2.0   (c) $\dfrac{x}{r_{ne}}$ = -3.0
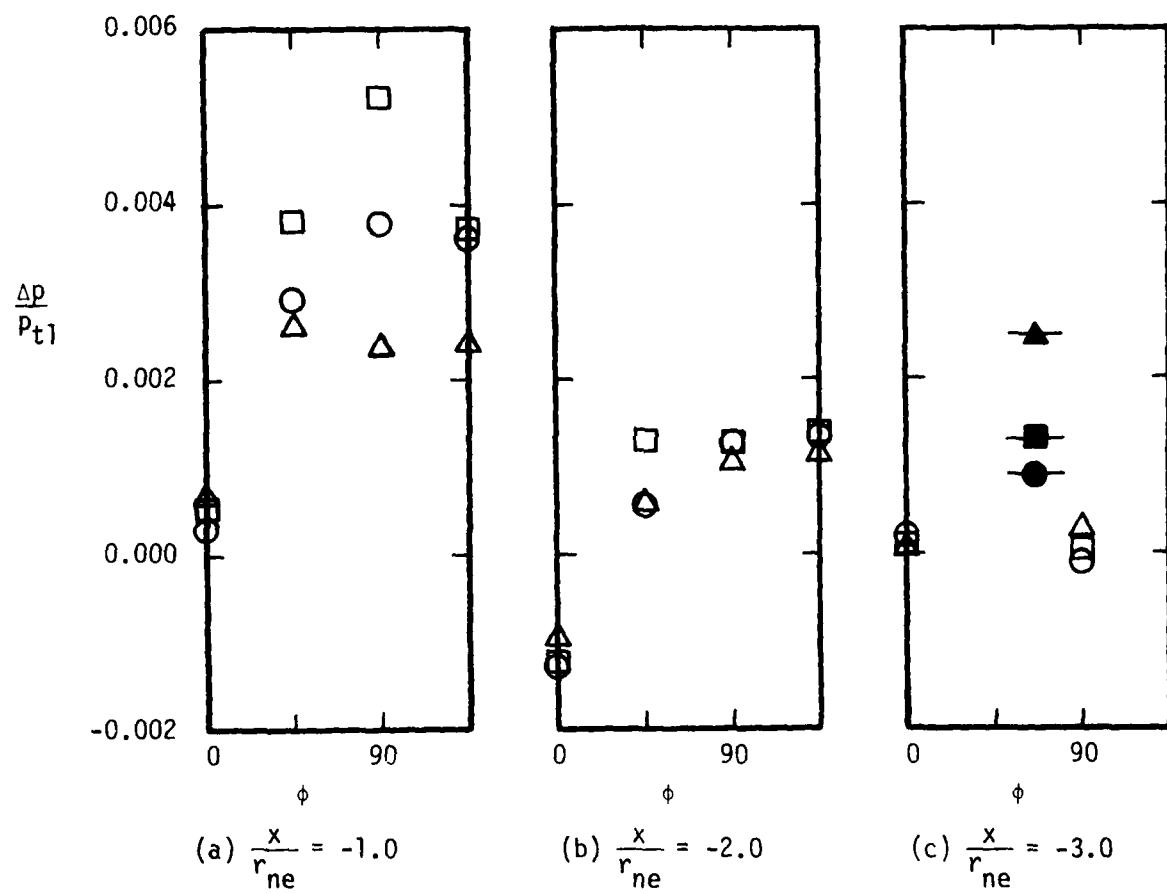
Figure 16. - The pressure distribution on the surface of the C1 nozzle during a blow-by test, $\tilde{x}_{ne}$ = 6.0h.

O p_{t1} = 7.375 x 10^6 N/m^2 (1069.7 psia)

$\square$ p_{t1} = 5.362 x 10^6 N/m^2 (777.7 psia)

$\triangle$ p_{t1} = 2.711 x 10^6 N/m^2 (393.2 psia)

Filled symbols are the corresponding values of Δp = 6.89 x 10^3 N/m^2 (1psi)

(d) $\dfrac{x}{r_{ne}}$ = -5.0

(e) $\dfrac{x}{r_{ne}}$ = -10.0

Figure 16. - Concluded.

$\bigcirc \ p_{t1} = 7.275 \times 10^6 \ N/m^2$ (1055.1 psia)

$\square \ p_{t1} = 5.396 \times 10^6 \ N/m^2$ (782.6 psia)

$\triangle \ p_{t1} = 2.745 \times 10^6 \ N/m^2$ (398.1 psia)

Filled symbols are the corresponding values of $\Delta p = 6.89 \times 10^3 \ N/m^2$ (1psi)

(a) $\dfrac{x}{r_{ne}} = -1.0$ (b) $\dfrac{x}{r_{ne}} = -2.0$ (c) $\dfrac{x}{r_{ne}} = -3.0$
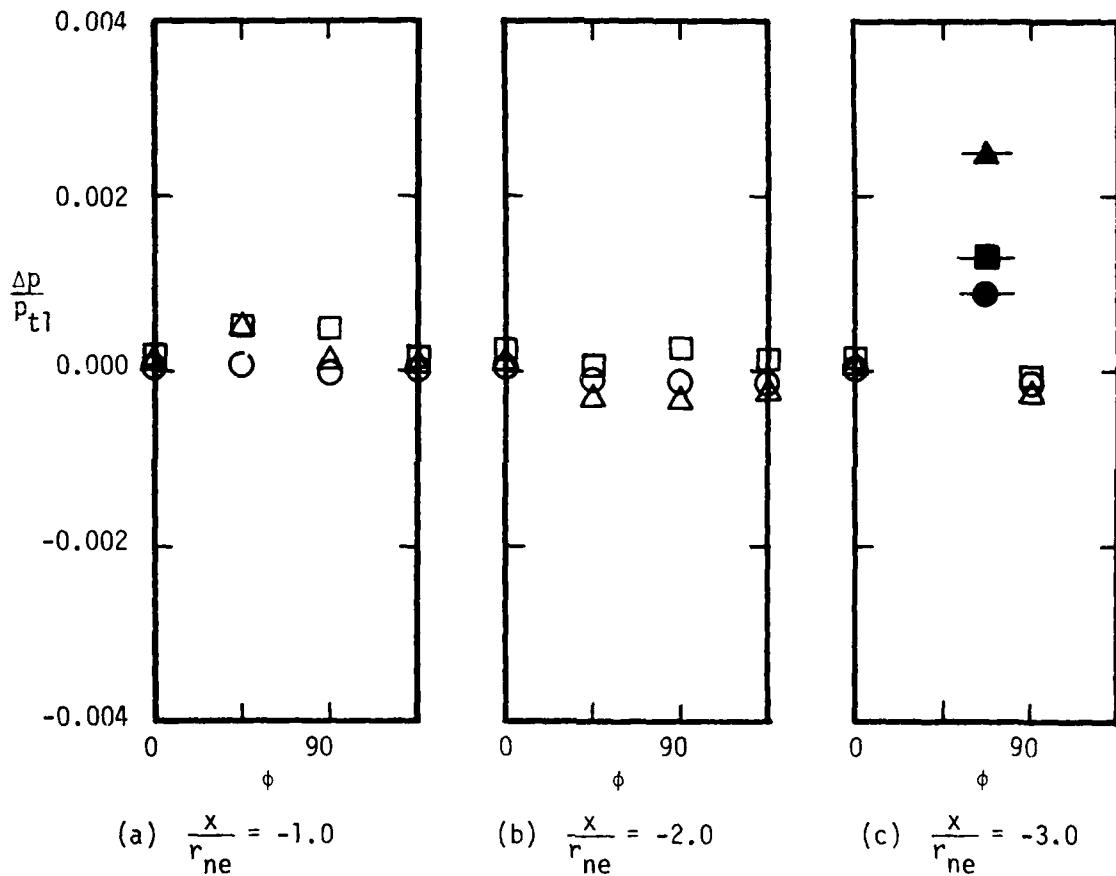
Figure 17. - The pressure distribution on the surface of the Cl nozzle during a blow-by test, $\tilde{x}_{ne} = 10.0h$.

$\bigcirc$ P_{t1} = 7.275 x 10^6 N/m^2 (1055.1 psia)

$\square$ P_{t1} = 5.396 x 10^6 N/m^2 (782.6 psia)

$\triangle$ P_{t1} = 2.745 x 10^6 N/m^2 (398.1 psia)

Filled symbols are the corresponding values of Δp = 6.89 x 10^3 N/m^2(1psi)

(d) $\dfrac{x}{r_{ne}}$ = -5.0   (e) $\dfrac{x}{r_{ne}}$ = -10.0
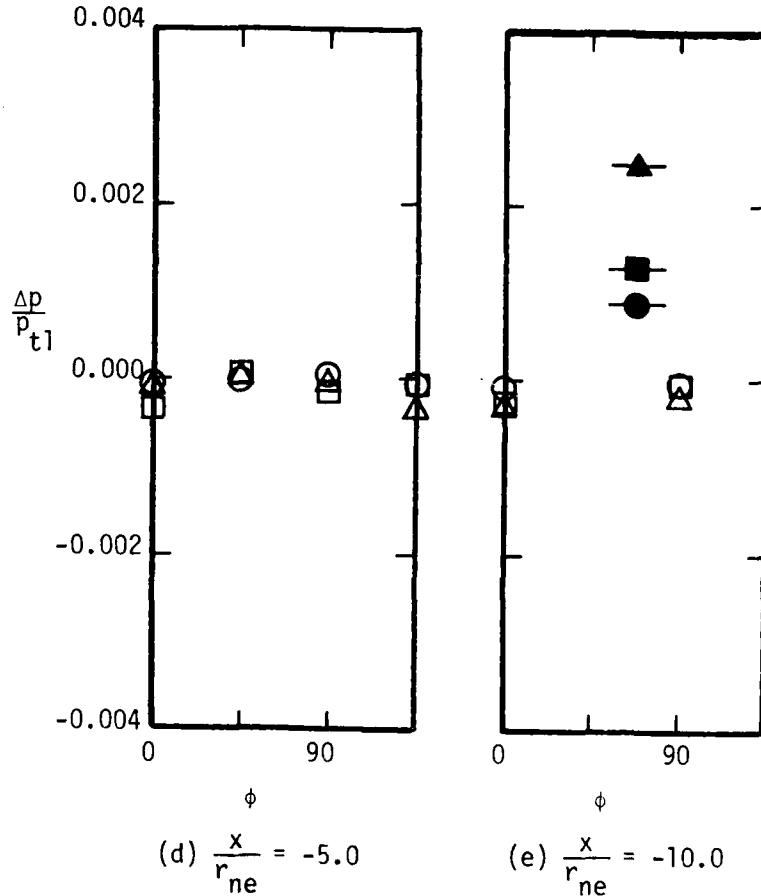
Figure 17. - Concluded.
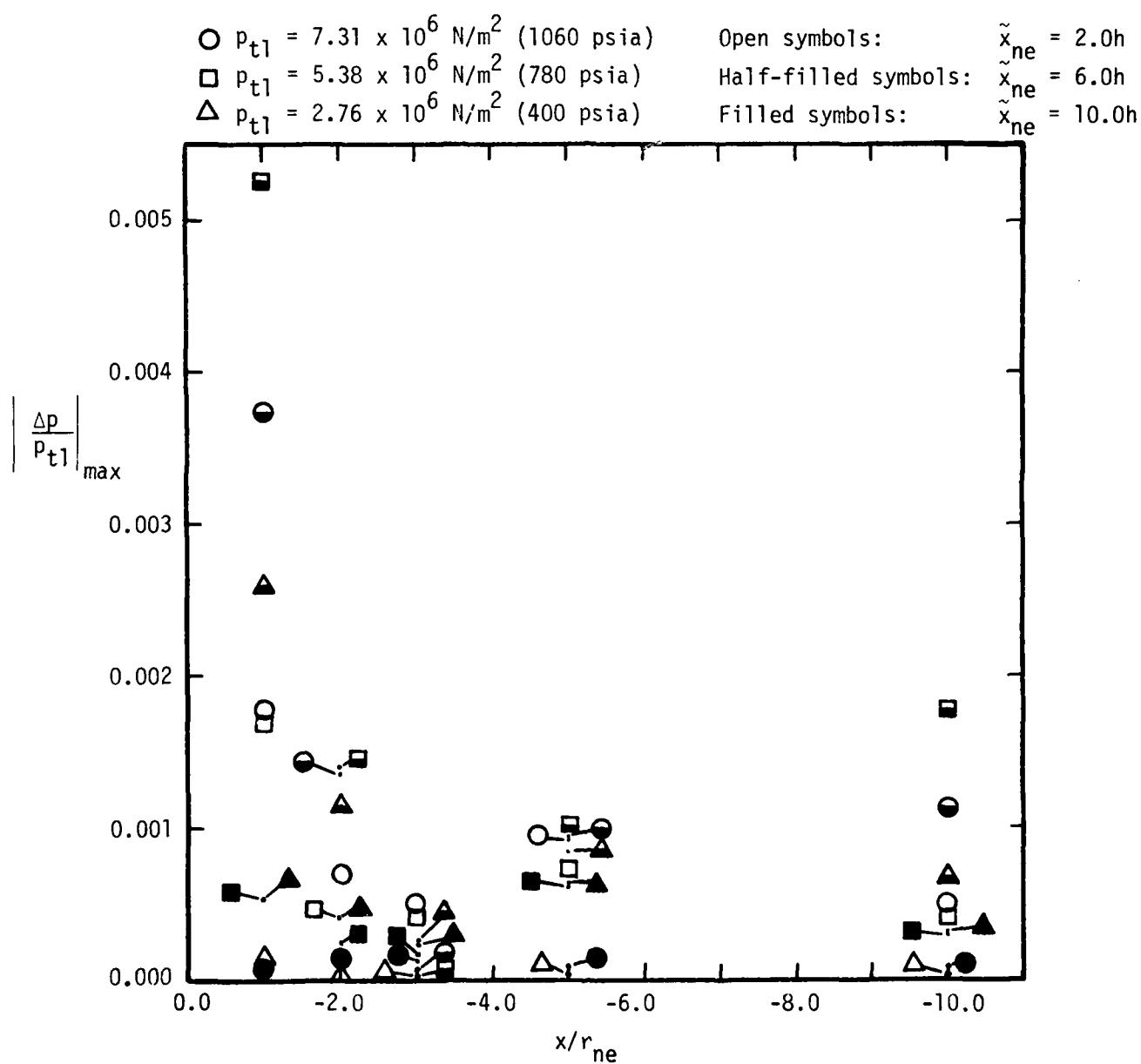
Figure 18. - The maximum absolute value of the differential pressure across the C1 nozzle as a function of the distance from the nozzle exit-plane during blow-by tests.
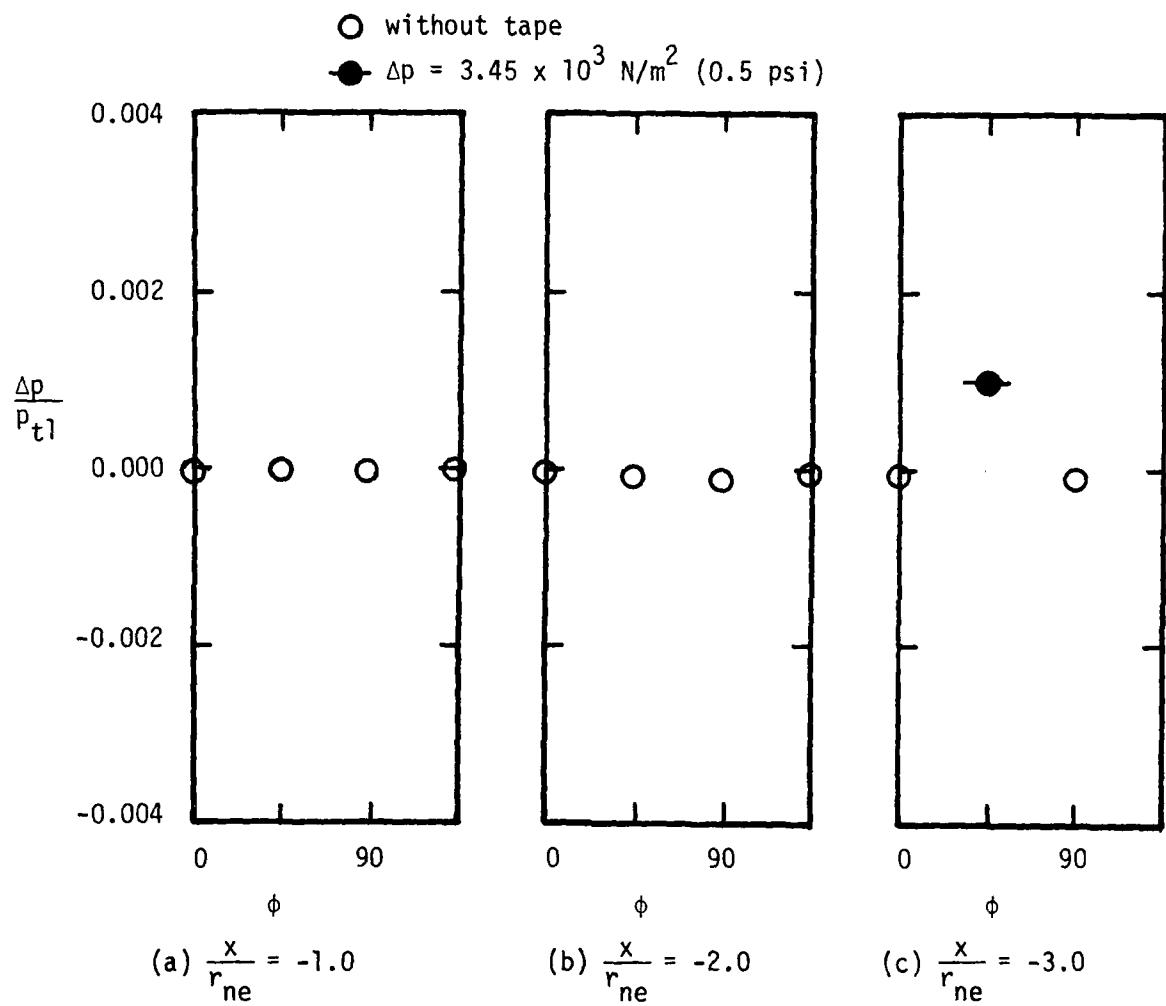
Figure 19. – The pressure distribution on the surface of the Cl nozzle during an ejector test, $p_{t1} = 3.38 \times 10^6$ N/m^2 (490.5 psia).
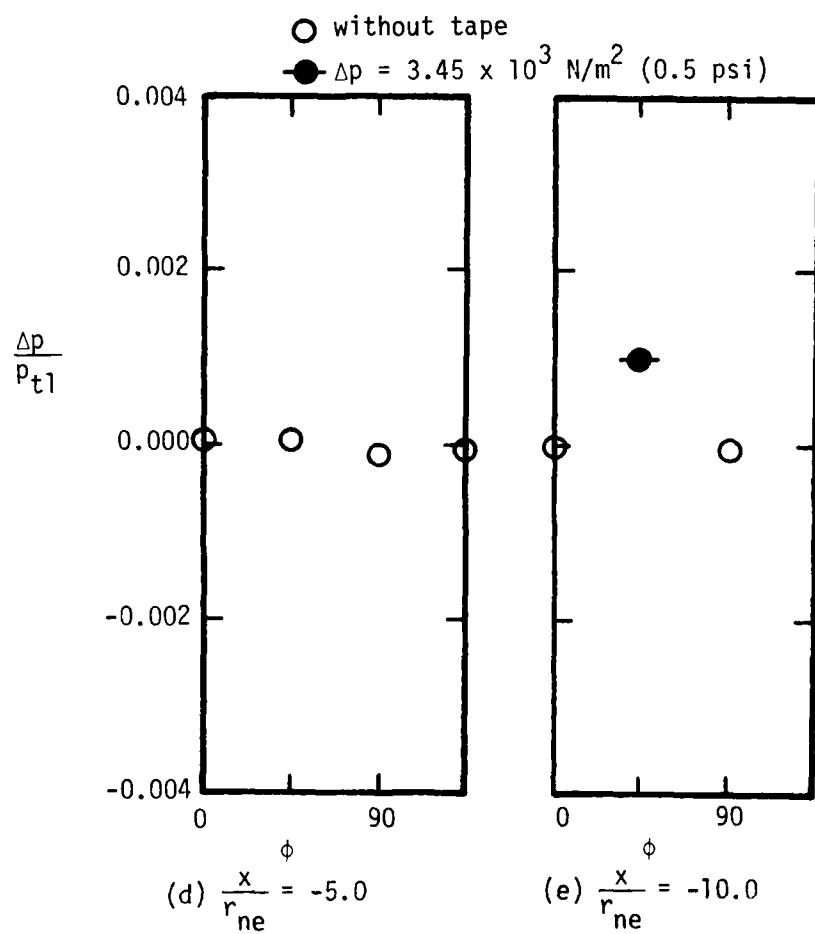
Figure 19. - Concluded.
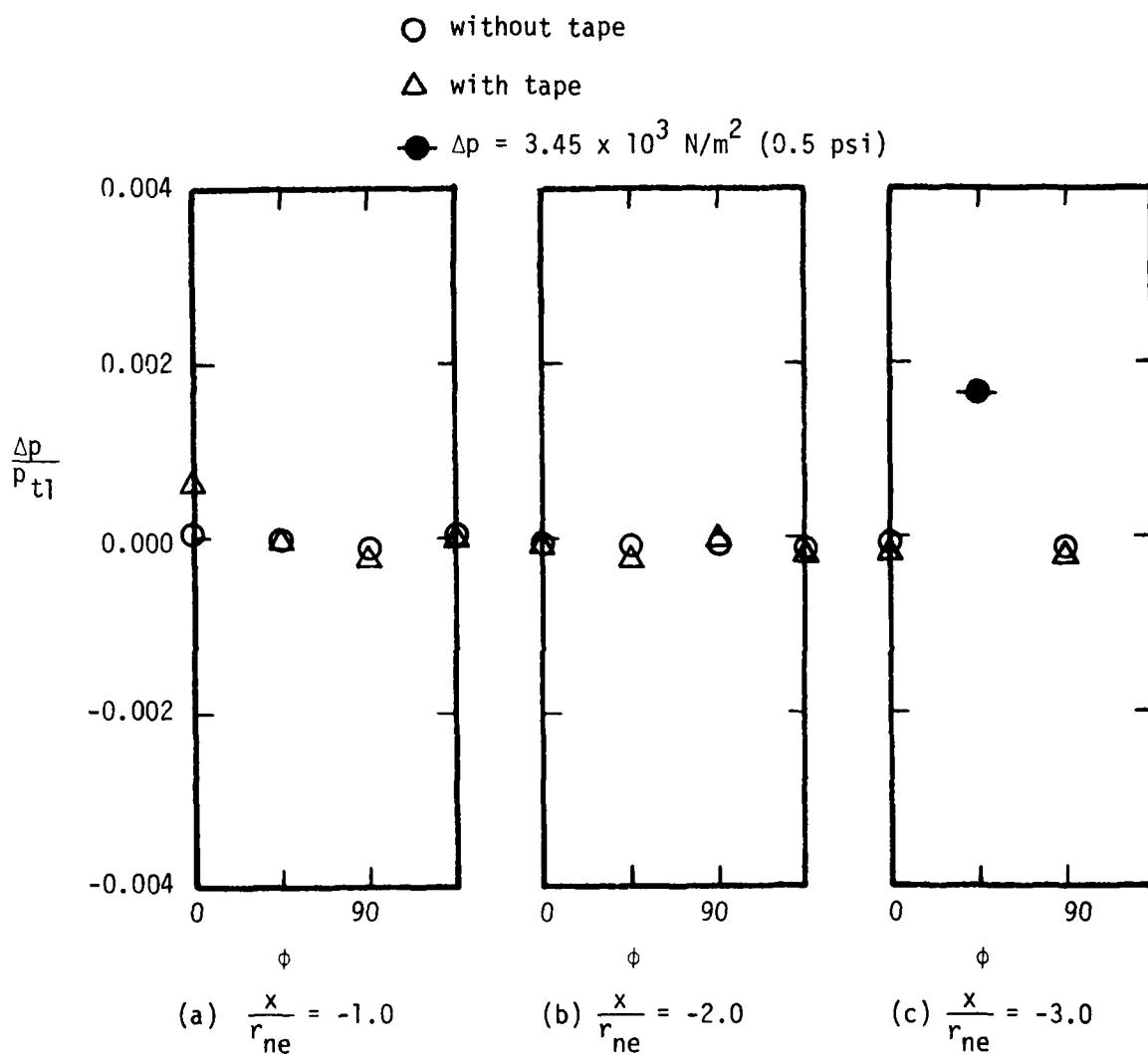
Figure 20. - The pressure distribution on the surface of the C1 nozzle during an ejector test, $p_{t1} = 2.04 \times 10^6$ N/m^2 (295.9 psia).
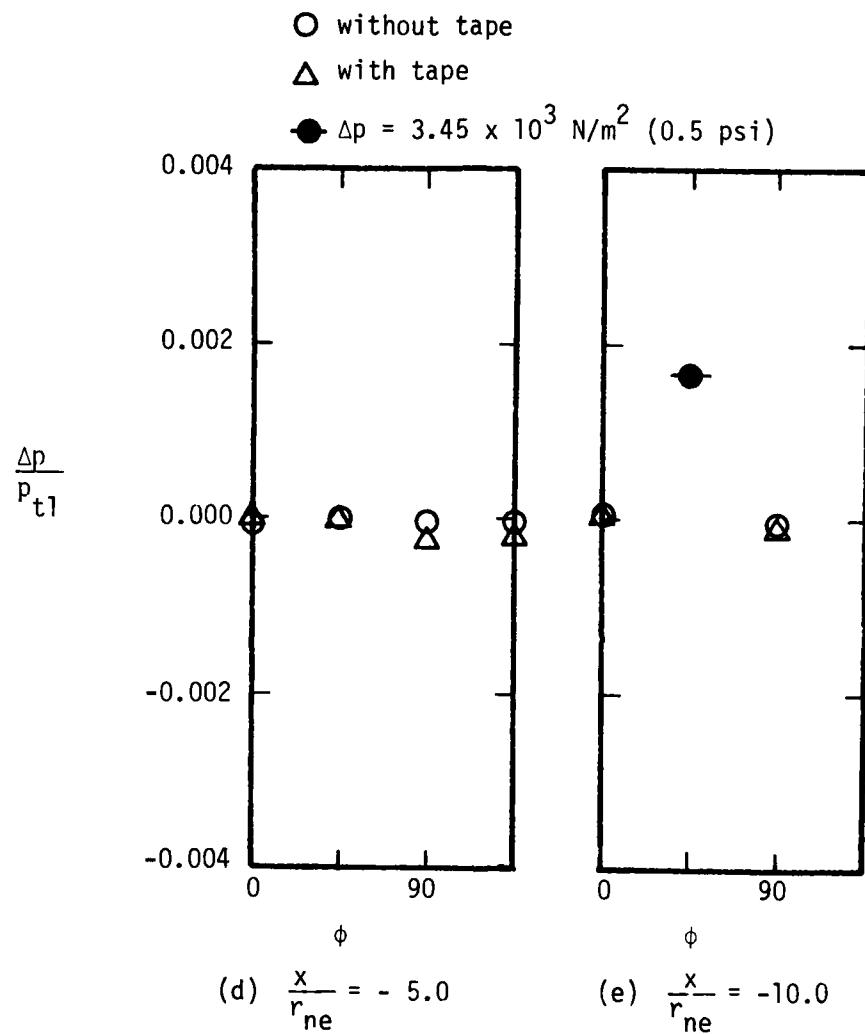
Figure 20. - Concluded.
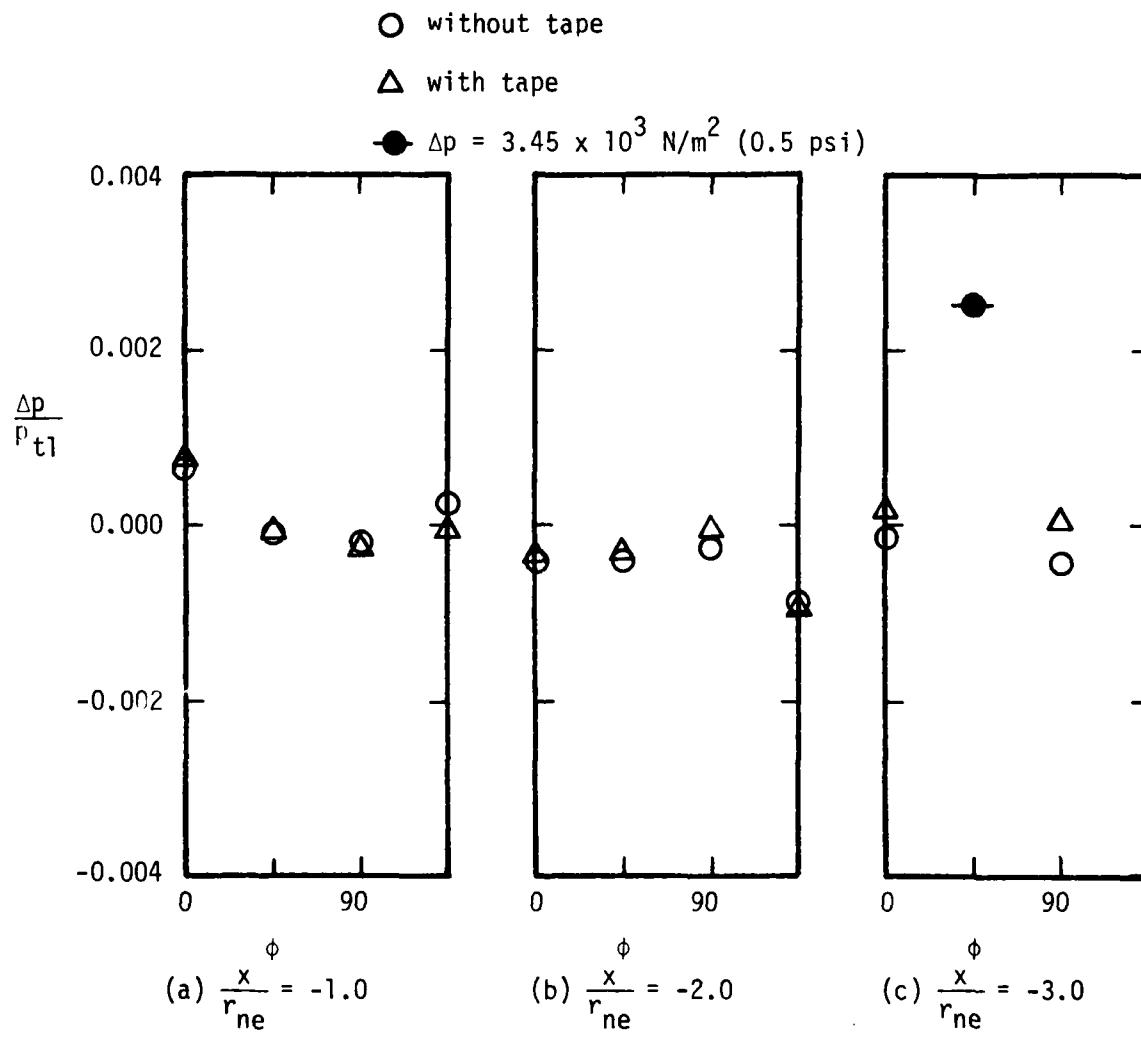
Figure 21. - The pressure distribution on the surface of the C1 nozzle during an ejector test, p_{t1} = 1.37 x 10^6 N/m^2 (198.5 psia).
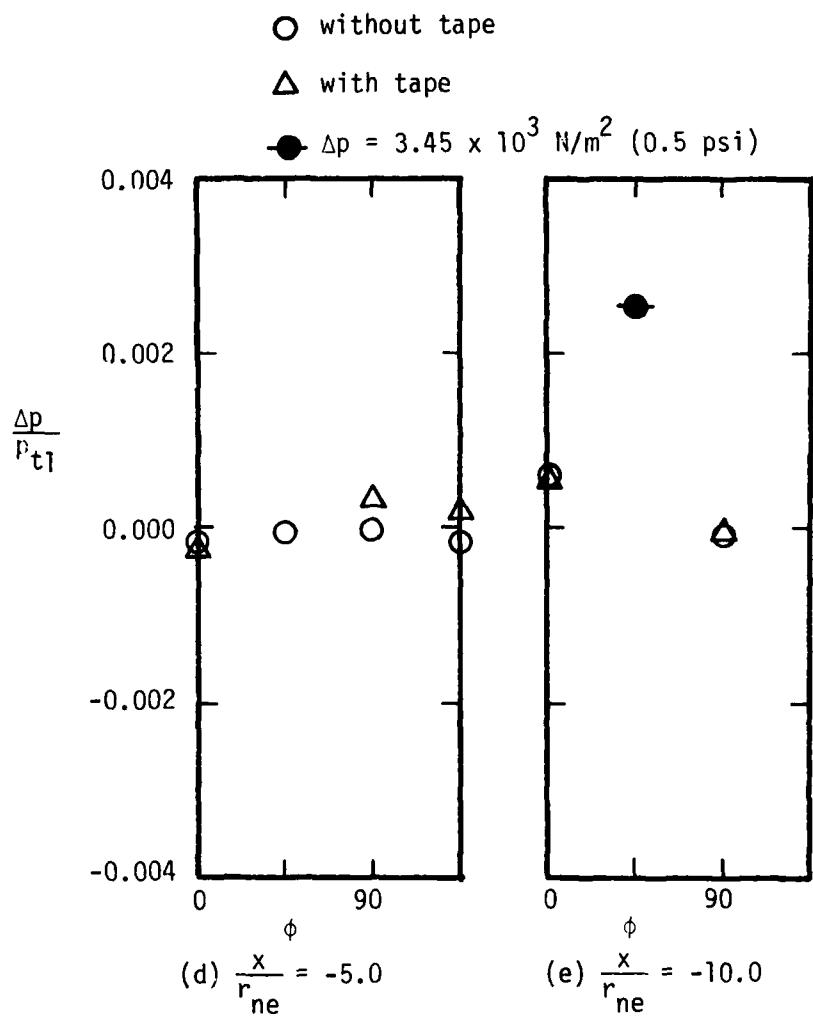
Figure 21. - Concluded.
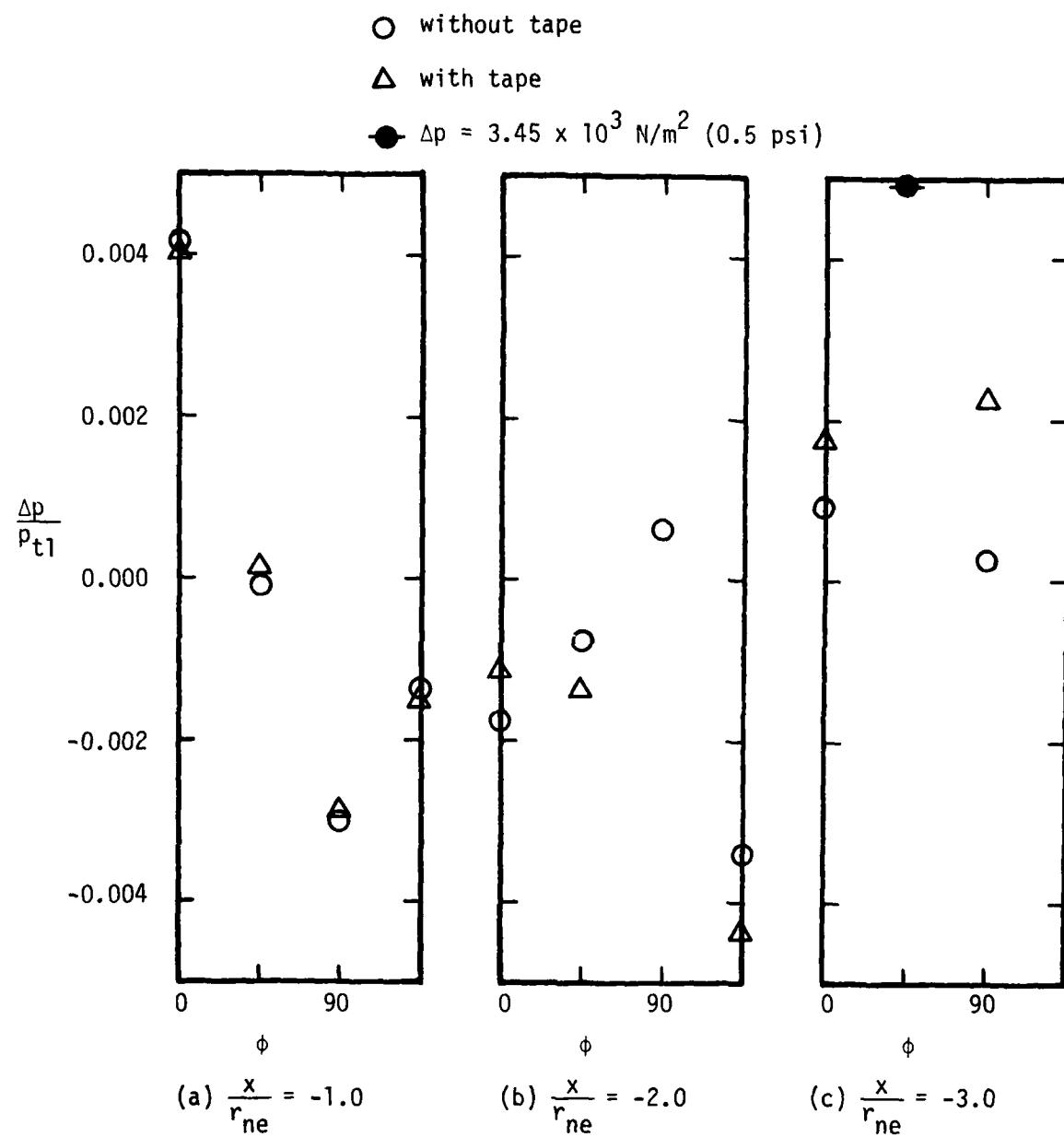
Figure 22. - The pressure distribution on the surface of the Cl nozzle during an ejector test, $p_{t1} = 6.98 \times 10^5$ N/m^2 (101.2 psia).
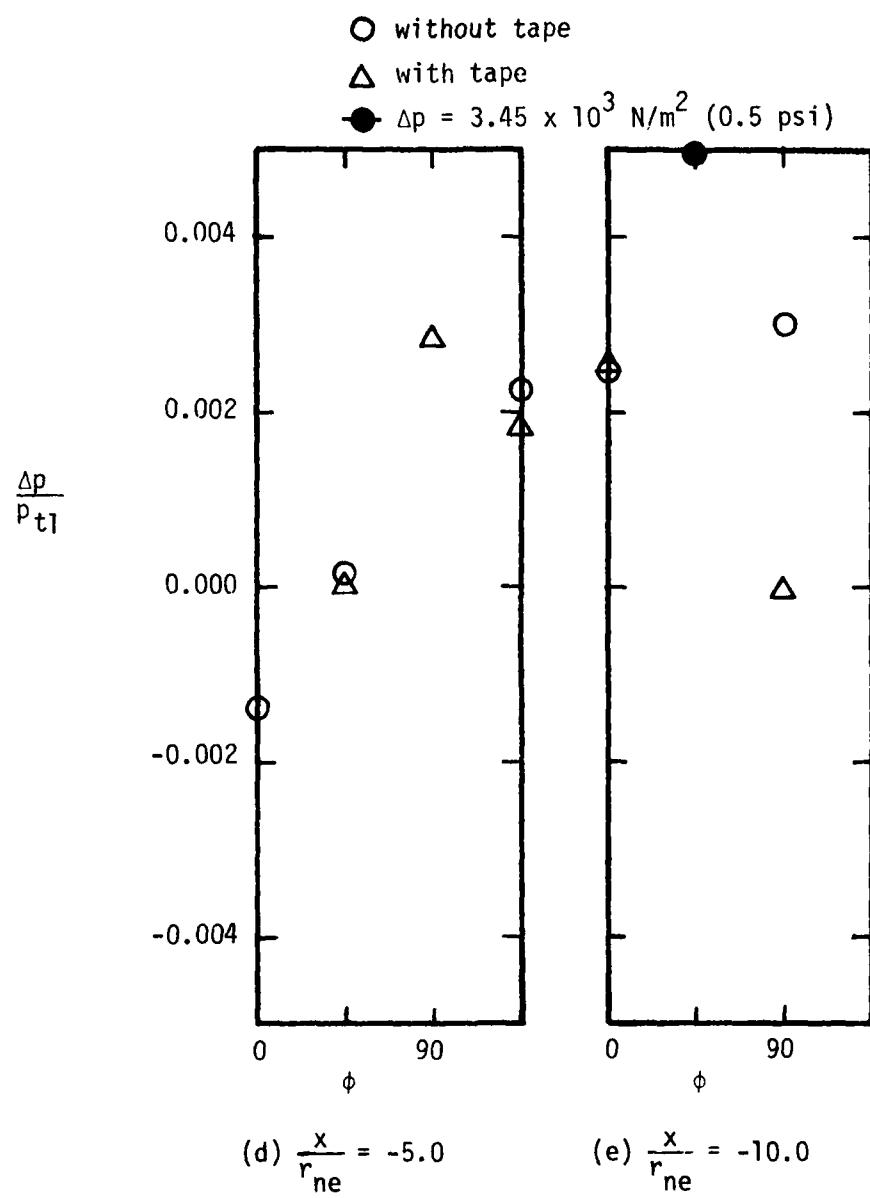
Figure 22. - Concluded.
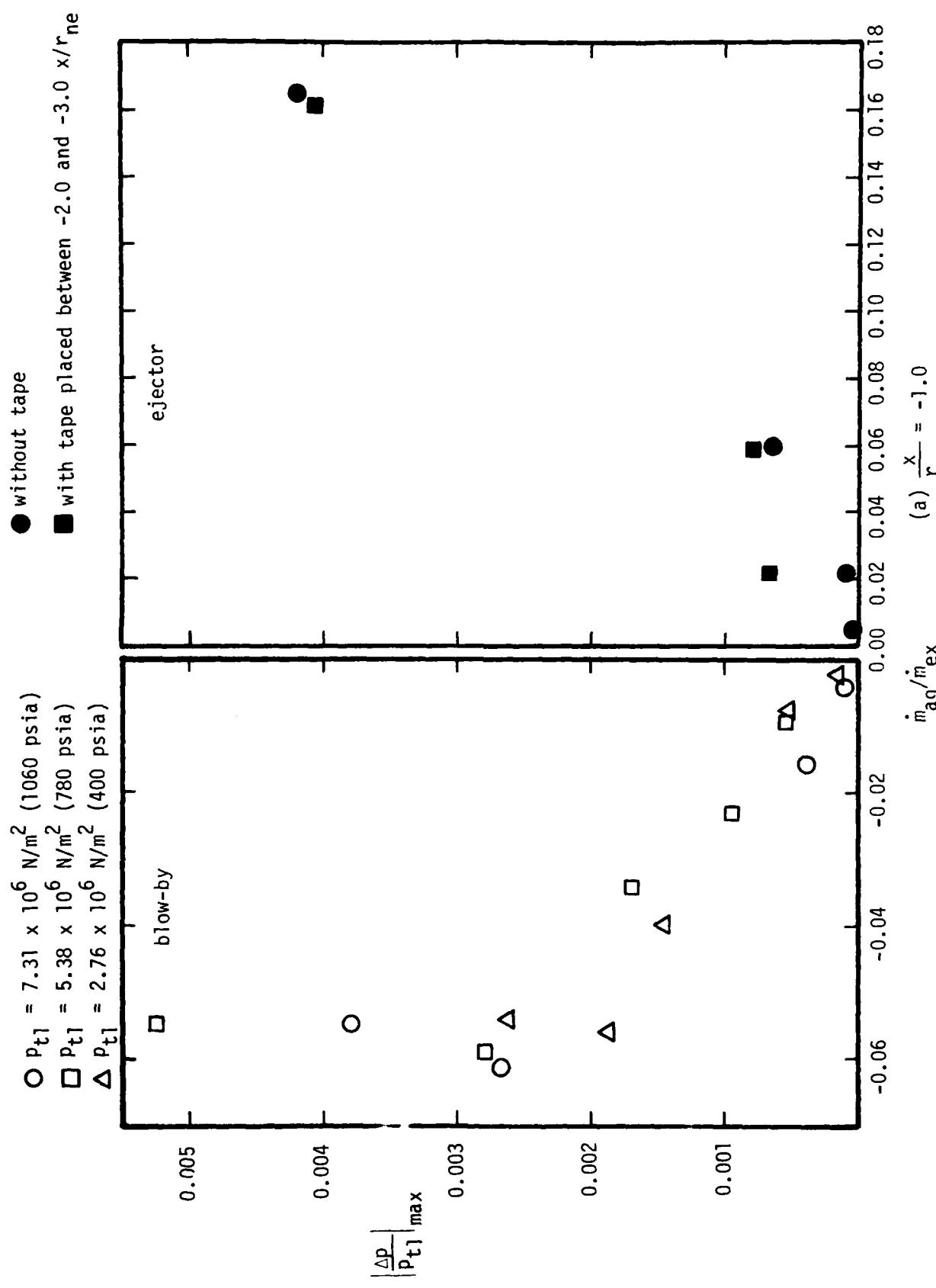
Figure 23. - A correlation between the mass flow-rate in the annular gap and the maximum differential pressure on the surface of the Cl nozzle.

(b) $\frac{x}{r_{ne}} = -2.0$
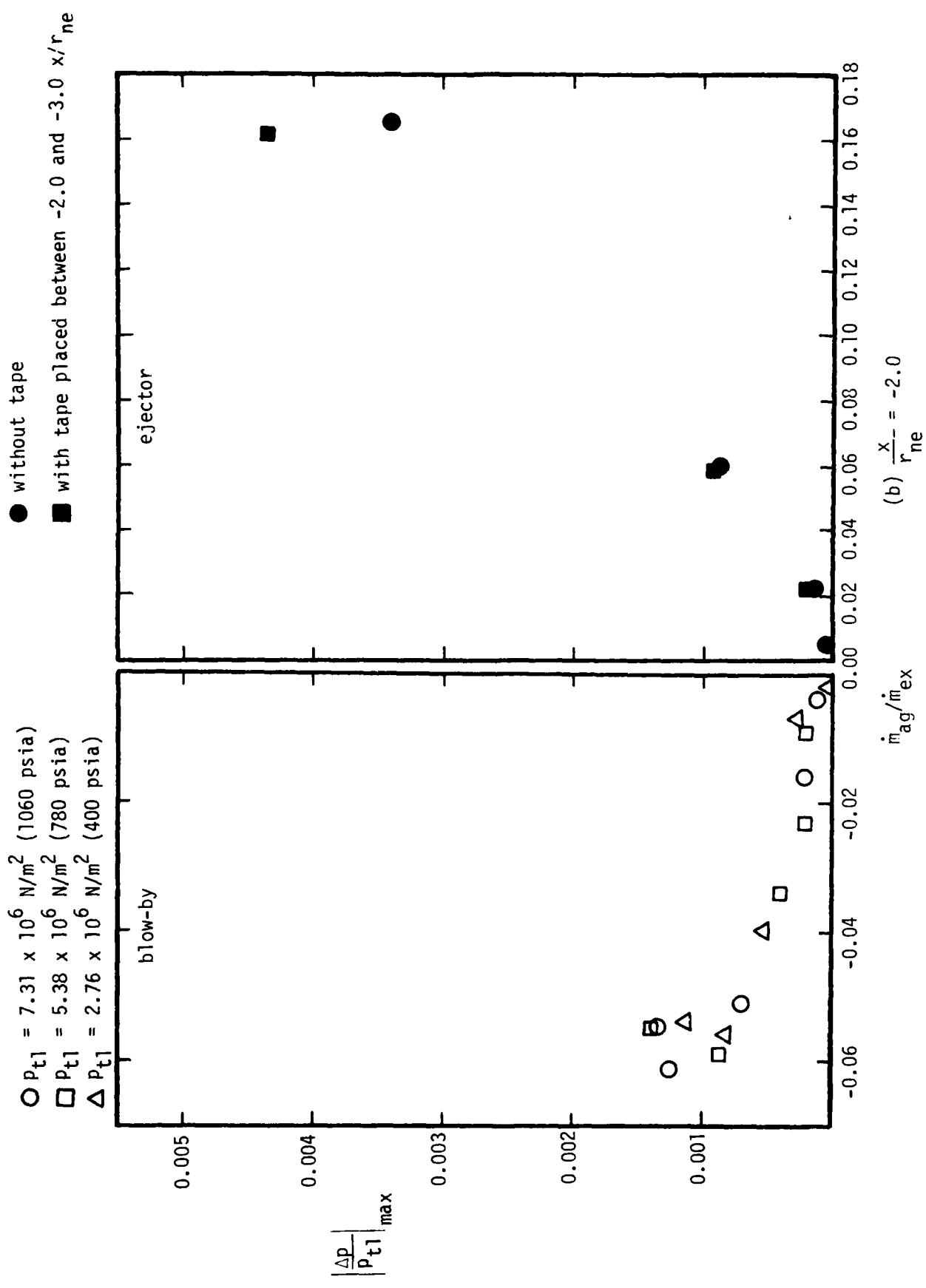
Figure 23. - Continued.
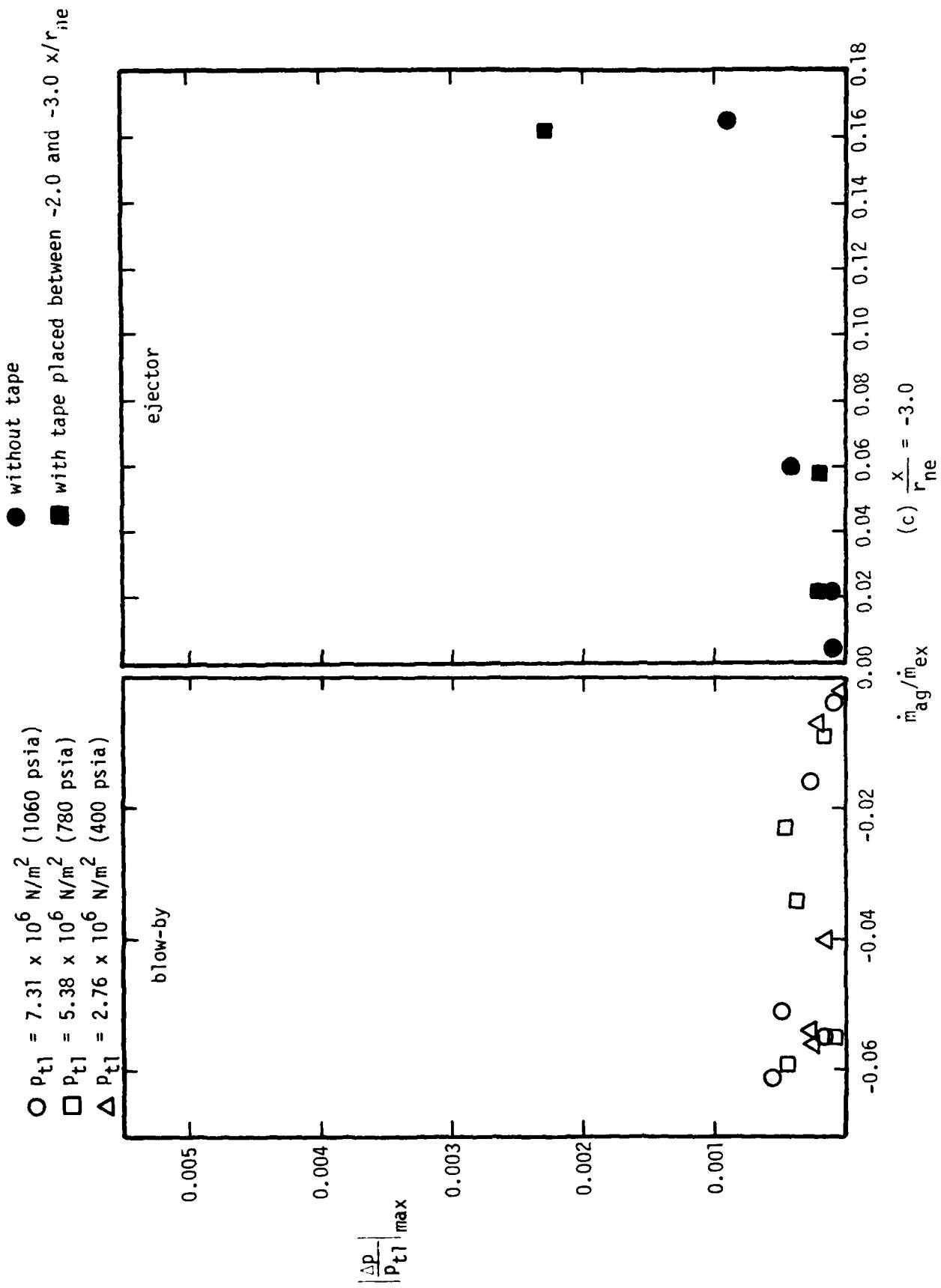
Figure 23. - Continued.
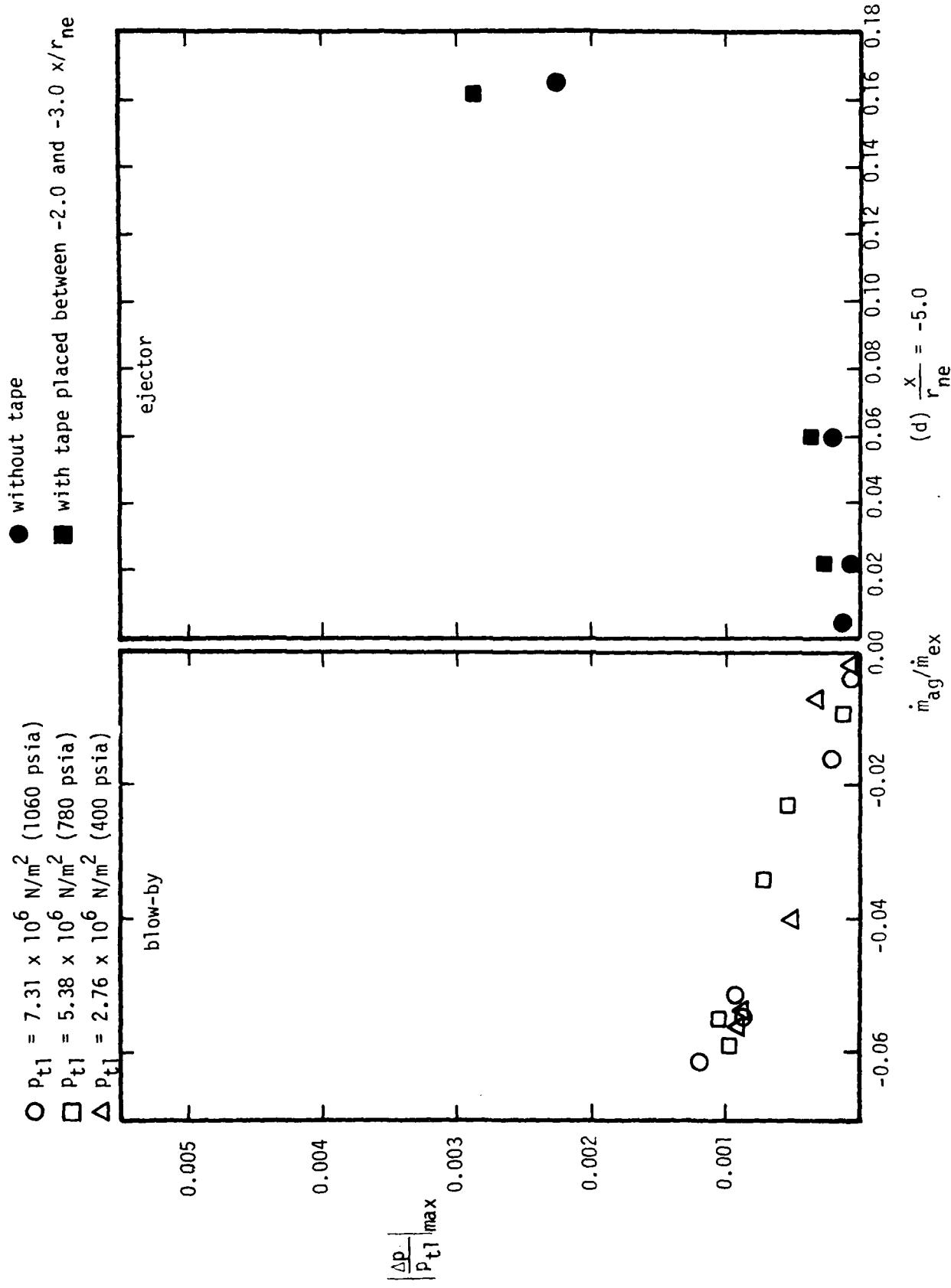
Figure 23. - Continued.
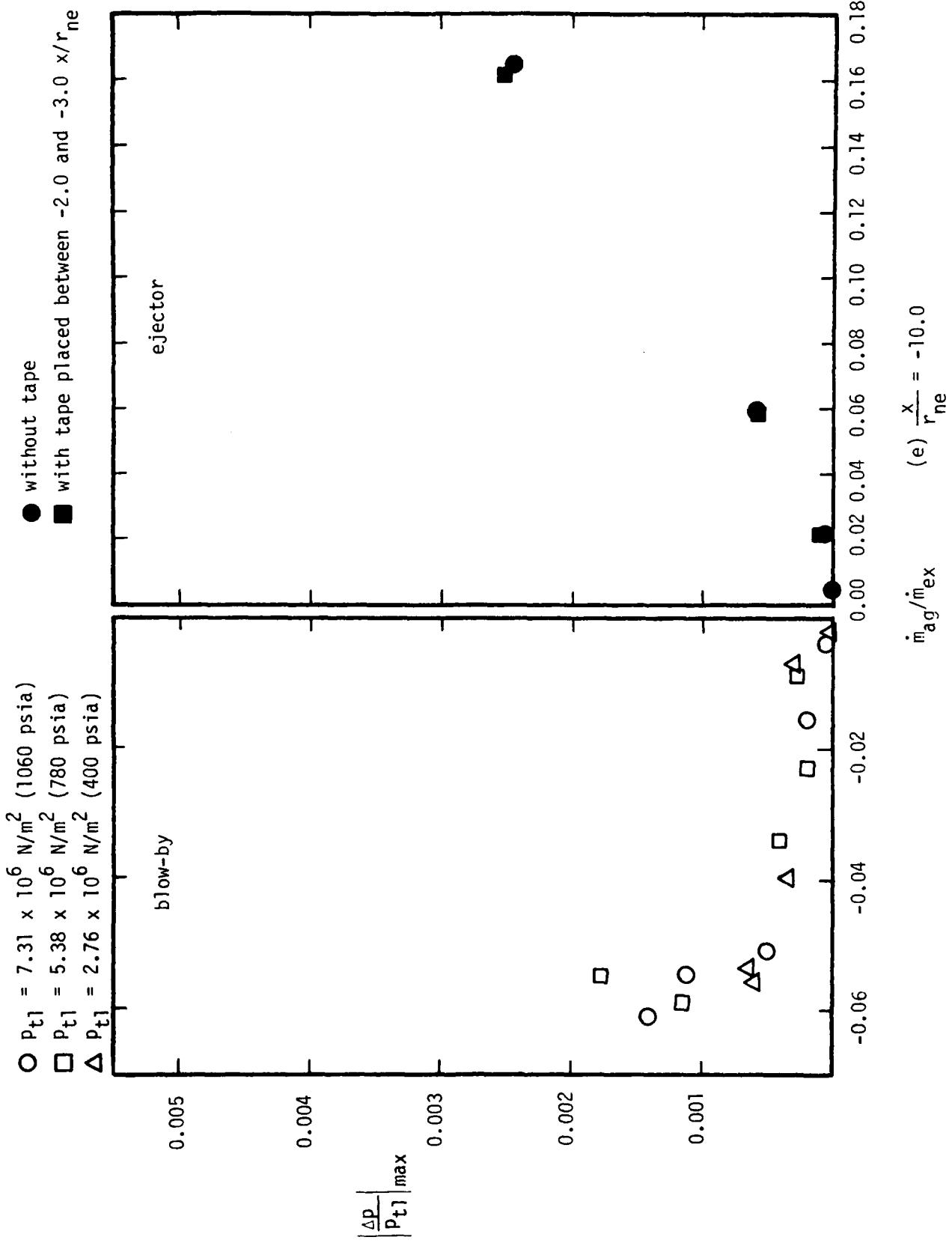
Figure 23. - Concluded.

APPENDIX A

The Static Wall-Pressure Distributions for the C4/L1 Configuration with a
Constrictive Ring

P/PT1

p_{atm}

-4.00   -3.00   -2.00   -1.00   0.00   1.00   2.00   3.00   4.00   5.00

X/RNE

0.00   0.05   0.10   0.15

(a) $p_{t1} = 2.71 \times 10^6$ N/m^2 (393 psia)
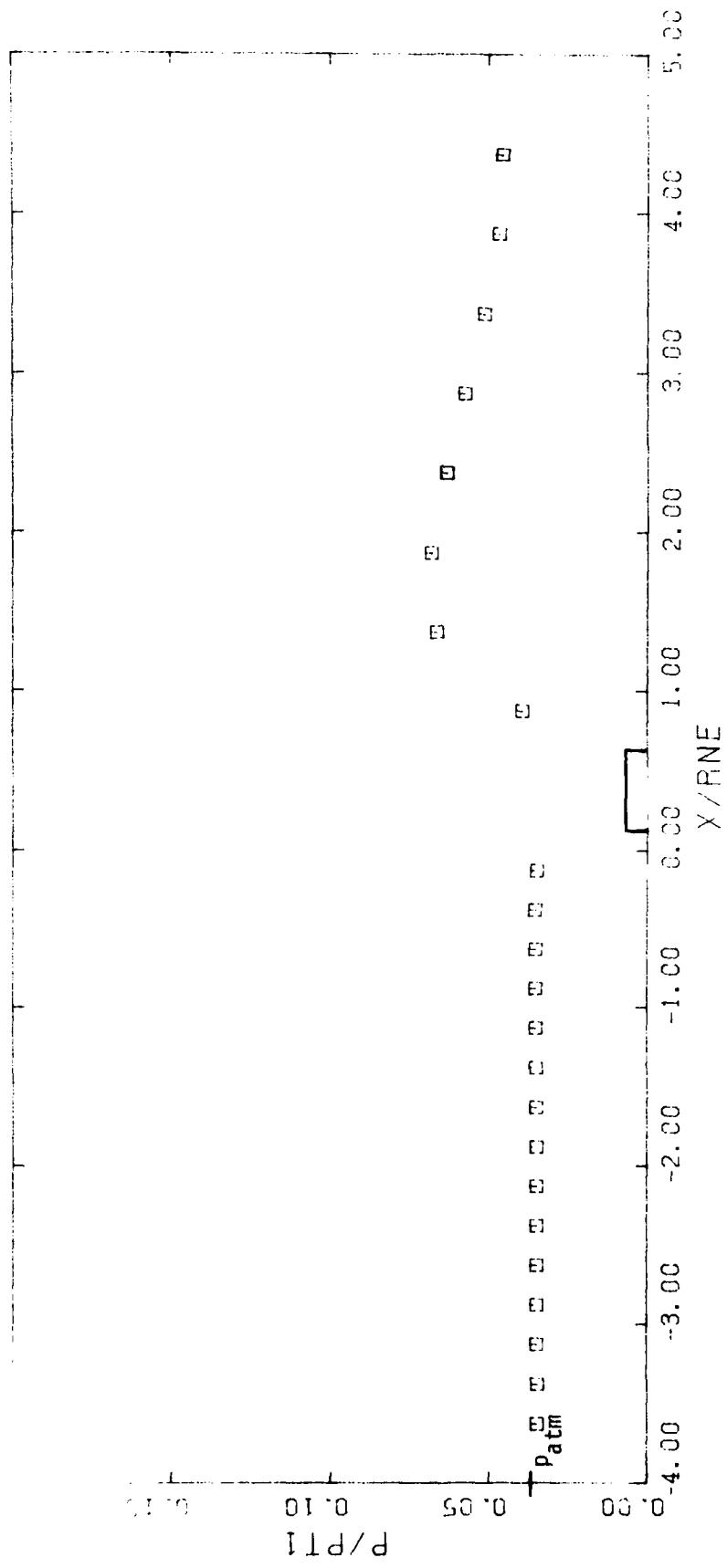
Figure A1. - The static wall pressure distribution for the C4/L1 configuration with constrictive ring, $\tilde{x}_{ne} = 1.0h$.
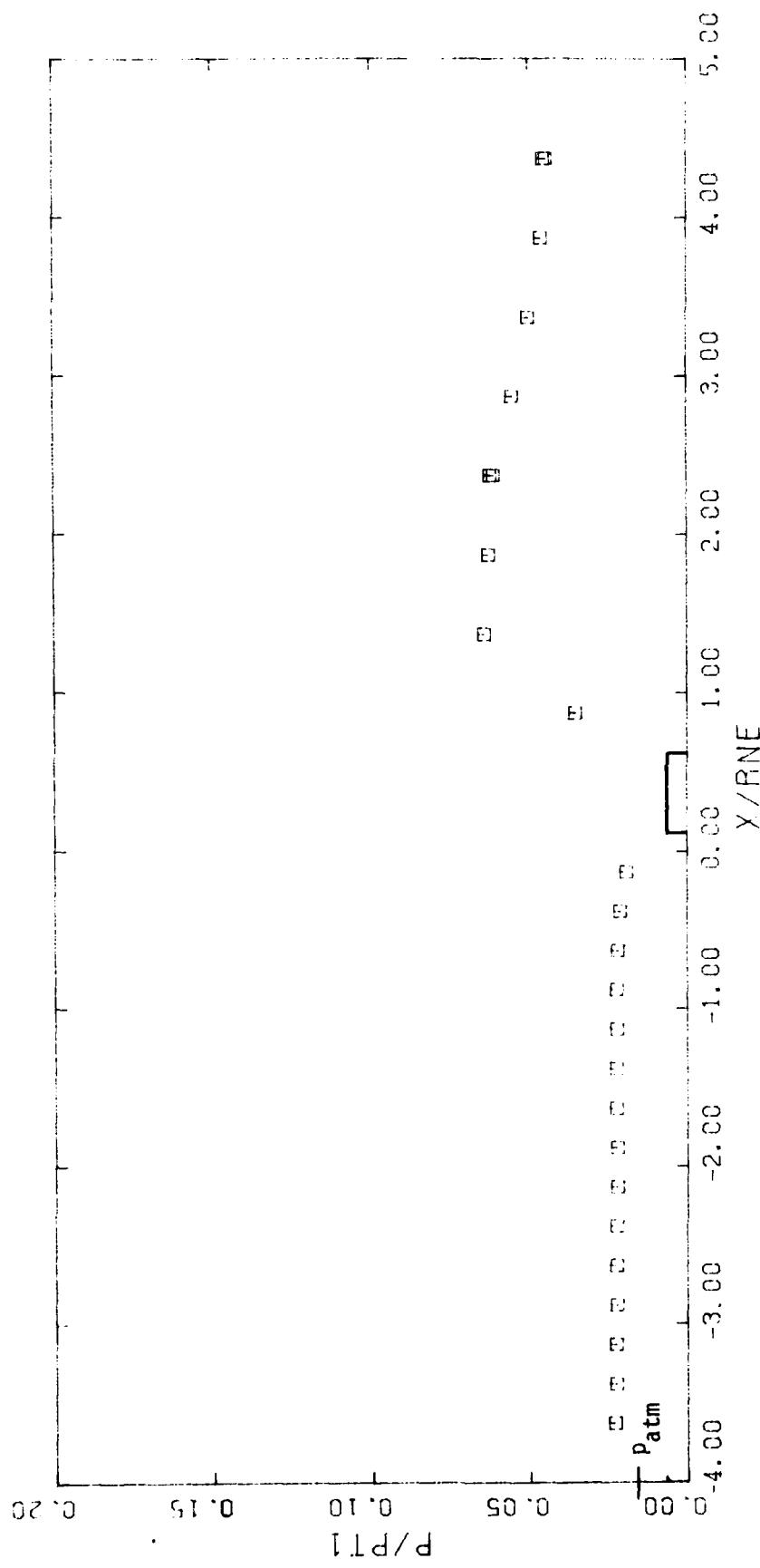
(b) $p_{t1} = 6.07 \times 10^6 \text{ N/m}^2$ (880 psia)

Figure A1. - Continued.
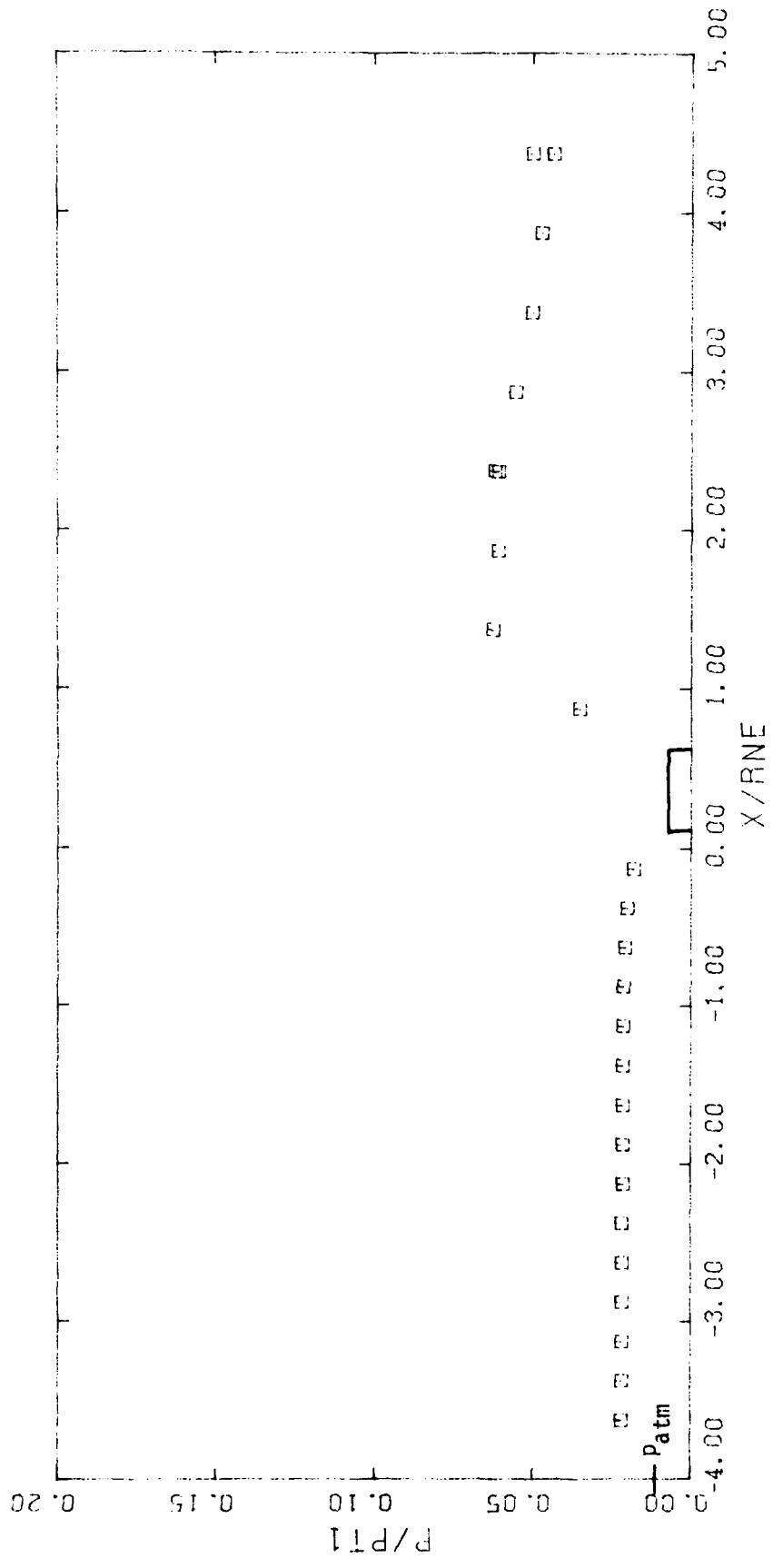
(c) $p_{tj} = 8.78 \times 10^6$ N/m^2 (1274 psia)

Figure A1. - Concluded.
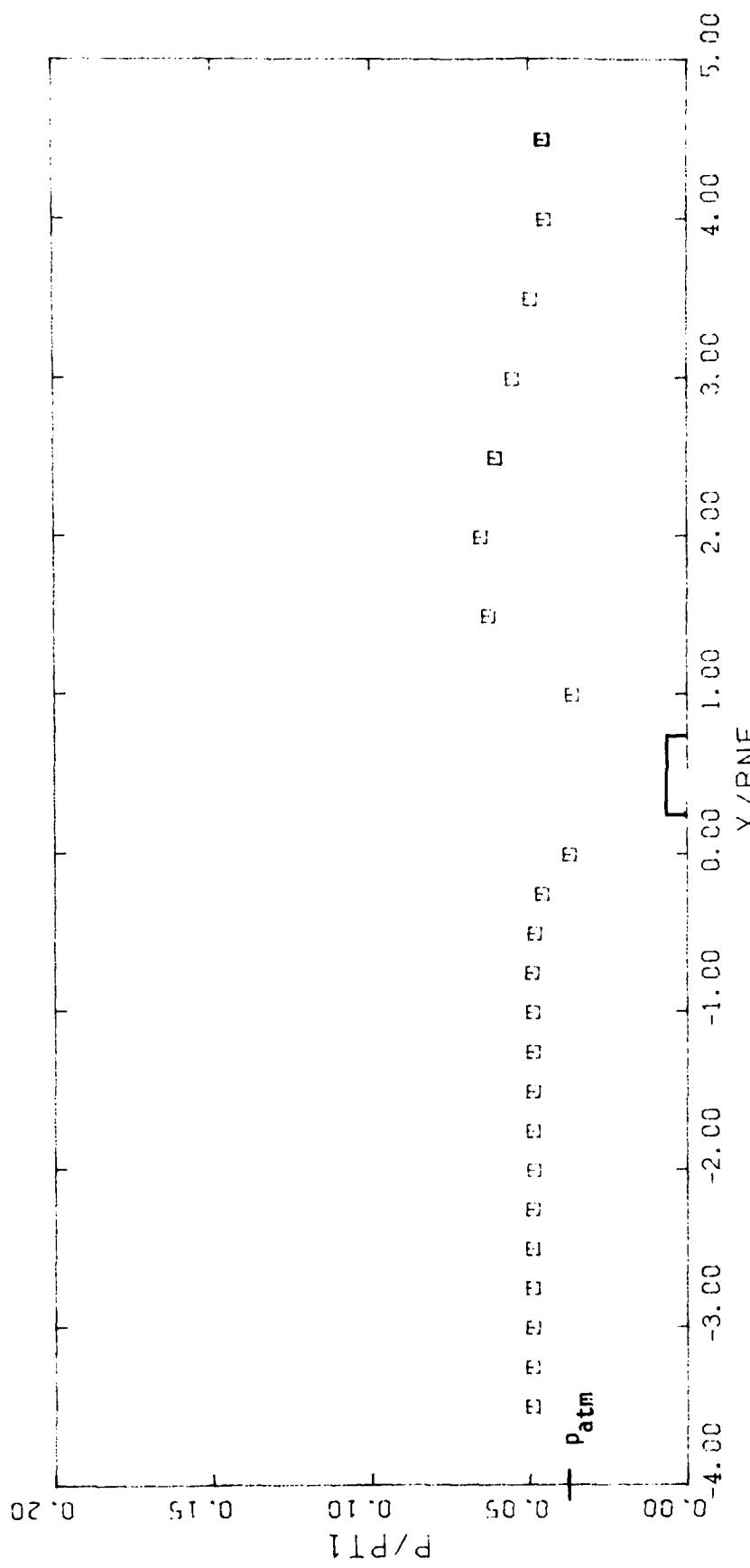
(a) $p_{t1} = 2.71 \times 10^6 \ N/m^2$ (393 psia)

Figure A2. – The static wall pressure distribution for the C4/L1 configuration constrictive ring, $\tilde{x}_{ne} = 2.0h$.
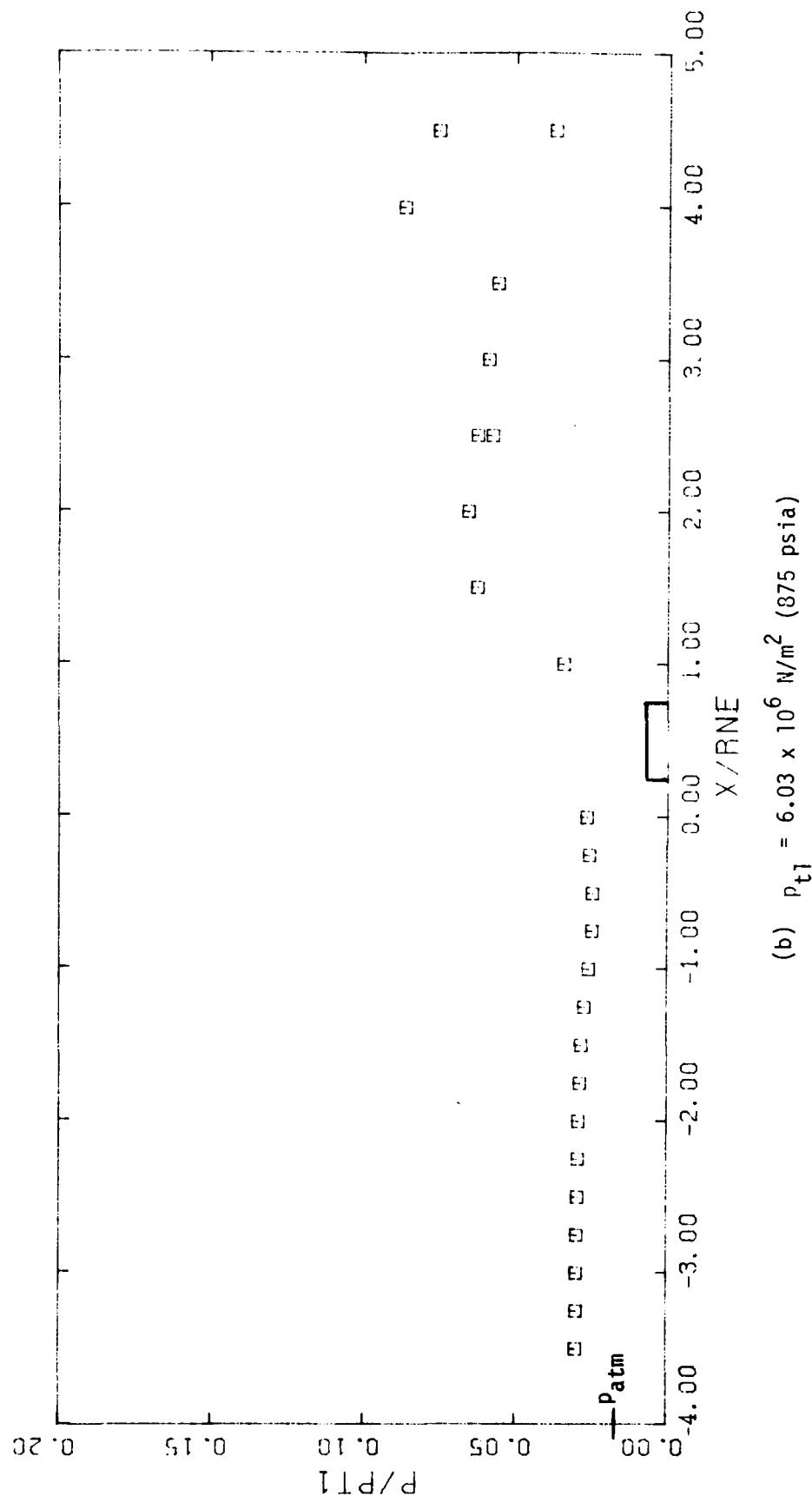
(b) $p_{t1} = 6.03 \times 10^6$ N/m^2 (875 psia)

Figure A2. - Concluded.

(a) $p_{t1} = 2.71 \times 10^6$ N/m^2 (393 psia)
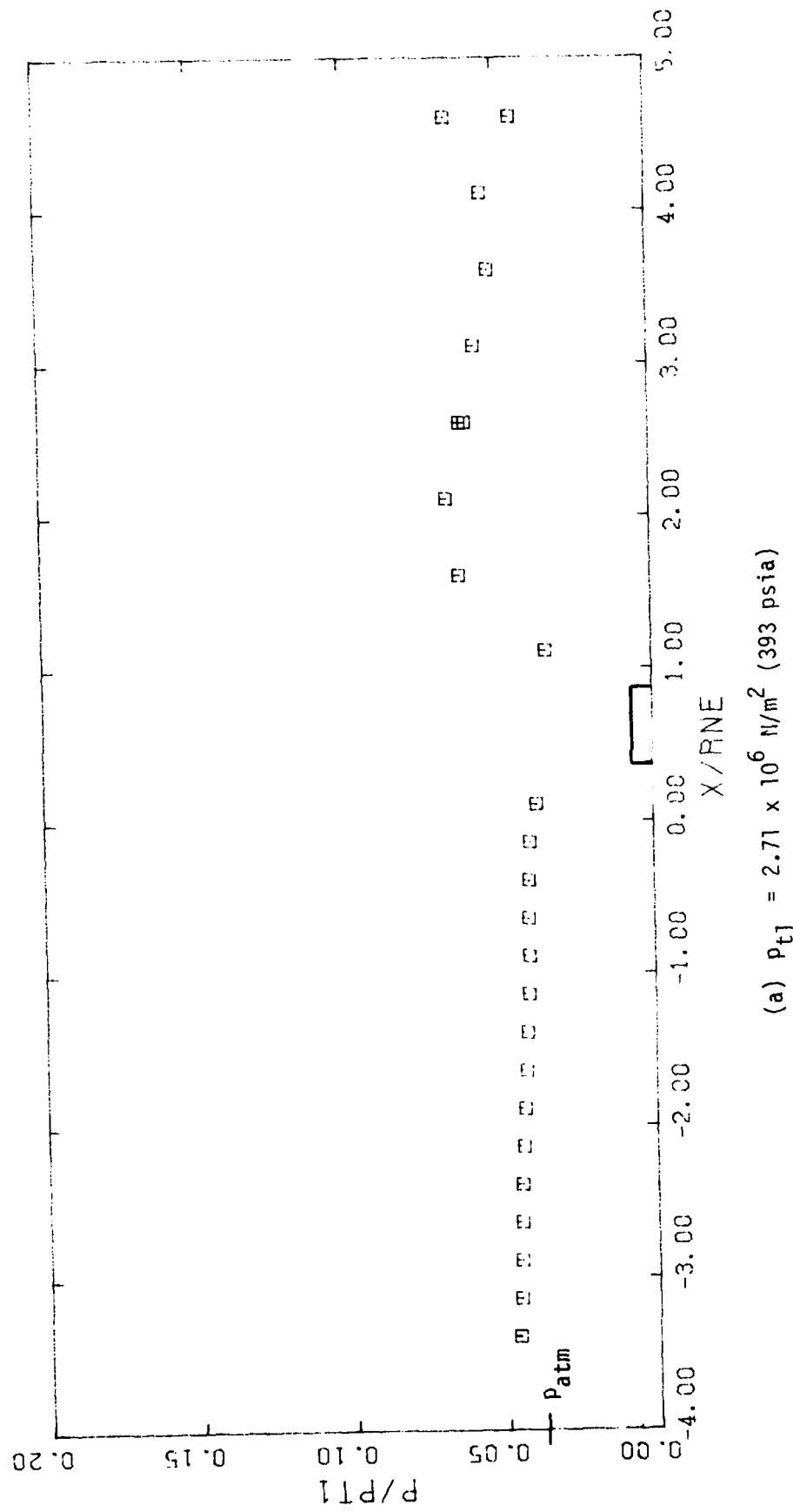
Figure A3. - The static wall pressure distribution for the C4/L1 configuration with constrictive ring, $\tilde{x}_{ne} = 3.0h$.
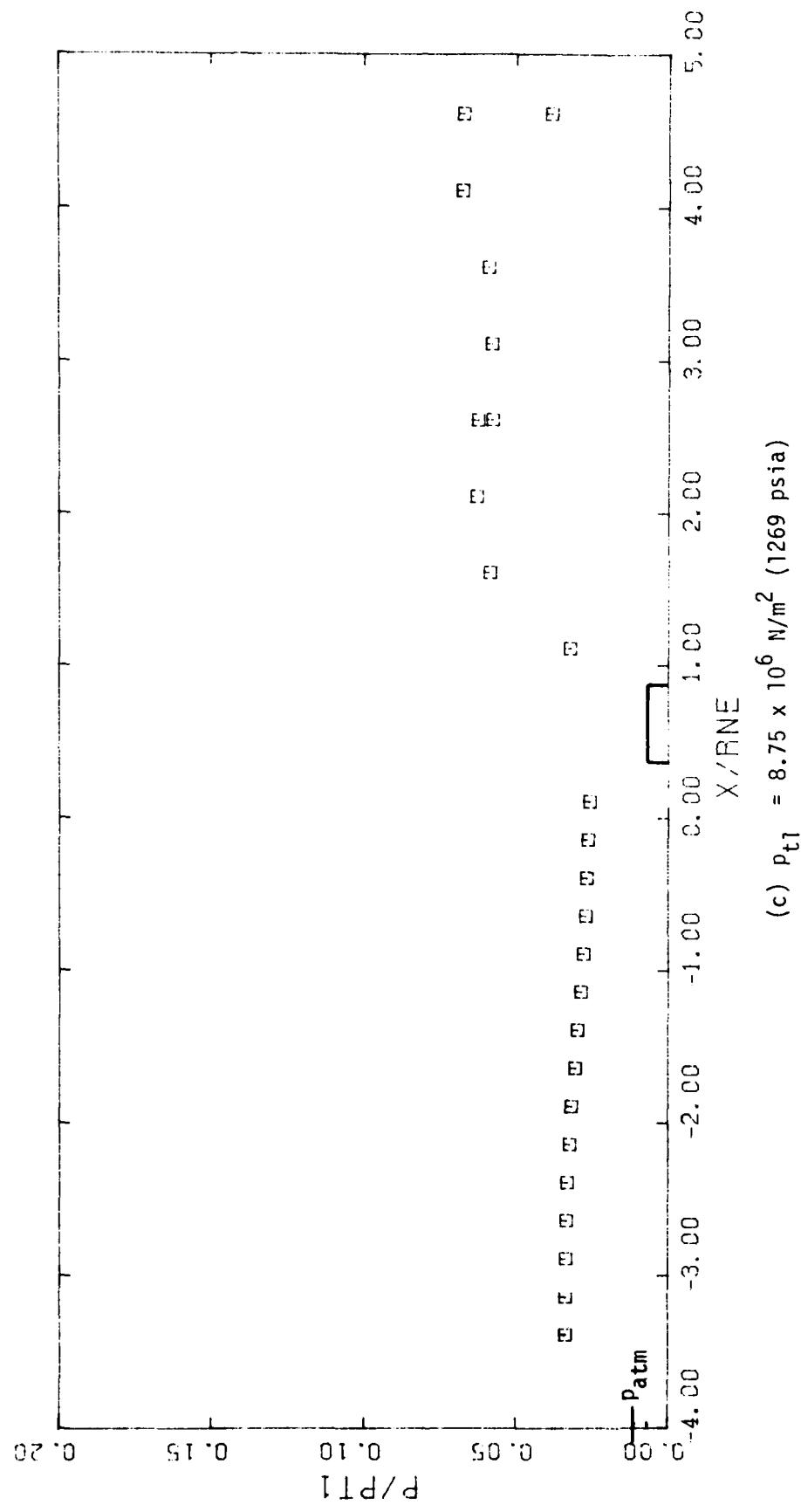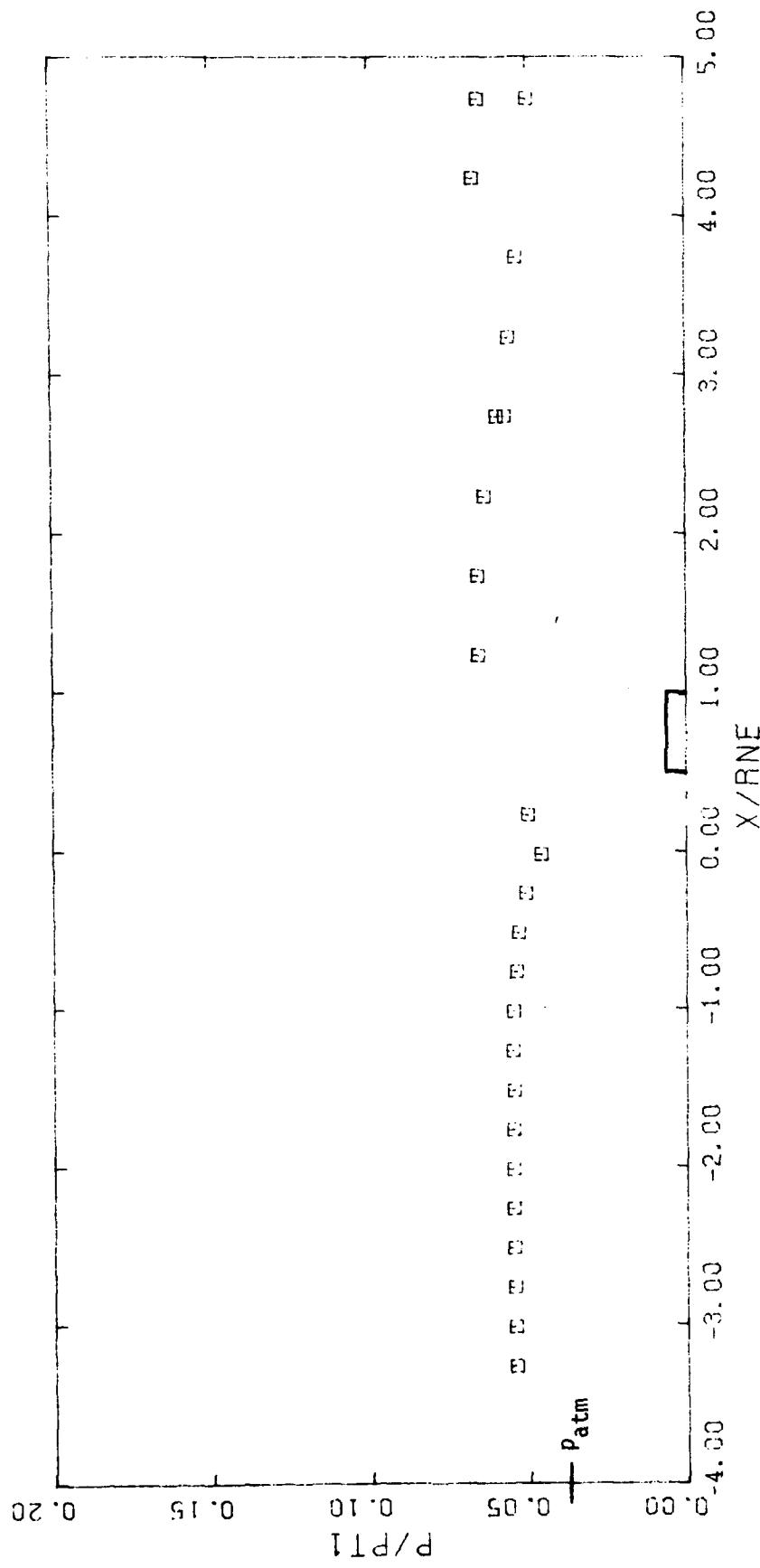
(b) p_{t1} = C.10 x 10^6 N/m^2 (885 psia)

Figure A3. - Continued.

X/RNE

$P/PT1$

P_{atm}

(c) $p_{t1} = 8.75 \times 10^6$ N/m^2 (1269 psia)

Figure A3. - Concluded.

(a) $p_{t1} = 2.71 \times 10^6$ N/m^2 (393 psia)

Figure A4. - The static wall pressure distribution for the C4/L1 configuration with constrictive ring, $\tilde{x}_{ne} = 4.0h$.

(b) $p_{t1} = 6.10 \times 10^6$ N/m^2 (885 psia)

Figure A4. - Continued.

(c) $p_{t1} = 8.75 \times 10^6$ N/m^2 (1269 psia)
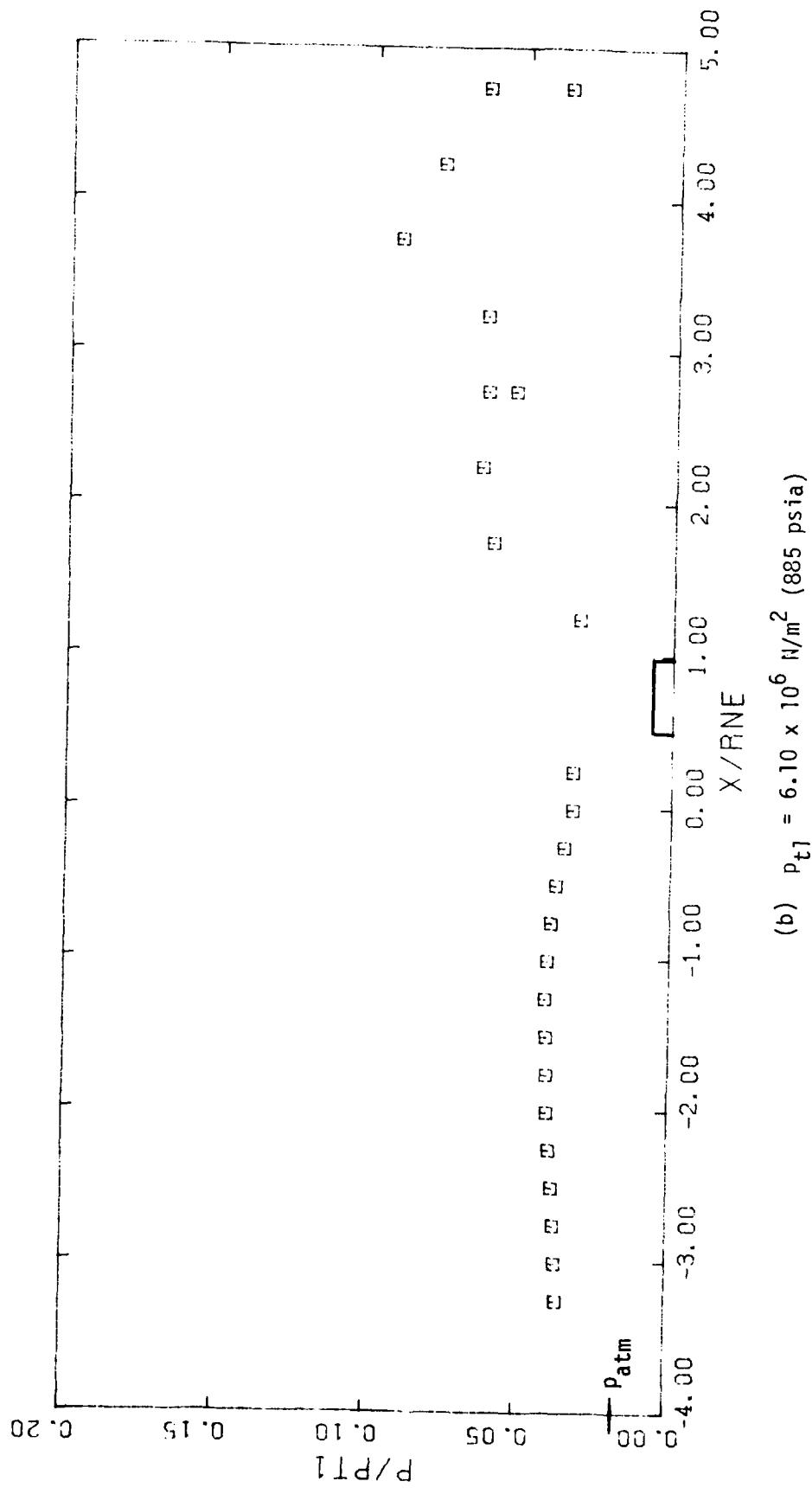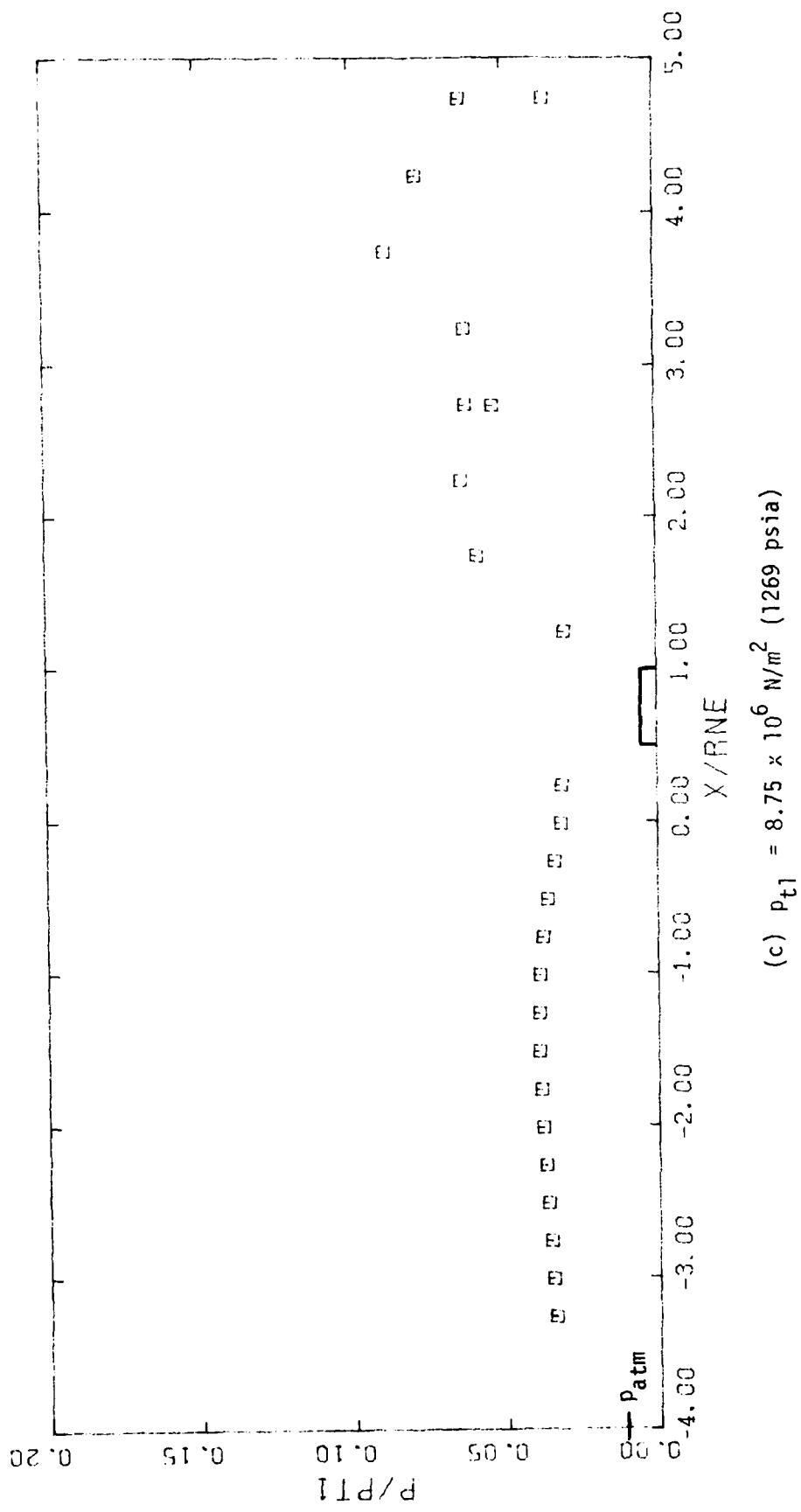
Figure A4. - Concluded.

(a) $p_{t1} = 2.71 \times 10^6$ N/m^2 (343 psia)
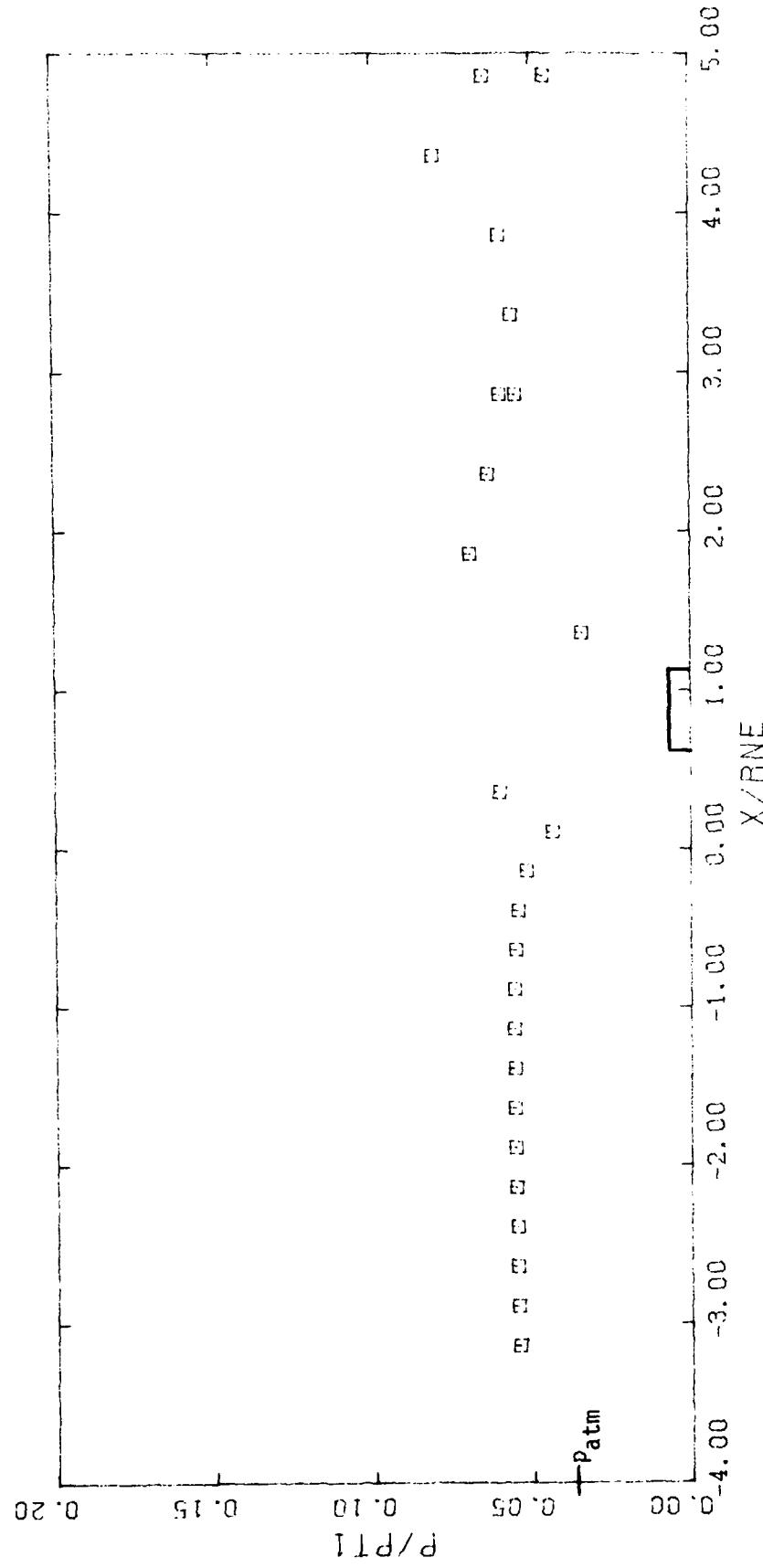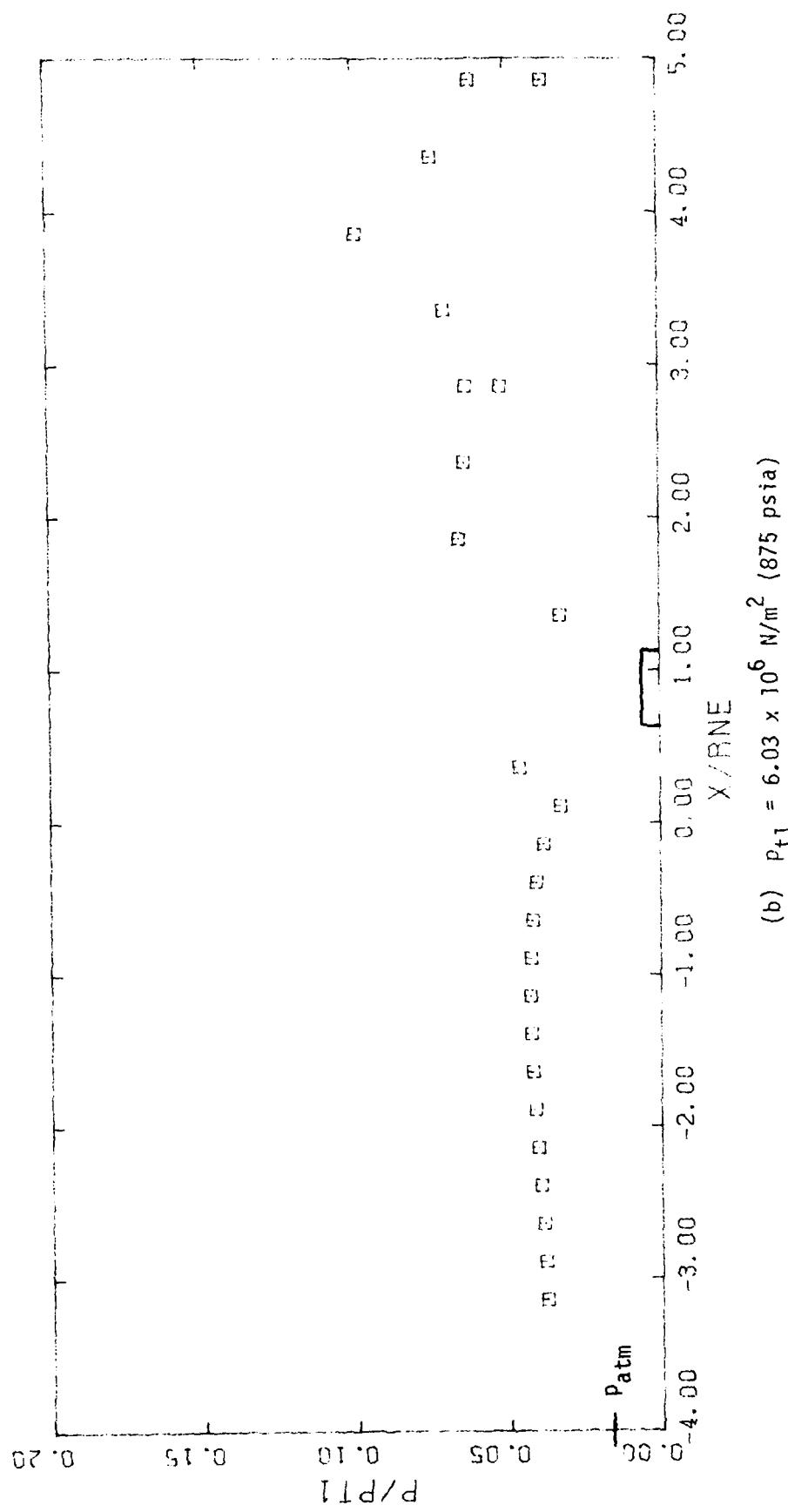
Figure A5. – The static wall pressure distribution for the C4/L1 configuration with constrictive ring, $\tilde{x}_{ne} = 5.0h$.

(b) $p_{t1} = 6.03 \times 10^6 \ N/m^2$ (875 psia)

Figure A5. - Continued.
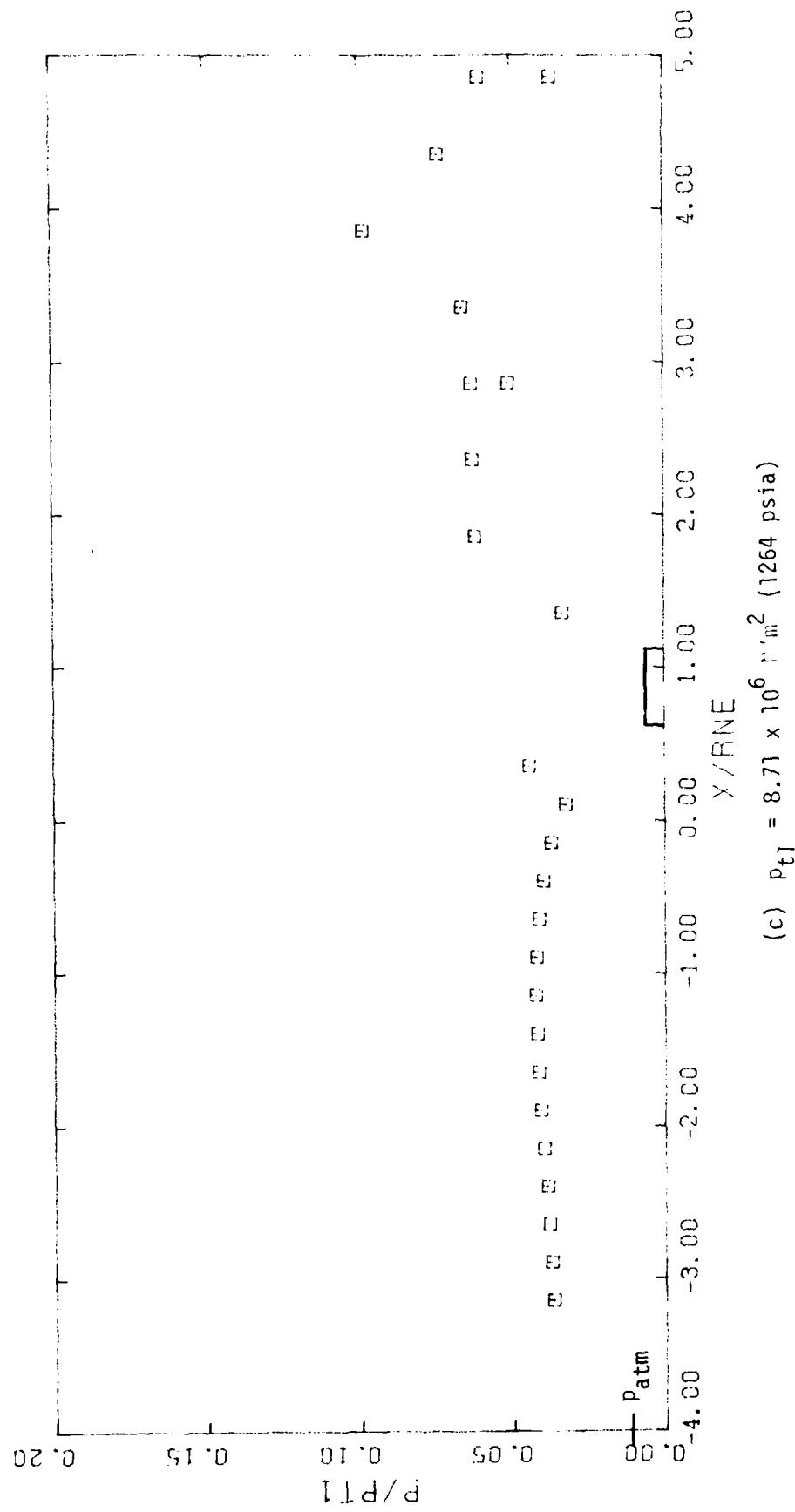
(c) $p_{t1} = 8.71 \times 10^6$ n/m^2 (1264 psia)

Figure A5. - Concluded.

P/PT1

0.20　0.15　0.10　0.05　0.00

P_{atm}

-4.00　-3.00　-2.00　-1.00　0.00　1.00　2.00　3.00　4.00　5.00

X/RNE
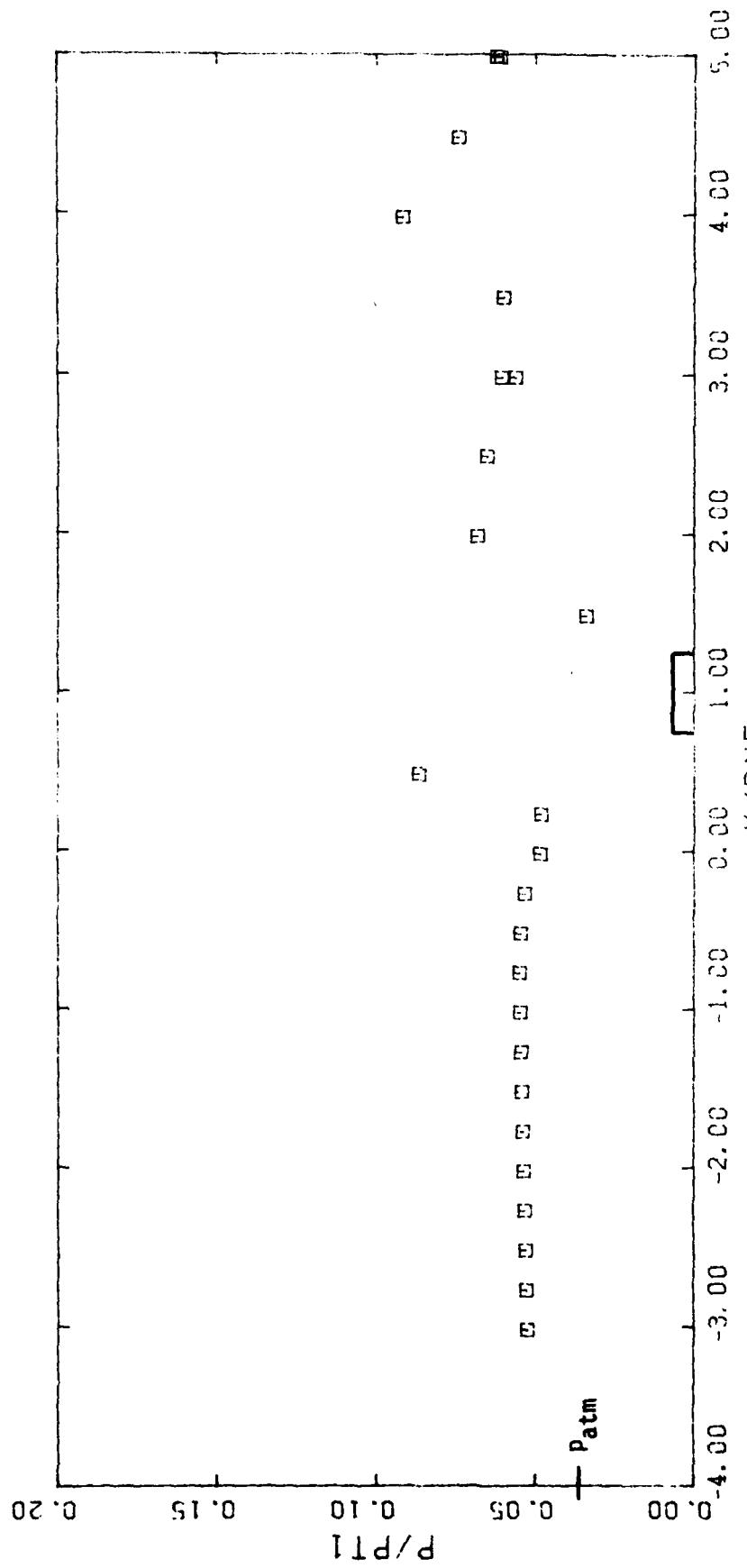
(a) p_{t1} = 2.71 × 10^6 N/m^2 (393 psia)

Figure A6. – The static wall pressure distribution for the C4/L1 configuration with constrictive ring, $\tilde{x}_{ne}$ = 6.0h.
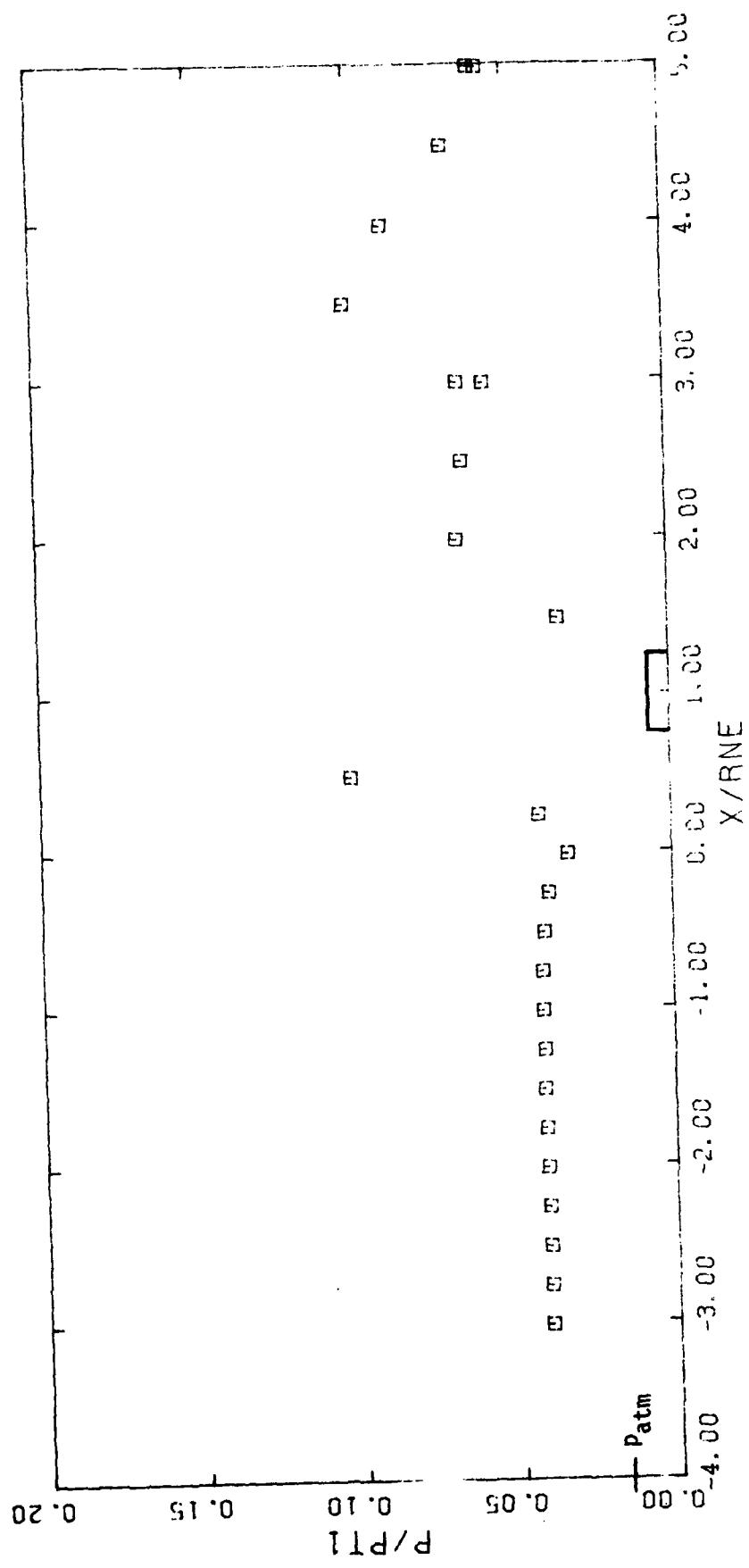
(b) $p_{t1} = 6.10 \times 10^6$ N/m^2 (885 psia)

Figure A6. - Concluded.
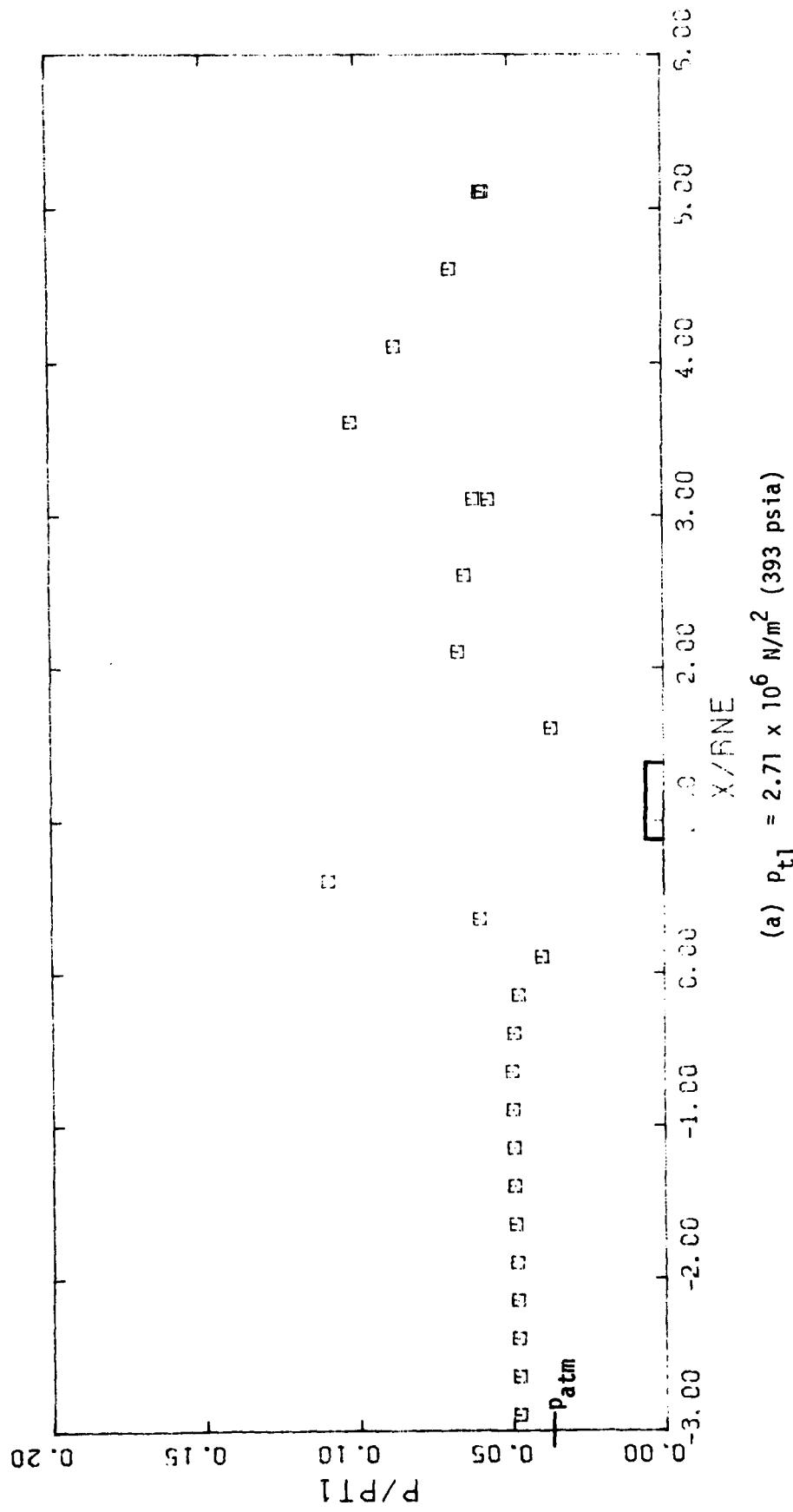
(a) $p_{t1} = 2.71 \times 10^6$ N/m^2 (393 psia)

Figure A7. - The static wall pressure distribution for the C4/L1 configuration with constrictive ring, $\tilde{x}_{ne} = 7.0$h.
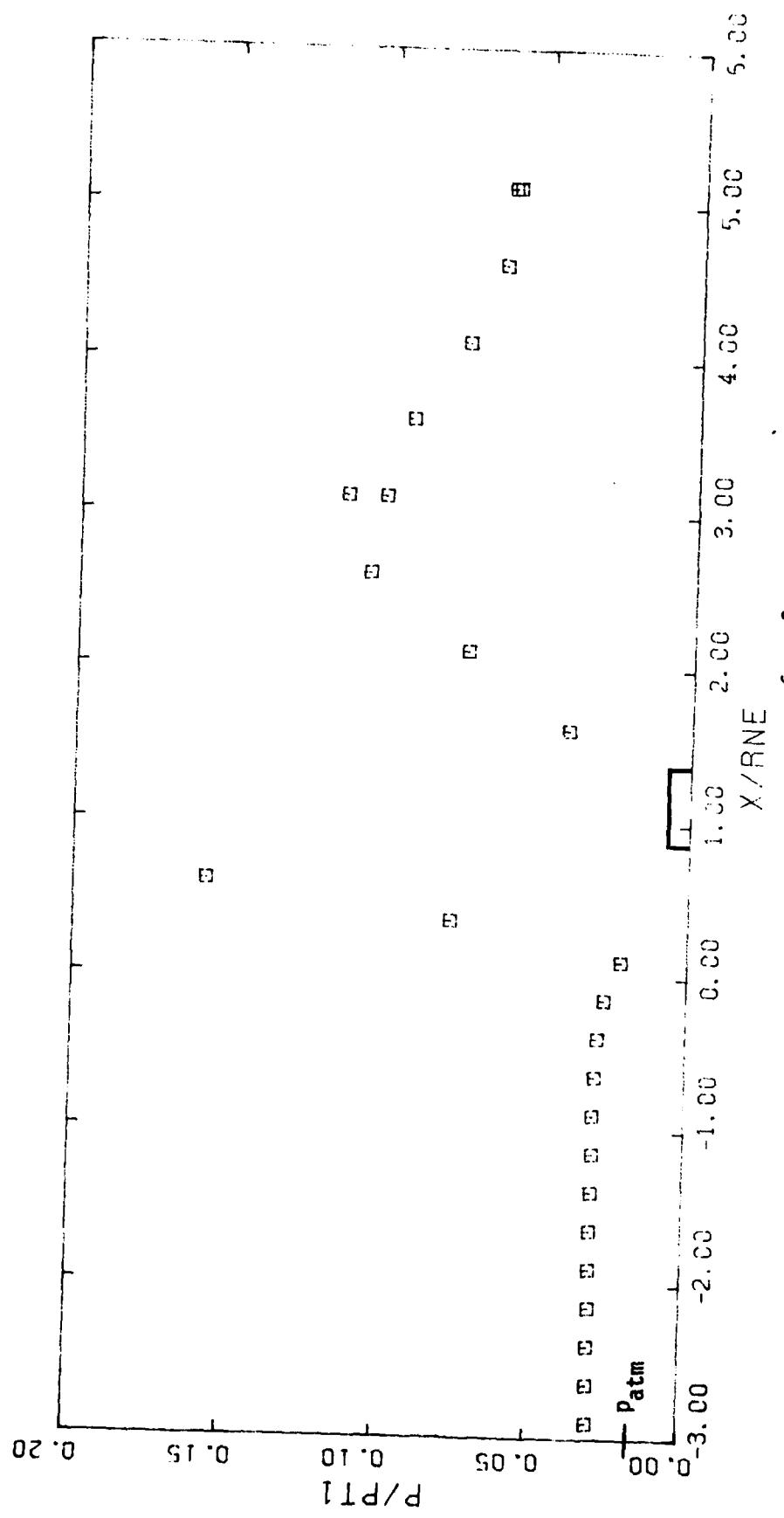
(b) $p_{t1} = 6.10 \times 10^6$ N/m^2 (885 psia)

Figure A7. - Continued.

(c) p_{t1} = 8.82 x 10^6 N/m^2 (1279 psia)
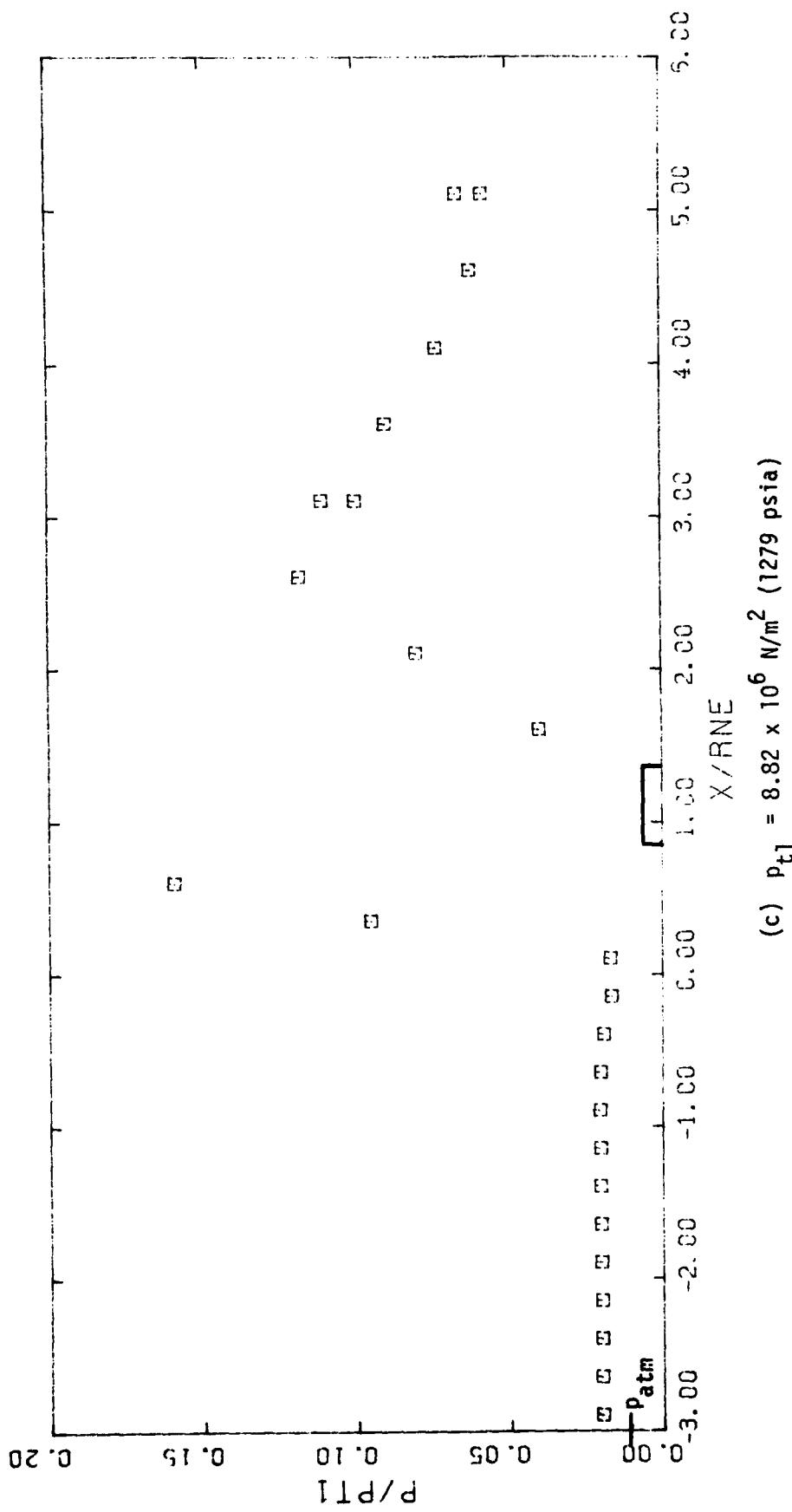
Figure A7. - Concluded.
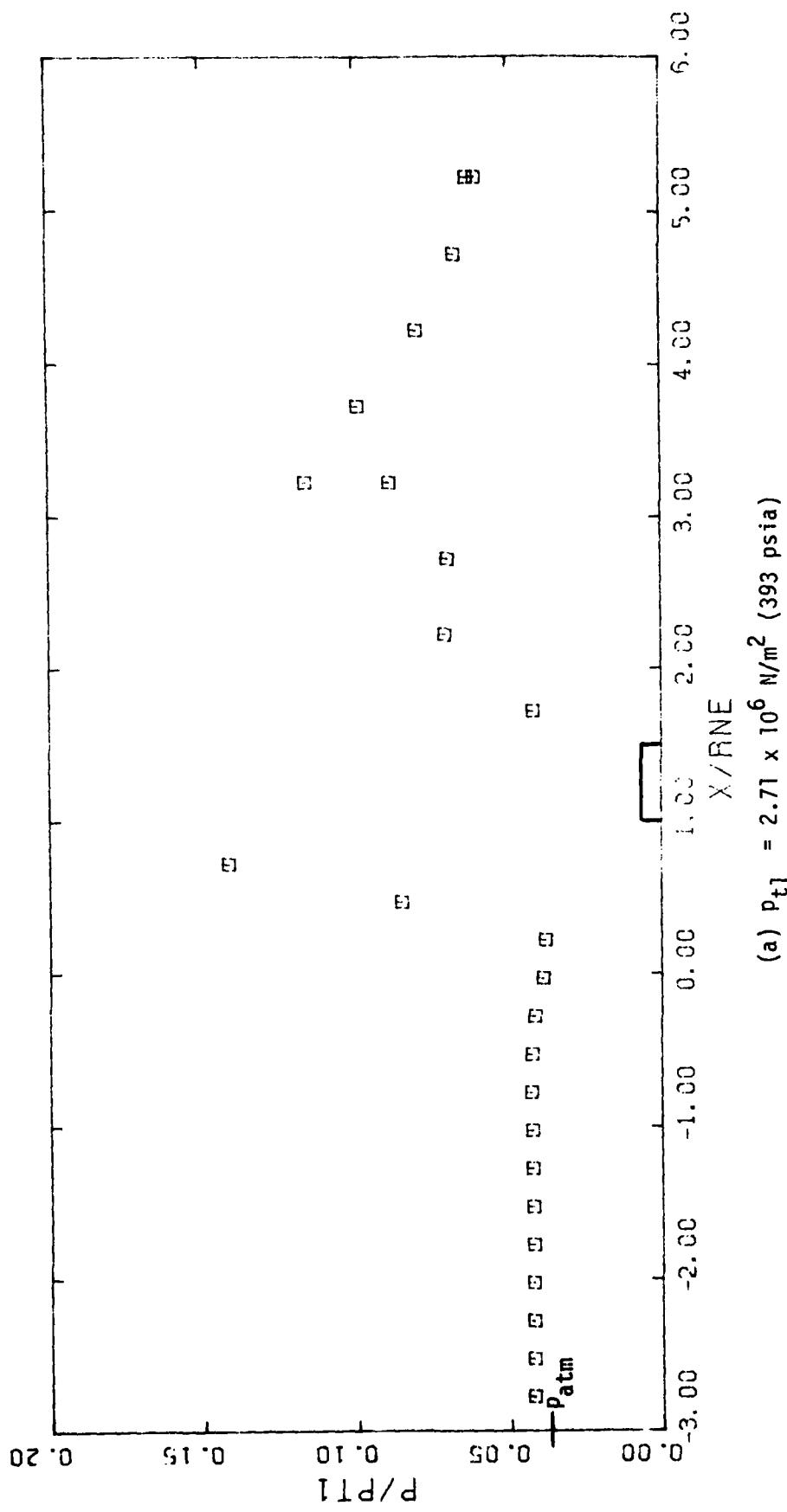
Figure A8. - The static wall pressure distribution for the C4/L1 configuration with constrictive ring, $\tilde{x}_{ne}$ = 8.0h.

(a) p_{t1} = 2.71 x 10^6 N/m^2 (393 psia)
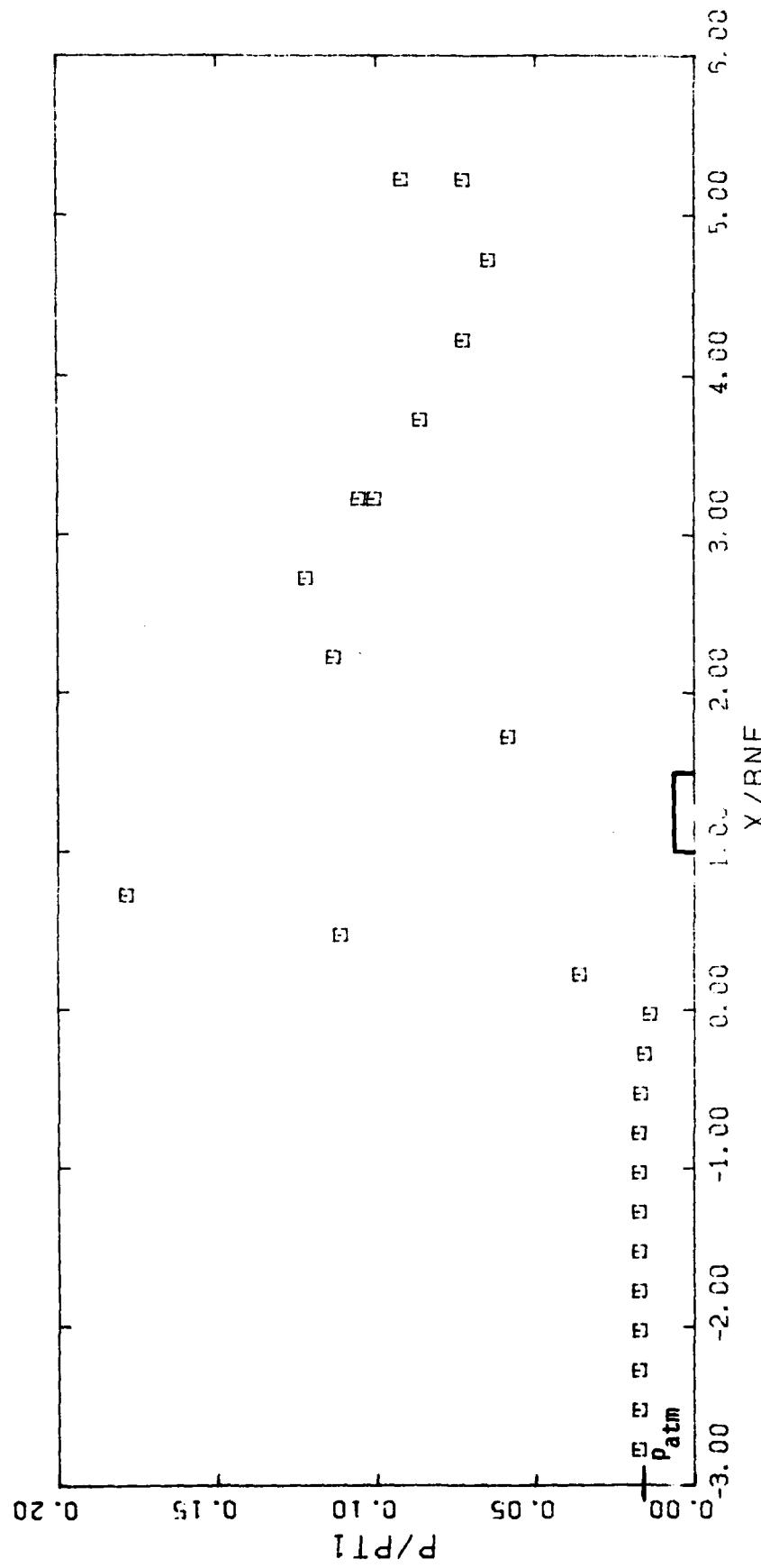
(b) $p_{t1} = 6.07 \times 10^6$ N/m^2 (880 psia)

Figure A8. - Continued.

(c) p_{t1} = 8.82 x 10^6 N/m^2 (1279 psia)
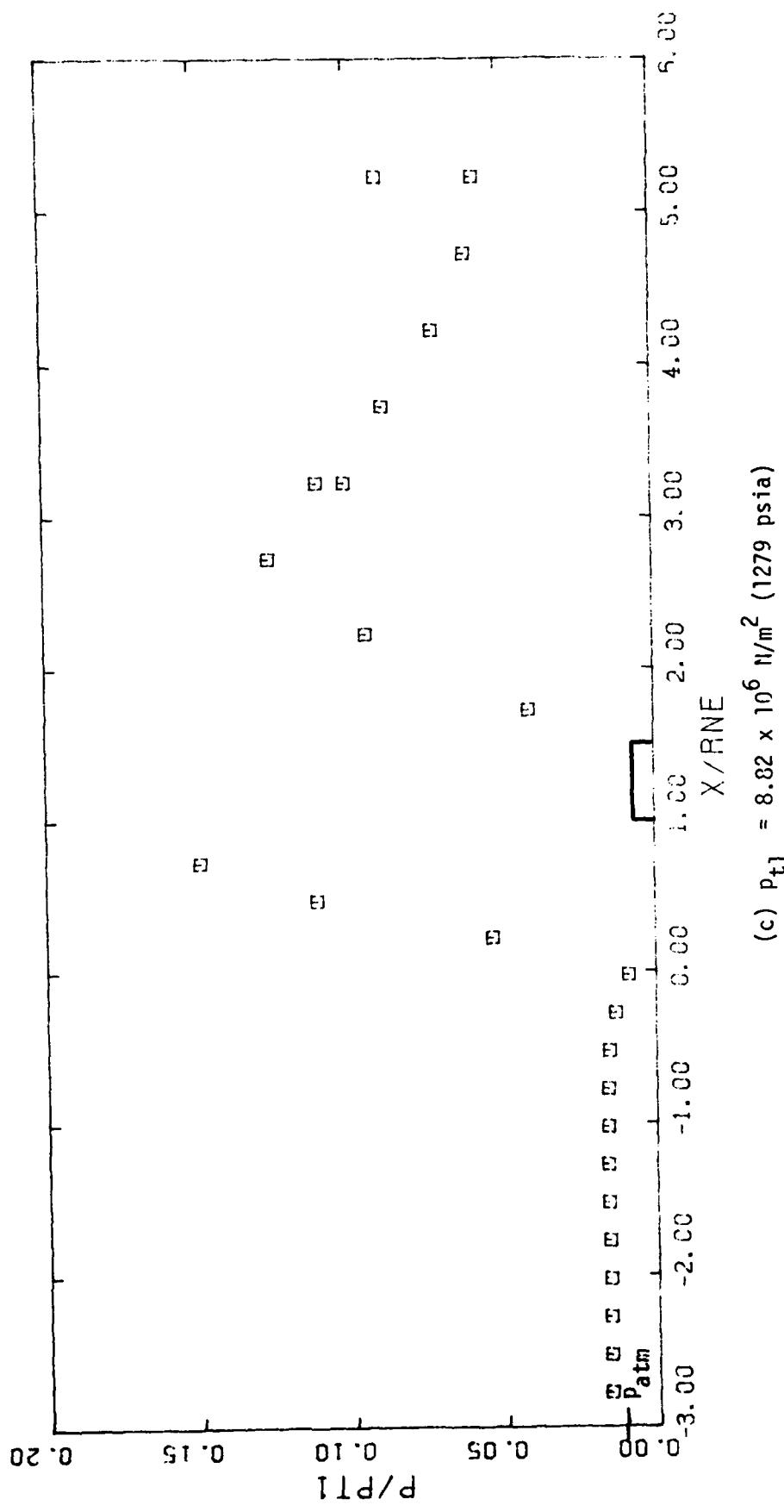
Figure A8. - Concluded.
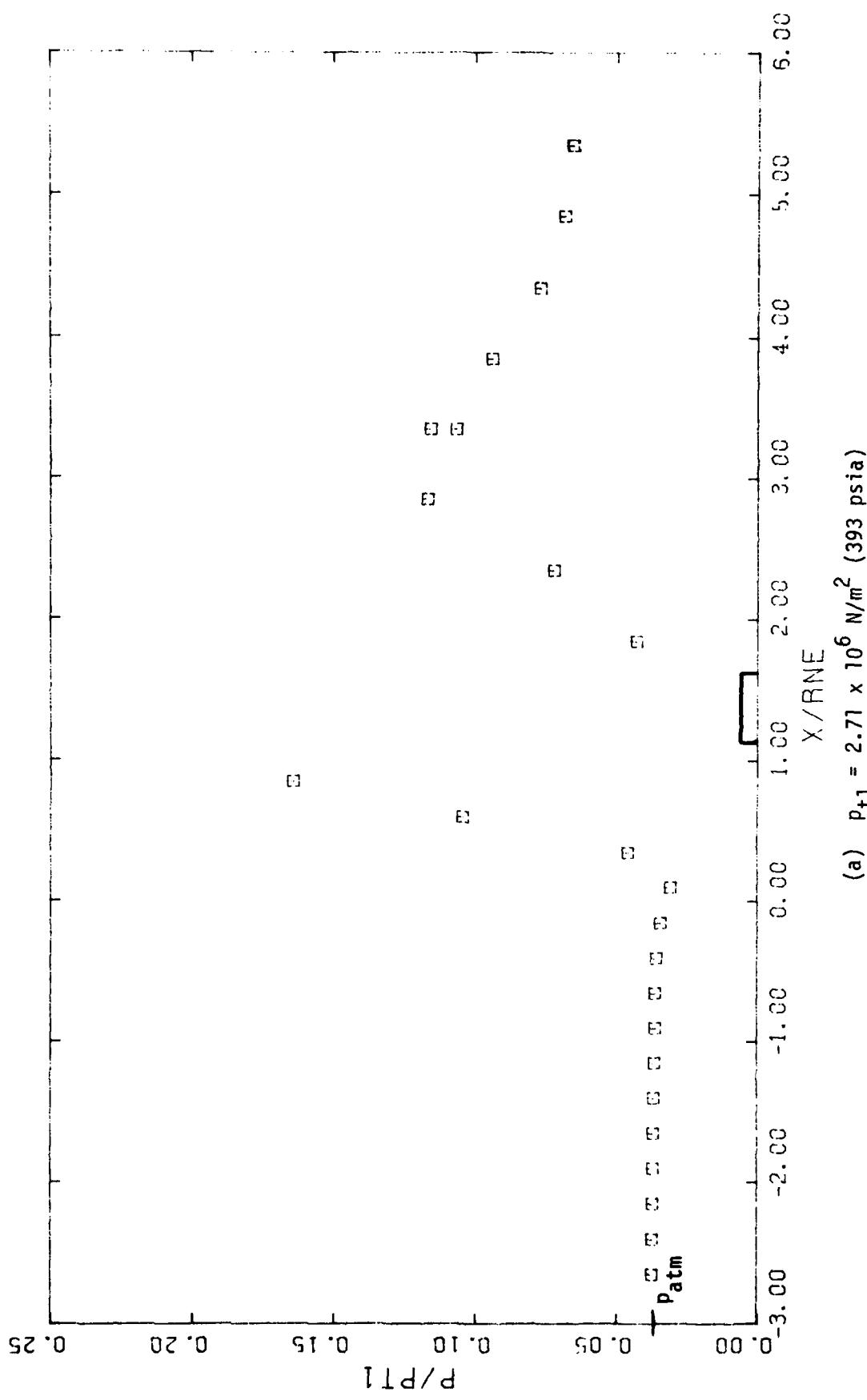
Figure A9. - The static wall pressure distribution for the C4/L1 configuration with constrictive ring, $\tilde{x}_{ne}$ = 9.0h.

(a) p_{t1} = 2.71 x 10^6 N/m^2 (393 psia)
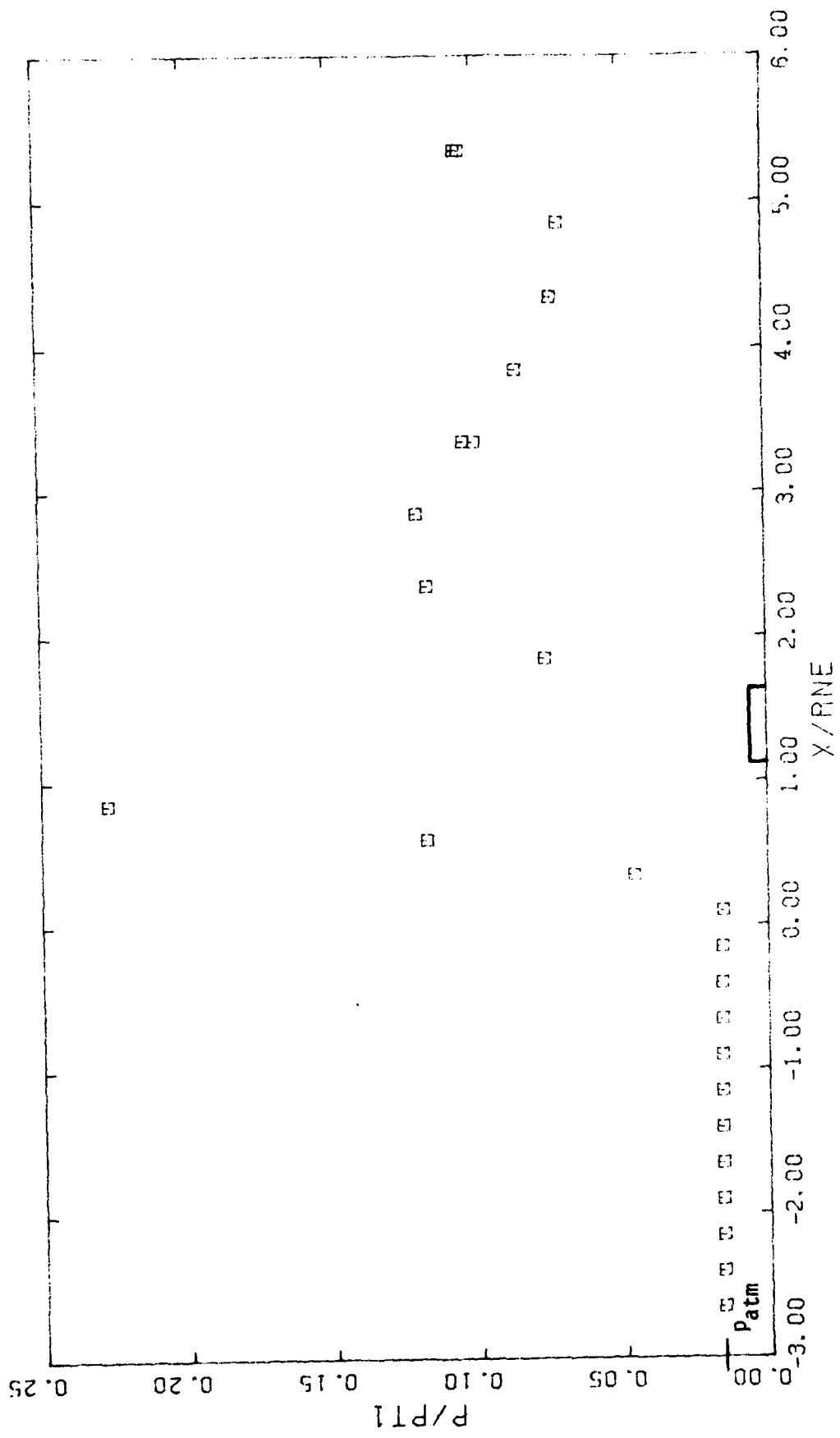
(b) $p_{t1} = 6.07 \times 10^6$ N/m^2 (880 psia)

Figure A9. - Continued.
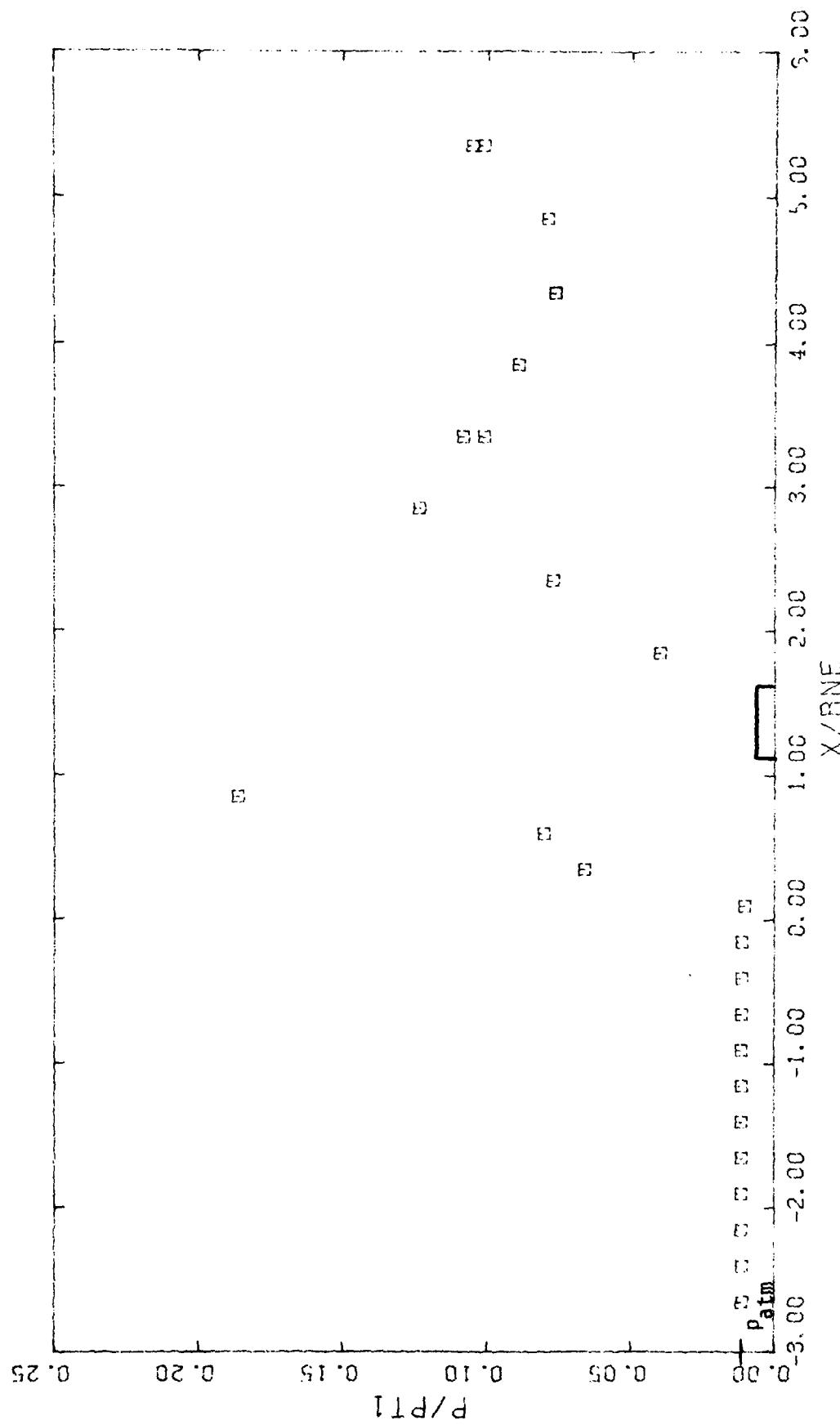
(c) $p_{t1} = 8.75 \times 10^6$ N/m^2 (1269 psia)

Figure A9. - Concluded.

(a) $p_{t1} = 2.71 \times 10^6$ N/m^2 (393 psia)
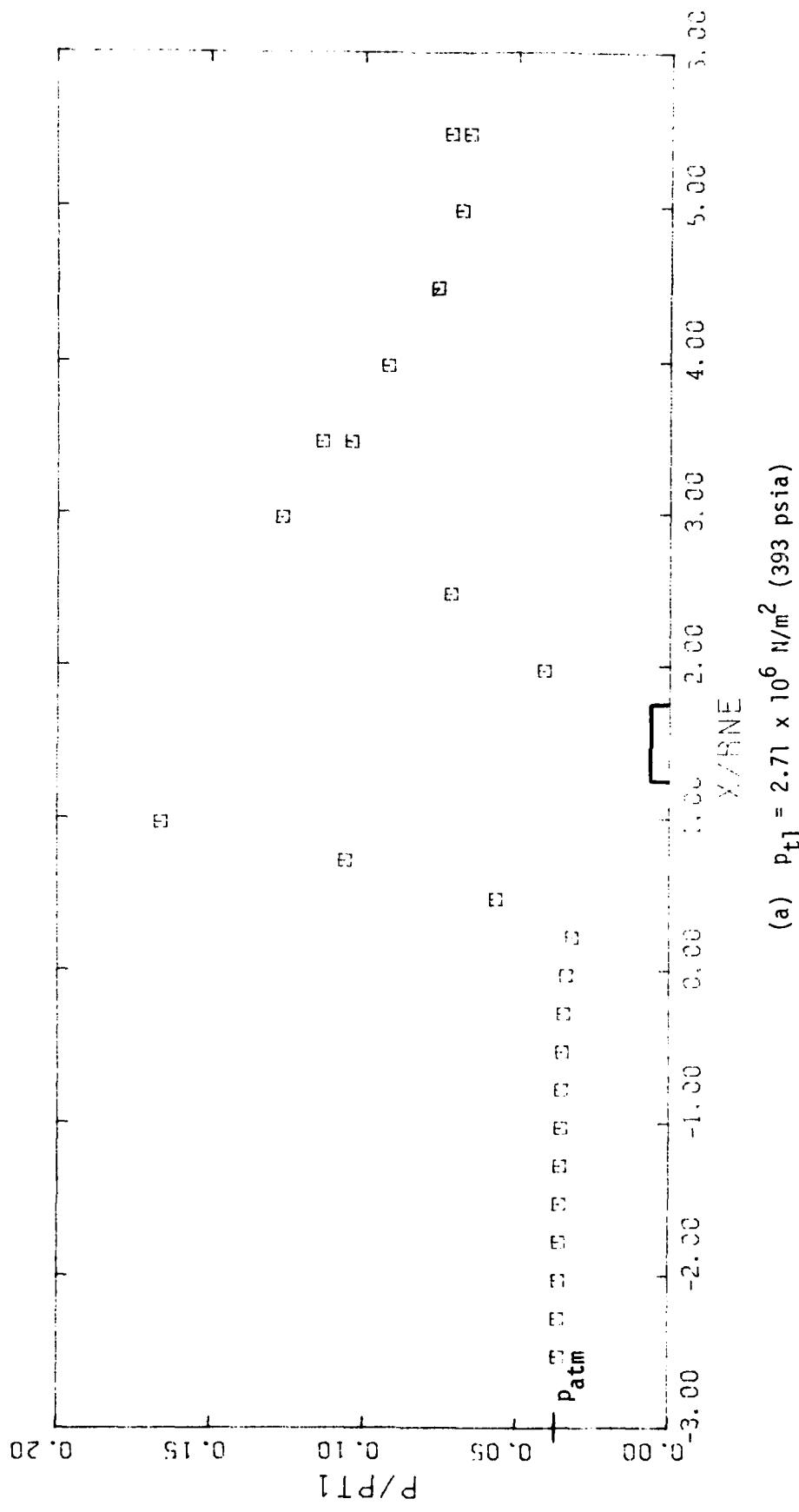
Figure A10. - The static wall pressure distribution for the C4/L1 configuration with constrictive ring, $\tilde{x}_{ne} = 10.0h$.
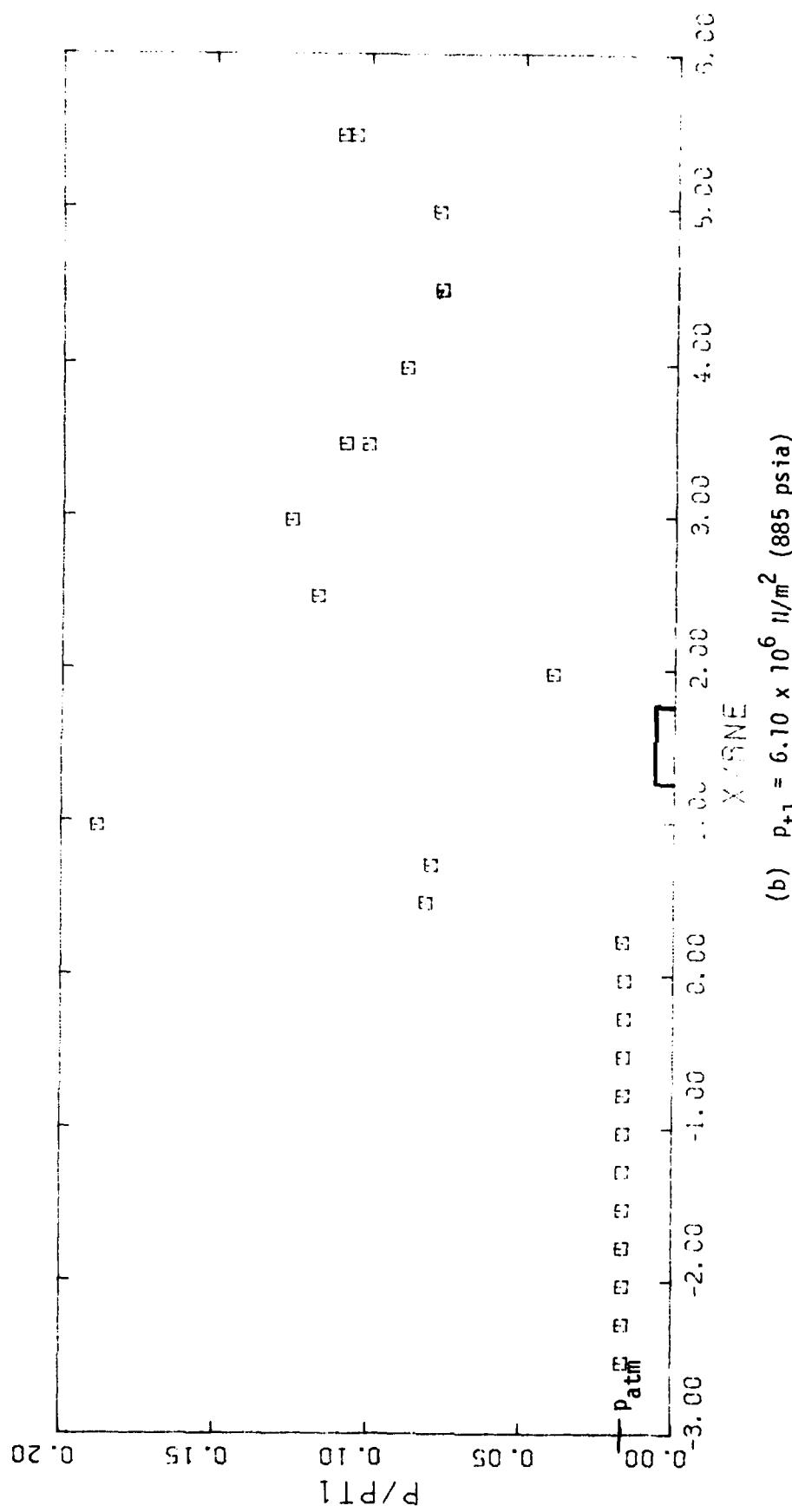
(b) $p_{t1} = 6.10 \times 10^6$ N/m² (885 psia)

Figure A10. - Concluded.

DISTRIBUTION

Defense Technical Information Center
Cameron Station
Alexandria, VA 22314   2

Commander
US Army Missile Command
Attn: DRSMI-0   3
        DRSMI-r, Dr. Kobler   1
        DRSMI-RLH   7
        DRSMI-ICBB, Barbara Roberts   1
        DRSMI-RPT   2
        DRSMI-RDK, Mr. Deep   2
        DRSMI-RPR   2
        DRSMI-LP, Mr. Voight   1
Redstone Arsenal, AL 35809

University of Illinois
Attn: Dr. H.H. Korst   1
Department of Mechanical Engineering
The University of Illinois at Urbana-Champaign
Urbana, Illinois 61801

US Army Material Systems Analysis Activity
Attn: DRXSY-MP   1
Aberdeen Proving Ground, MD 21005